A comprehensive analysis of (p)ppGpp signaling in bacteria

Molly Hydorn

Submitted in partial fulfillment of the
requirements for the degree of
Doctor of Philosophy
under the Executive Committee
of the Graduate School of Arts and Sciences

COLUMBIA UNIVERSITY

2025

Abstract

A comprehensive analysis of (p)ppGpp signaling in bacteria

Molly Hydorn

(p)ppGpp is a signaling molecule produced by bacteria in response to stresses, particularly amino acid starvation. RelA/SpoT homolog (RSH) enzymes synthesize (p)ppGpp when an uncharged tRNA enters an actively translating ribosome, stalling protein synthesis. (p)ppGpp slows bacterial growth by inhibiting translation, transcription, and DNA replication, and it upregulates the transcription of stress response genes. (p)ppGpp has also been shown to increase pathogenicity, virulence, and antibiotic tolerance. For example, persister cells — cells that are tolerant to antibiotic exposure and result in persistent and chronic infections — are thought to arise from a subpopulation of cells that are high in (p)ppGpp. Current methods of detecting (p)ppGpp are limited to bulk measurements using inaccessible techniques, making analysis of (p)ppGpp metabolism and its physiological consequences challenging. Here, I develop RsFluc, a novel tool for (p)ppGpp detection in *B. subtilis,* and validate it using HPLC-MS and known (p)ppGpp induction methods. I use RsFluc to assess (p)ppGpp metabolism in *B. subtilis* and assay the environmental stimuli that trigger (p)ppGpp signaling. I evaluate the downstream responses to (p)ppGpp using RsFluc, transcriptional reporters, and protein synthesis labeling techniques. I develop RsGFP, a tool for (p)ppGpp detection at the single-cell level. Using

RsGFP, I evaluate heterogeneity in (p)ppGpp throughout growth and the factors that contribute to that heterogeneity. I utilize these (p)ppGpp detection tools to develop a novel single-cell RNA sequencing (scRNA-seq) technique that enables researchers to assay heterogeneity in (p)ppGpp while simultaneously assessing differential gene expression at the single-cell level. I use RsGFP to evaluate the relationship between heterogeneity in (p)ppGpp and heterogeneity in regrowth and antibiotic tolerance. Lastly, collaborators and I developed a technique for labeling cells for protein synthesis while performing scRNA-seq, gaining insights into physiological states and how these states may affect transcription.

Table of Contents

List of Figures

List of Tables

Acknowledgments

Firstly, I would like to acknowledge my advisor, Dr. Jonathan Dworkin, and the entire Dworkin Lab. His insight and support throughout my training have been truly invaluable, and his guidance has shaped me into the scientist I am today. I want to thank my former lab member, Sathya Nagarajan, Ph.D., who advised on many of the experiments in this thesis, trained me in new techniques and analyses, and provided a strain construct used in this work. I want to thank my former lab member, Kiera Englehart, for keeping the lab running smoothly during her tenure. I would also like to thank former members, Simon Diez, Ph.D., for my early training in the lab, and Abigail Whalen, for her initial work on the riboswitch construct design, which informed my future designs. I want to thank current lab members, Gilberto Padron, Ph.D., and Evan Waldron, MD, Ph.D., for their continued input on the project. I want to thank Katrina Ralwins de la Rosa for supporting lab operations.

I want to thank Tyler Detomasi, Ph.D., for encouraging me to pursue a doctorate and for his training throughout my early development as a researcher. I would also like to thank Dr. Michael Marletta for recognizing my potential and welcoming me into his lab for my undergraduate research experience, which would not have been possible without his guidance.

I want to thank the Cellular Physiology and Biophysics department for their support of me on the departmental T32 grant, as well as for providing guidance and direction throughout the training through the Data Club meetings. I want to thank Drs. Filippo Mancia and Jane Dodd for their input as Directors of Graduate Studies. I want to thank the Microbiology and Immunology department for their support of my work on the T32 grant and for their feedback on my research in the Research in Progress meetings.

Finally, I'd like to thank Drs. Anne Moscona, Ruben Gonzalez, and Lars Dietrich for serving on my committee and providing feedback throughout my training. I want to thank Dr. Sam Sternberg for his advice and feedback on the thesis work in previous meetings and Dr. David Dubnau for serving as an external committee member during my thesis defense.

Dedication

This thesis is dedicated to my family. We're all Dr. Hydorn.

This thesis is also dedicated to Gabe Schumm, Ph.D., for always being by my side. I couldn't have done it without you.

Chapter 1

1 Introduction

1.1 A history of (p)ppGpp

Bacteria must adapt to their constantly changing environment to grow and divide. To meet the challenges and demands of growth and division, bacteria have evolved various strategies for signaling and physiological reprogramming to respond to stress. One key stress is nutrient depletion. In 1969, Cashel and Gallant initiated an investigation into the bacterial response to amino acid starvation in the Gram-negative model organism, *Escherichia coli*. They were inspired by work showing that when an *E. coli* culture was starved for their amino acids, the bacteria exhibited drops in the levels of stable RNA synthesis needed for growth and division (1), indicating some coordination of amino acid metabolism and nucleic acid synthesis. Fangman and Neidhart demonstrated that the trigger for this response was an increase in the population of uncharged transfer RNA (tRNA) molecules in cells (2, 3). The same response was also observed when antibiotics blocked protein synthesis in the Gram-positive pathogenic bacterium *Staphylococcus aureus* (4) and in *E. coli* (5). This phenomenon was referred to as the "stringent control" (6), or more commonly, the stringent response. Notably, the RC locus in *E. coli* was identified, and Stent and Brenner showed that when mutated, the bacterium no longer exhibited this coordination between nucleic acids and amino acid availability (7). They referred to this mutated strain as RC^{rel} (7). However, the function of this RC gene, later known as *relA*, remained unclear, and Cashel and Gallant aimed to clarify it.

Cashel and Gallant cultivated a wild-type (WT) RC gene strain of *E. coli* in the presence of amino acids until the culture reached an exponential growth phase. The cultures were then

filtered, and the cells were resuspended in medium supplemented with radioactive phosphate, both with and without amino acids. After a brief labeling period in the new media, both samples were analyzed using thin-layer chromatography (TLC) to separate the different phosphate compounds. When the cells were resuspended with amino acids, 18 distinct spots appeared on the autoradiograph, four of which were previously identified as ribonucleotide triphosphates (GTP, ATP, UTP, and CTP). When the cells were resuspended without amino acid supplementation, a 19th spot emerged on the chromatogram, which Cashel and Gallant referred to as the "magic spot" (6). They showed that the WT strain, but not the RC^{rel} strain, could form this magic spot when starved for a single amino acid, leading them to hypothesize that the compound at the magic spot was the product of the RC gene. They also found that the RC^{rel} strain did not undergo a downshift in RNA biosynthesis, as observed in the WT strain after starvation, suggesting that this newly identified compound may be essential for the downregulation of freshly formed RNA.

The following year, Cashel and Kalbacher identified one of these magic spot nucleotides (MSI) as a tetra-phosphorylated guanosine with diphosphate groups on both the 5' and 3' carbons, coining it ppGpp (8). They reasoned that the second magic spot nucleotide (MSII) was pppGpp, collectively coined (p)ppGpp (Figure 1.1). It was later described that the ppGpp molecule was made by adding a pyrophosphate group donated by an ATP molecule to the 3' hydroxyl group of a GDP molecule (9). Haseltine and Block showed that the biosynthesis of (p)ppGpp required a translating ribosome complex with an uncharged, codon-specific tRNA stalled in the ribosome's active site (10). This stalled complex was required for the "stringent factor," the enzyme responsible for producing (p)ppGpp, which is located at the *E. coli* RC^{rel} locus, to initiate the conversion of GDP and GTP into ppGpp and pppGpp, respectively.

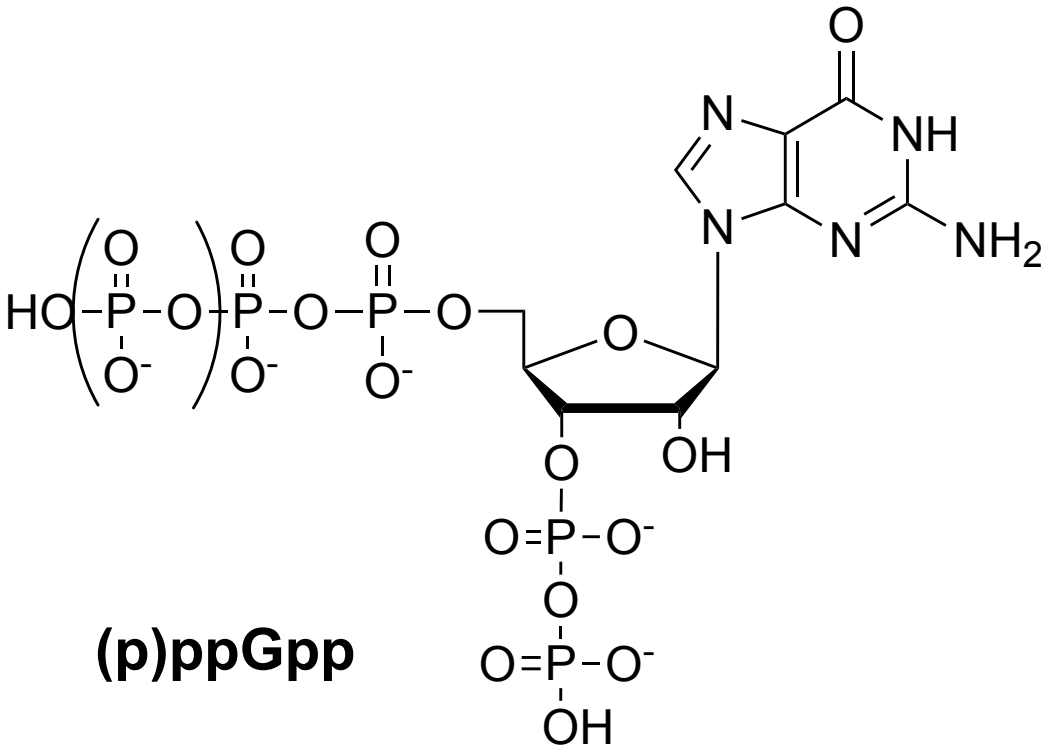

Figure 1.1 Chemical structure of guanosine penta- and tetraphosphate, (p)ppGpp. Line structure drawing of (p)ppGpp.

Rhaese *et al.* demonstrated that the accumulation of (p)ppGpp also occurs in *Bacillus subtilis*, a spore-forming Gram-positive model organism (11). They showed that the formation of (p)ppGpp is triggered by the stalling of protein synthesis, as confirmed by inhibiting protein synthesis with chloramphenicol (12). Since (p)ppGpp accumulation was demonstrated in both *E. coli* and *B. subtilis*, researchers now had two model organisms—one Gram-positive and one Gram-negative—to study (p)ppGpp metabolism and its physiological effects. This expanded our understanding of the bacterial stringent response, laying the foundation for a new field of research into how these molecules impact microbes, both commensal and pathogenic.

1.2 (p)ppGpp metabolism

1.2.1 (p)ppGpp synthesis

(p)ppGpp synthesis is primarily mediated by the superfamily of proteins called long RelA/SpoT homologue proteins (RSH) (13, 14). These enzymes feature a bifunctional N-terminal domain (NTD) that includes both a hydrolase (HD) and synthetase (SYNTH) domain, along with a regulatory C-terminal domain (CTD) that often contains a ThrRS, GTPase, SpoT domain (TGS), and an aspartate kinase, chorismate mutase, and TyrA domain (ACT) (14) (Figure 1.2).

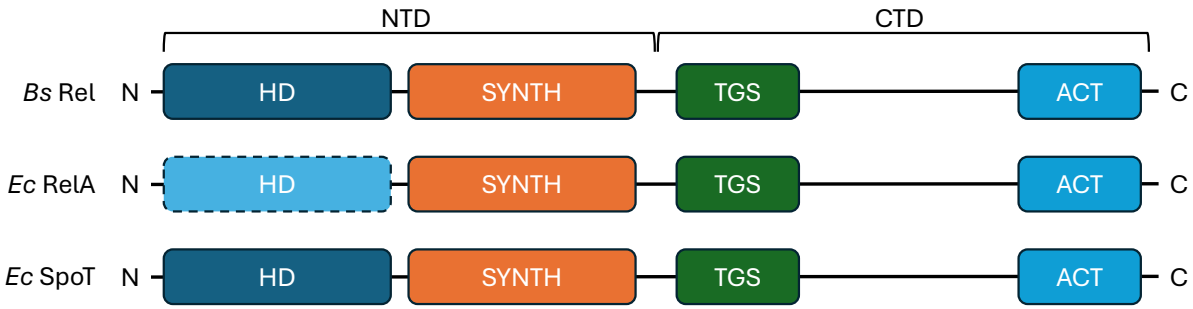

Figure 1.2 Domain architecture of RSH proteins.
Schematic depicting the typical RSH domain architecture of bifunctional *B. subtilis* Rel, monofunctional *E. coli* RelA, and bifunctional *E. coli* SpoT, containing HD and SYNTH domains in the NTD, and regulatory TGS and ACT domains in the CTD.

The most extensively characterized (p)ppGpp synthetases are *E. coli* monofunctional synthetase RelA, which has a vestigial hydrolase domain (15), and *B. subtilis* bifunctional Rel enzyme, which initiates (p)ppGpp synthesis during amino acid starvation in their respective species. *E. coli* also contains a bifunctional RSH protein called SpoT, which produces a small amount of (p)ppGpp (16). Phylogenetic analysis has shown that most β- and γ-Proteobacteria possess both a monofunctional RelA and a bifunctional Rel/SpoT, indicating that an evolutionary duplication event occurred. Conversely, other bacteria, such as Firmicutes like *B. subtilis*, have only a single bifunctional Rel/SpoT (14).

These RSH proteins function as (p)ppGpp synthetases when deacylated tRNA enters the A site of an actively translating ribosome, causing stalling and stopping protein synthesis at that

site (10, 17). RSH proteins often serve as the primary (p)ppGpp hydrolases, and their synthetase domains are typically in a closed or inactive state, acting as hydrolases unless they detect starvation signals. Monofunctional RSH proteins are usually held in an inactivated conformation until they detect starvation signals. RSH CTD RNA binding motifs interact with ribosomes to regulate hydrolase and synthetase activity, as shown by structural studies (18). This switching between hydrolase and synthetase is controlled by the CTD TGS and ACT motifs in RSH enzymes, which bind to uncharged tRNAs and rRNA, inducing a conformational change that switches the enzyme to the active, synthetase-on state (19–22). Once this signal is recognized, the enzymes adopt the active synthetase form and begin converting cellular GTP and GDP into pppGpp and ppGpp, respectively (Figure 1.3). Structural analysis identified the catalytic site of these RSH proteins, revealing a conserved catalytic aspartic acid residue—Asp264 in *B. subtilis* Rel, Asp275 in *E. coli* RelA, and Asp259 in *E. coli* SpoT (19).

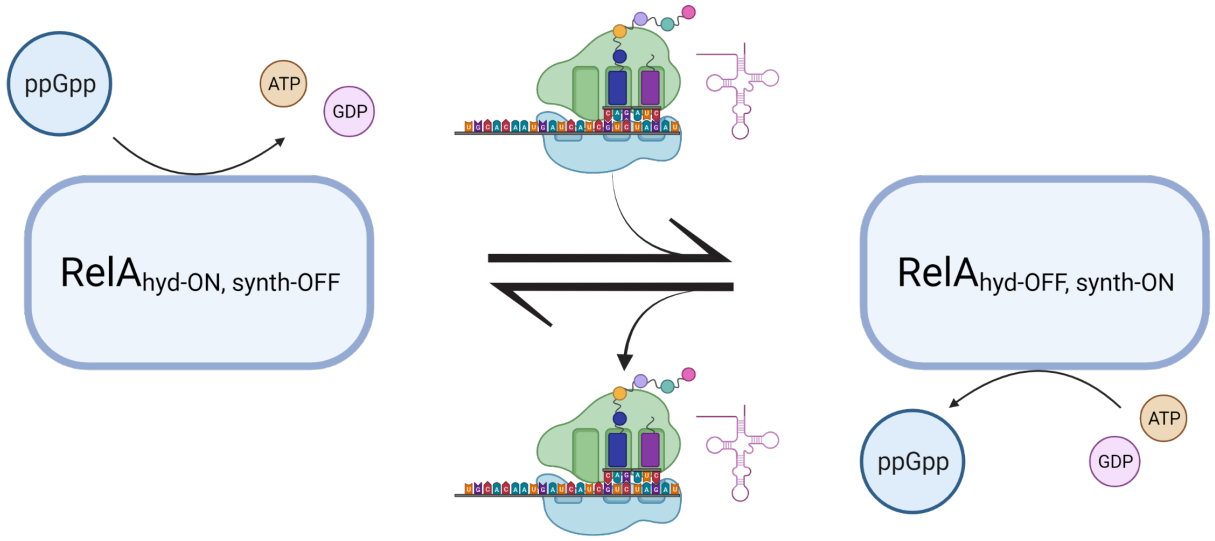

Figure 1.3. RSH HD to SYNTH switch regulated by CTD recognition of de-acylated tRNA and ribosome.
RSH proteins function primarily as (p)ppGpp hydrolases, unless bound to an actively translating ribosome with a deacylated tRNA entering the A-site of the ribosome, triggering stalling and indicating amino acid starvation. This signal confers a conformational change in RSH proteins, allowing the enzymes to become synthetase active and start converting GTP and GDP into pppGpp and ppGpp, respectively.

This synthesis of (p)ppGpp has also been shown to be positively allosterically regulated by (p)ppGpp itself, the very product that is produced by RSH proteins, leading to a commitment to a stringent response during starvation conditions (23, 24). This allosteric activation can be initiated by both pppGpp and ppGpp but has been found to generate higher enzymatic activity when stimulated with pppGpp using *E. coli* RelA (24). The allosteric site was identified as a binding pocket containing a conserved tyrosine residue essential for allosteric activation (24), specifically Tyr200 in *B. subtilis* Rel and Tyr211 in *E. coli* RelA. Interestingly, *E. coli* SpoT does not display this allosteric activation despite the conservation of the allosteric site (24). Allosteric activation is crucial for full enzyme activity *in vitro* and for growth in minimal media in living bacteria, suggesting that this mechanism evolved to coordinate the different Rel/RelA molecules within a cell that would otherwise not interact (24).

While RSH proteins are the primary (p)ppGpp synthetases, there are also small alarmone synthetases (SAS) that produce (p)ppGpp in specific species. These enzymes contain only a SYNTH domain, excluding the CTD and HD domains. Different bacteria have these enzymes in various combinations (25). *E. coli* has two RSH proteins, RelA and SpoT, while *B. subtilis* has one RSH protein, Rel, and two SAS proteins, SasA and SasB (Figure 1.4). These SAS proteins were identified through sequence analysis, and their (p)ppGpp synthetase activity was confirmed both *in vitro* and in a *relA* deletion strain, which restored (p)ppGpp synthesis (26). While Rel activity in *B. subtilis* is regulated by amino acid starvation, the regulation of SAS proteins has been an ongoing area of research. SasA is upregulated in response to cell wall stress via the two-component signaling system WalKR (27–29). SasB is expressed during exponential growth in LB (26), but its activity is enhanced by allosteric activation with pppGpp and inhibited by pGpp (30, 31). Interestingly, RelQ, a SasB homolog in *Enterococcus faecalis*, is allosterically inhibited when mRNA is present, and this inhibition can be overcome by (p)ppGpp binding (32).

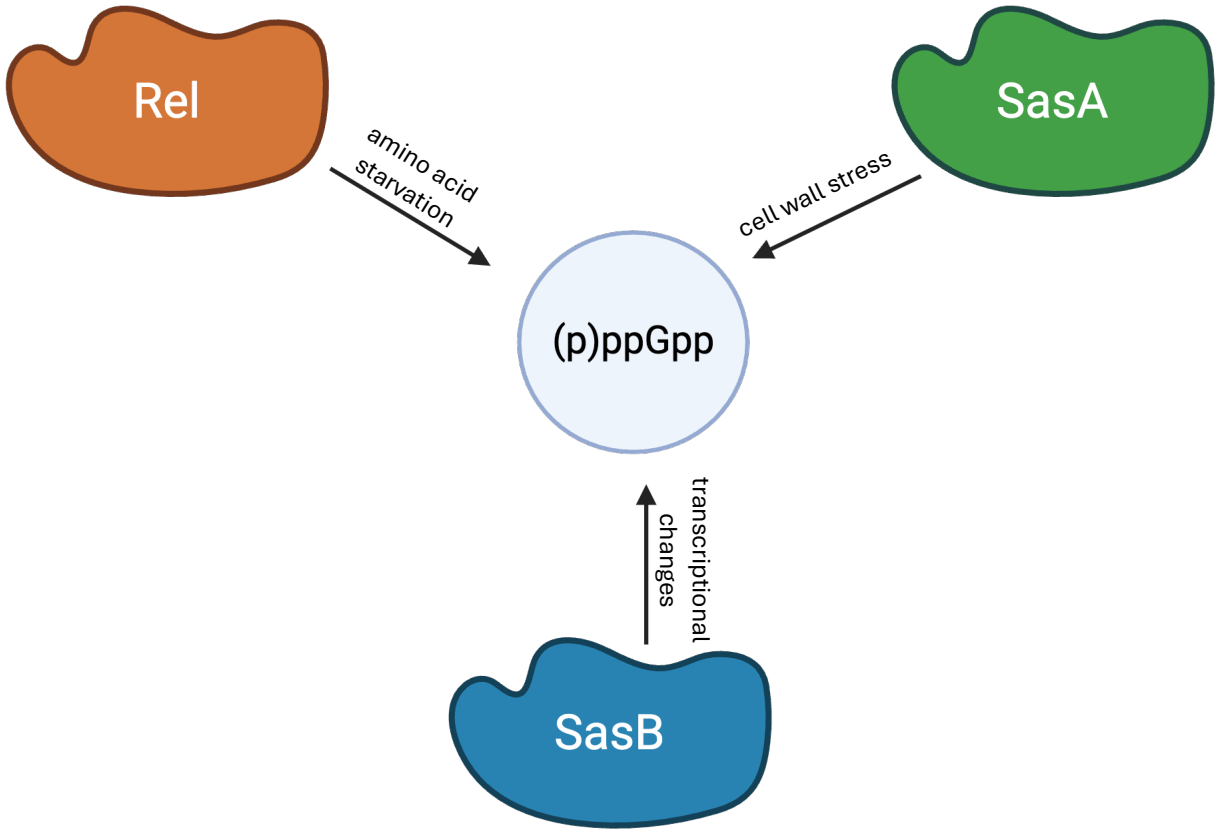

Figure 1.4 Schematic of *B. subtilis* (p)ppGpp synthetases.
B. subtilis contains three identified (p)ppGpp synthetases, one RSH enzyme, Rel, and two SAS enzymes, SasA and SasB. SasA is upregulated in response to cell wall stress. SasB is regulated transcriptionally and allosterically.

1.2.2 (p)ppGpp hydrolysis

The main hydrolases of (p)ppGpp in bacteria are the RSH family enzymes (14–16). As mentioned earlier, *B. subtilis* Rel and *E. coli* SpoT are bifunctional, containing active SYNTH and HD domains, enabling them to degrade (p)ppGpp from cells back to GDP and free pyrophosphates. However, *E. coli* RelA has a nonfunctional HD domain, acting only as a (p)ppGpp synthetase.

The primary conformation of bifunctional RSH proteins is the hydrolase state unless otherwise triggered by amino acid starvation (14). This RSH enzyme activity may support a low

basal level of cellular (p)ppGpp, which is essential for cell maintenance. This low, basal level of (p)ppGpp homeostasis is thought to be crucial for maintaining cell shape (33, 34), energy levels after exponential growth (34), stability of rRNAs (35), growth rate and DNA synthesis (35, 36), and amino acid biosynthesis (16, 37).

While RSH enzymes are the primary (p)ppGpp hydrolases, there are some reports of secondary (p)ppGpp hydrolases, mainly small alarmone hydrolases (SAH) and *B. subtilis* NahA. SAHs are duplications of the hydrolase domain in the genome that break down (p)ppGpp into GDP and free pyrophosphates (14). These SAH enzymes are rare but have been found in certain bacteria and even in the mitochondria of some eukaryotes ((14), Table 1). Recent research on the *B. subtilis* Nudix-hydrolase enzyme (NahA) has shown that this enzyme helps degrade and prevent the overaccumulation of (p)ppGpp in *B. subtilis* by converting (p)ppGpp into the smaller alarmone, pGpp (38, 39). However, because NahA hydrolyzes (p)ppGpp into pGpp, it is not considered a true (p)ppGpp hydrolase and may serve other roles, such as removing a pyrophosphate from the 5' end of mRNA (40). This hydrolysis activity will be discussed in more detail in section 1.2.3.

1.2.3 Crosstalk with other signaling molecules

(p)ppGpp is among the many signaling molecules that bacteria produce in response to stimuli. For example, cyclic AMP (cAMP), a signaling nucleotide in eukaryotes, was first discovered in *E. coli* and shown to be involved in stress signaling triggered by glucose depletion (41). Other crucial bacterial signaling nucleotides include cyclic-di-GMP (42), cyclic-di-AMP (43), AppppA (44), and the small alarmone pGpp (38). While each has a wide range of specific trigger stimuli and regulatory mechanisms, there are some similarities and overlaps in their

metabolisms and downstream signaling, particularly in crosstalk with (p)ppGpp and among themselves (45).

c-di-GMP is produced from two GTP molecules by diguanylate cyclase (DGC) (46) and broken down by c-di-GMP-specific phosphodiesterases (PDEs) into pGpG (47). The synthesis of c-di-GMP is believed to be triggered by various environmental signals, including oxygen stress (48), nutrient starvation (49), and antibiotics (50). c-di-GMP interacts with several effector proteins, such as those involved in cell replication, cellulose production, motility, and extracellular polymeric substance (EPS) synthesis (51). Additionally, this molecule influences gene expression by binding sigma factors and RNA elements called riboswitches (51). Its overall role is to regulate bacterial life cycles, switching between planktonic and biofilm states (51). A study in *Caulobacter crescentus* demonstrated that the small molecule binding protein SmbA binds both c-di-GMP and (p)ppGpp, with each binding producing opposing effects (52). When (p)ppGpp binds to SmbA, it activates the protein, leading to increased growth on glucose and enhanced reactive oxygen species (ROS) quenching in response to redox stress (Figure 1.5A). Conversely, when c-di-GMP binds to SmbA, it inhibits the protein, triggering a metabolic switch that suppresses growth on glucose.

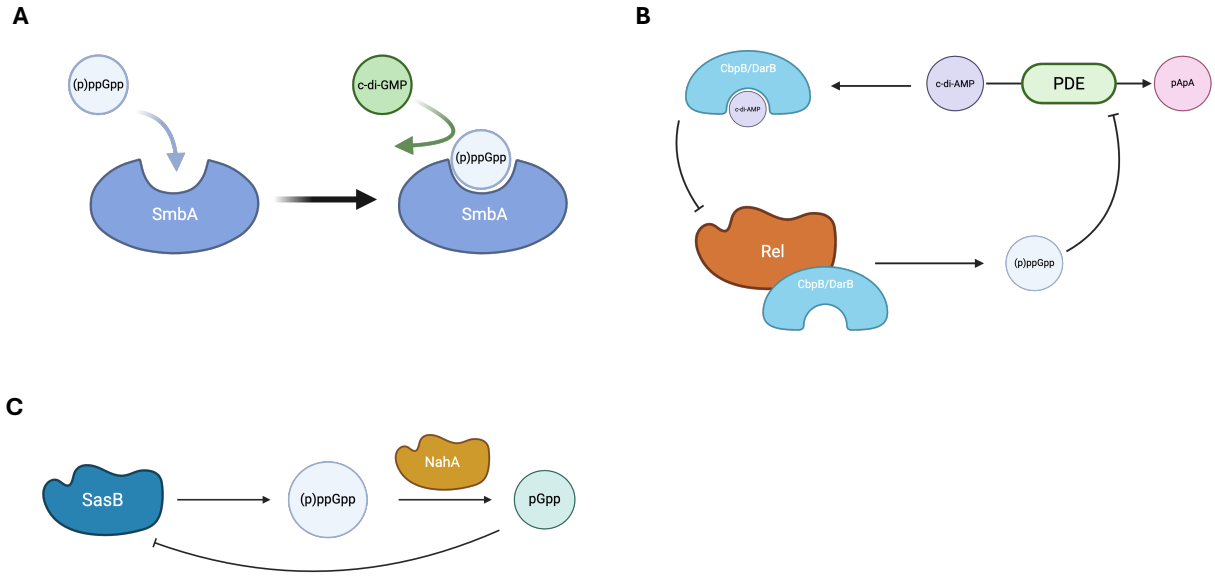

Figure 1.5 Crosstalk between (p)ppGpp and other signaling nucleotides.
A) (p)ppGpp inhibits c-di-GMP binding of effector protein SmbA in *Caulobacter crescentus* by competitively binding, affecting downstream c-di-GMP regulatory processes. B) (p)ppGpp inhibits c-di-AMP degradation by binding PDE in *B. subtilis* and *S. aureus*. c-di-AMP binding protein CbpB in *Listeria monocytogenes* and DarB in *B. subtilis* stimulate (p)ppGpp production when in apo form, leading to a regulatory feedback mechanism of crosstalk between c-di-AMP and (p)ppGpp. C) NahA processes (p)ppGpp to pGpp in *B. subtilis*. pGpp then inhibits (p)ppGpp synthetase SasB activity through allosteric competitive inhibition, introducing a negative feedback mechanism.

Bacteria also use c-di-AMP signaling, often referred to as the "essential poison" in literature (53). c-di-AMP is produced from two ATP molecules by diadenylate cyclase (DAC) and is broken down by c-di-AMP-specific PDEs into pApA (54–57). This molecule is vital for managing osmotic stress, surviving acid stress, protecting DNA, and resisting antibiotics (57). Its targets include potassium (K^+) and osmolyte transporters (58) as well as proteins that maintain DNA integrity (43). Crosstalk between c-di-AMP and (p)ppGpp occurs through mechanisms such as allosteric regulation or direct inhibition of enzymes involved in nucleotide metabolism. In *B. subtilis* (59) and *S. aureus* (60), (p)ppGpp binds to c-di-AMP PDE, preventing its breakdown and raising c-di-AMP levels. Notably, c-di-AMP can also inhibit Rel activation

through the c-di-AMP binding protein CbpB in *Listeria monocytogenes* (61) and the homolog DarB in *B. subtilis* (62). When CbpB/DarB are in their apo form, they bind to Rel to promote (p)ppGpp synthesis, even without a stalled ribosome. When c-di-AMP binds to CbpB/DarB, this complex cannot form, resulting in no (p)ppGpp production. This creates a feedback loop between c-di-AMP and (p)ppGpp (Figure 1.5B).

pGpp is a smaller alarmone signaling nucleotide, previously thought to be another form of (p)ppGpp. However, recent studies show it has distinct functions and should be considered a separate pathway (38, 39). This smaller alarmone nucleotide can be produced by the same enzymes that generate (p)ppGpp themselves, such as Rel (63) and SAS (64) enzymes. pGpp regulates a small subset of (p)ppGpp targets in *B. subtilis* (38), and it also controls (p)ppGpp production. The Wang Lab found that when SasA was expressed in an otherwise (p)ppGpp^0 background, pGpp accumulated (39). However, this buildup did not occur when cells lacked NahA due to a Δ*nahA* mutation. This led to the discovery that NahA is a pyrophosphohydrolase that converts (p)ppGpp to pGpp by releasing pyrophosphate or phosphate groups (38). pGpp has also been shown to inhibit *B. subtilis* ppGpp synthetase SasB activity by competitively binding to an allosteric site, which is stimulated by pppGpp binding (31). This creates a negative feedback loop to prevent (p)ppGpp overaccumulation (Figure 1.5C).

1.3 Physiological significance of (p)ppGpp signaling

1.3.1 Translation

One of the main effects of (p)ppGpp signaling is growth arrest. In part, this occurs because (p)ppGpp inhibits bacterial translation. In bacteria, translation happens in four main steps: initiation, elongation, termination, and ribosome recycling (65–67). These steps are facilitated by GTPases, including initiation factor 2 (IF2), elongation factor G (EF-G), EF-Tu, and HflX.

(p)ppGpp targets several of these GTPases to regulate translation by competitively inhibiting them.

Initiation of protein synthesis involves assembling the large (50S) and small (30S) ribosomal subunits with mRNA, initiating tRNA (fMet-tRNA^{fMet}), and initiation factors to start new polypeptide production. One of these initiation factors, IF2, was identified as a (p)ppGpp-binding protein and metabolic sensor (68–70). Diez *et al.* confirmed that IF2 binds to (p)ppGpp in *B. subtilis* using Differential Radial Capillary (DRACaLA) binding assays (71). The binding of (p)ppGpp to IF2 inhibits ribosomal assembly *in vitro*, as shown by fluorescence resonance energy transfer (FRET). Additionally, (p)ppGpp binding to IF2 prevents recognition of fMet-tRNA^{fMet} (69, 70). (p)ppGpp also interacts with the ribosome assembly GTPase ObgE in *E. coli* (72), further extending the influence of (p)ppGpp on translation initiation.

EF-Tu facilitates translation elongation in complex with GTP and aminoacyl-tRNA (aa-tRNA), which delivers aa-tRNA to the A-site to enable transpeptidation and ongoing polypeptide synthesis (73). After EF-Tu hydrolyzes GTP during delivery, it becomes free to repeat the process until termination (74). EF-G coordinates the translocation of tRNA and mRNA from the A- to P-site and P- to E-site, driven by GTP hydrolysis (75). Both EF-Tu and EF-G have long been recognized as targets of (p)ppGpp inhibition (76–79).

Ribosome recycling is a vital process for maintaining cell function and preserving energy (80). HflX is a ribosomal recycling factor recently identified in *E. coli* (81). HflX operates by dissociating 70S ribosomes and then remaining bound to the 50S subunit, before detaching from it upon GTP hydrolysis (82). (p)ppGpp was shown to bind HflX in both *E. coli* (83) and *S. aureus* (84). Although the exact mechanism remains unclear, (p)ppGpp is thought to inhibit ribosome recycling, which slows protein synthesis and contributes to growth arrest (67).

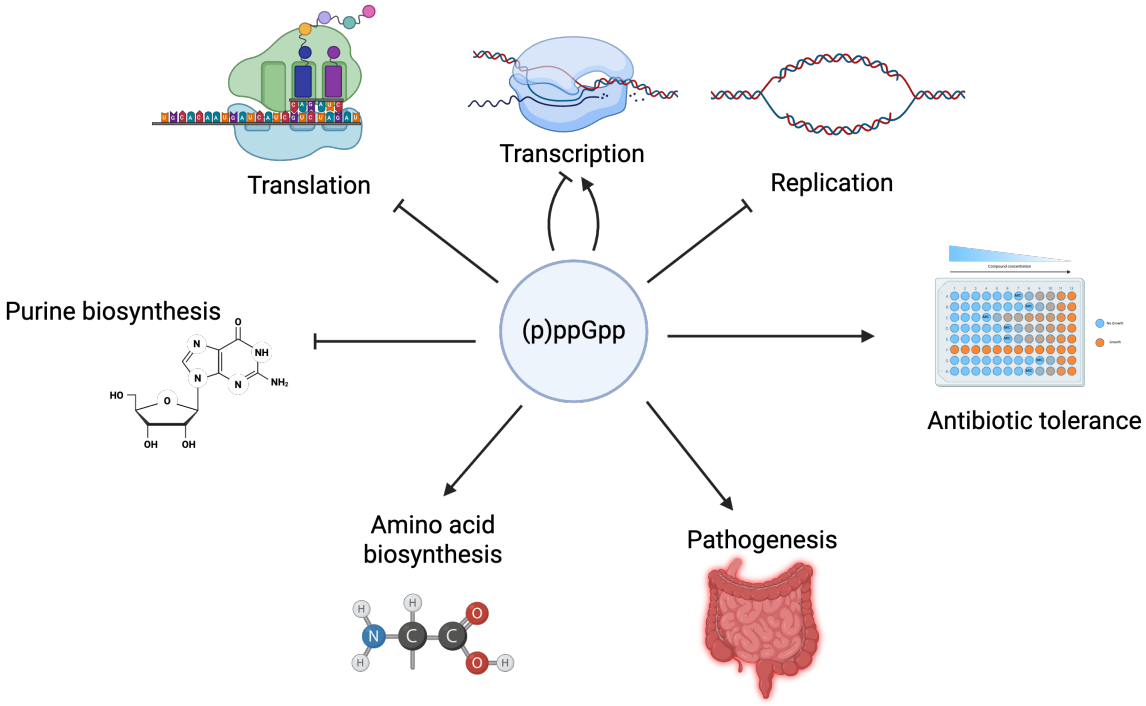

Figure 1.6 (p)ppGpp signaling affects numerous bacterial physiologies. (p)ppGpp has been shown to inhibit translation, DNA replication, and purine biosynthesis in various bacterial species. (p)ppGpp has been shown to upregulate amino acid biosynthetic pathways and those involved in pathogenesis, and to increase antibiotic tolerance. (p)ppGpp has been shown to play a role in upregulation of specific genes and downregulation of others via various mechanisms across bacterial species.

1.3.2 Transcription

Amino acid starvation leads to a widespread reduction in stable RNA synthesis (1). In *E. coli*, (p)ppGpp regulates transcription by directly binding to the RNA polymerase (RNAP) machinery (85), initiating a response through the transcriptional regulator DksA (86–89). DksA, a transcriptional regulator that is constantly expressed, interacts with RNAP, and both DksA and (p)ppGpp bind simultaneously to RNAP to control specific promoters. When (p)ppGpp and DksA bind to RNAP, the expression of genes for flagella, ribosomal proteins, and fatty acid synthesis is suppressed, while genes involved in amino acid biosynthesis are activated (90–92). This regulatory response enables the cell to prepare for environments with limited nutrients by

downregulating genes associated with rapid growth and upregulating those involved in stress response.

Potrykus *et al.* demonstrated that ribosomal RNA (rRNA) content is regulated by (p)ppGpp and that the coupling of growth rate to rRNA content is lost in *an E. coli* mutant lacking (p)ppGpp synthesis (35). (p)ppGpp, DksA, and RNAP work together to conserve energy by downregulating ribosome biogenesis during amino acid starvation, with these promoter regions typically being GC-rich and targeted for downregulation through sequence recognition by RNAP (93–95). While (p)ppGpp signaling downregulates rRNA, amino acid biosynthetic pathways are upregulated because they contain AT-rich promoter regions. In *B. subtilis*, however, (p)ppGpp does not directly bind RNAP, nor does it have a DksA homolog. The decreased GTP pools resulting from increased (p)ppGpp signaling (37) regulate transcriptional changes since G-start transcripts are not highly transcribed when GTP levels fall (96). rRNA-initiating nucleotides in *B. subtilis* are mostly GTP, which requires high levels of the nucleotide to initiate ribosome biogenesis.

(p)ppGpp-dependent transcriptional changes in *B. subtilis* are mainly mediated indirectly through the GTP-binding regulator CodY (97). CodY is a transcriptional repressor—although in some cases it has been shown to act as an activator—of hundreds of *B. subtilis* genes, including those involved in sporulation, competence, flagellar function, amino acid and sugar transporters, and amino acid biosynthetic operons (98–101). When GTP binds to CodY, it acts as a repressor of the genes downstream of the DNA-binding site. (p)ppGpp levels inhibit GTP synthesis (37), causing apo CodY to no longer bind to the DNA upstream of these genes, which allows transcription to proceed. (p)ppGpp modulates transcription by inhibiting translation, leading to a decrease in response regulator levels (102). When (p)ppGpp levels are high, protein synthesis

rates decline, transcriptional repressor levels decrease, and the transcription of genes within the repressor's regulon increases.

1.3.3 DNA synthesis and genome maintenance

(p)ppGpp coordinates the transition from high growth to the stationary phase by targeting central dogma processes in bacteria, as discussed in previous sections. In bacteria, these processes are closely linked and occur simultaneously. While a transcript is being synthesized from DNA, it is actively translated by polysome complexes of ribosomes. Similarly, DNA replication and transcription are tightly coupled, as they occur on the same template simultaneously. Maintaining genome integrity during replication is essential for keeping these processes closely linked and ensuring bacterial survival. (p)ppGpp has been shown to support this maintenance in model organisms *like E. coli* and *B. subtilis* (25).

In *E. coli*, (p)ppGpp has been shown to inhibit replication initiation (103, 104) and block DNA replication elongation in *B. subtilis* (104, 105). DNA replication is usually measured by the ratio of the abundance of *ori*, the origin of replication, to the abundance of DNA in the termination region, *ter*, often expressed as the *ori*/*ter* ratio. Fernández-Coll *et al.* found that *ori*/*ter* ratios are high during exponential growth and decrease as growth rates slow, and this regulation occurs in a (p)ppGpp-dependent manner in *E. coli* (36). They demonstrated that (p)ppGpp targets the expression of DNA gyrase machinery, slowing replication initiation by altering supercoiling at the origin of replication. Wang *et al.* demonstrated that in *B. subtilis,* DNA primase is the primary target of (p)ppGpp inhibition, and that initiation of replication is not affected by increased (p)ppGpp levels (105).

(p)ppGpp also plays a key role in DNA repair (106–110), often through its interaction with transcription machinery (111, 112). Weaver *et al.* suggested a mechanism for this regulation in

E. coli based on structural insights (113). RNAP has an additional (p)ppGpp binding site during elongation rather than initiation, and binding of (p)ppGpp to this site encourages DNA repair in response to stress and genotoxin exposure by promoting RNAP backtracking. This also provides a new perspective on previous findings that (p)ppGpp induces DNA repair by causing transcriptional pausing (114, 115). Overall, these fundamental processes of the central dogma are carefully managed by (p)ppGpp signaling to slow growth during nutritional stress, safeguard genome integrity, and enable cells to reprogram for environments with fewer nutrients.

1.3.4 Purine and amino acid biosynthesis

Guanosine nucleotide metabolism, especially GTP and GDP, is closely linked to amino acid starvation (37). This link is crucial for conserving energy and responding to nutrient shortages. When cells detect amino acid starvation, they must adapt by producing the amino acids needed for cellular maintenance and growth. This shift redirects metabolism from purine synthesis to amino acid production and is controlled through (p)ppGpp signaling mechanisms.

A key response to amino acid starvation is increased amino acid synthesis from the carbon and nitrogen sources available in the cell. An inability to produce amino acids is called amino acid auxotrophy. Bacteria that cannot make (p)ppGpp due to mutations in (p)ppGpp synthetase genes are known as (p)ppGpp^0. There is increased amino acid auxotrophy in (p)ppGpp^0 bacteria, especially in branched-chain amino acid biosynthetic pathways, as reported across different bacterial species (16, 37, 88, 101, 116–118).

(p)ppGpp signaling downregulates purine biosynthetic pathways by directly inhibiting metabolic enzymes and altering the expression of genes involved in purine biosynthesis. (p)ppGpp^0 has been shown to cause GTP dysregulation, leading to toxic overaccumulation of the nucleotide (37, 118). In *E. coli*, (p)ppGpp signaling targets the GTPases Hpt, Gpt, PurF, and Gsk

to lower GTP production through competitive inhibition (118). In *B. subtilis*, the GTPases Hpt, Gpt, and Gsk are also targeted by (p)ppGpp (37). Additionally, the 12-gene *pur* operon responsible for converting phosphoribosyl pyrophosphate (PRPP) into the purines ATP and GTP in *B. subtilis* is anti-induced by (p)ppGpp binding to PurR, the repressor of the *pur* operon (119).

1.3.5 Pathogenesis and virulence

During infection and host colonization, bacteria encounter stresses such as low pH, temperature fluctuations, hypoxia, and oxidative stress, all of which (p)ppGpp helps mediate in stress response. For example, some gut microbes rely on (p)ppGpp signaling within the gut during fasting and feeding periods (120). Additionally, certain virulence factors may be expressed differently depending on whether (p)ppGpp signaling is present or absent. (p)ppGpp has been identified as a key molecule for the pathogenesis and virulence of specific bacterial pathogens during human infections (121).

One such pathogen that requires a complete stringent response for successful host infection is *Staphylococcus aureus*, which has become increasingly important as methicillin-resistant *S. aureus* (MRSA) cases rise in hospitals. Clinical isolates have been identified that are defective in (p)ppGpp hydrolysis, leading to increased colonization during nutrient stress (122). (p)ppGpp is also necessary for the upregulation of virulence factors in *S. aureus* (123). In *Streptococcus pneumoniae*, one of the most common human pathogens, (p)ppGpp plays a critical role in modulating translation during a mouse infection model, as well as in gene expression required for producing pneumolysin toxin (124). *Mycobacterium tuberculosis*, the pathogen responsible for tuberculosis in humans, shows decreased pathogenicity and virulence in *rel* mutant strains during guinea pig infection (125). *Pseudomonas aeruginosa*, the pathogen involved in most cystic fibrosis-related fatalities, displays decreased cytotoxicity in human lung cell lines and

reduced inflammatory cell infiltration in a mouse infection model when mutated to (p)ppGpp^0, indicating that (p)ppGpp signaling is essential during infection (126).

1.3.6 Antibiotic tolerance and resistance

Antibiotics generally target bacteria by blocking essential macromolecular synthesis, such as DNA, RNA, or proteins. Since (p)ppGpp inhibits these key processes, a well-known association exists between (p)ppGpp and antibiotic resistance and tolerance. For this thesis, resistance is defined as a higher minimal inhibitory concentration (MIC) caused by the genetic presence of a resistance factor, while tolerance is defined as the ability to survive brief exposure to lethal antibiotic levels without an increase in MIC (127).

In MRSA, the link between methicillin resistance and the stringent response has been widely examined. Methicillin resistance results from the *mecA* gene, which encodes a penicillin-binding protein (PBP) with very low affinity for methicillin and other β-lactam antibiotics (128). Researchers found that when amino acid starvation was induced and cells were treated with methicillin, MRSA showed resistance to oxacillin due to increased expression of *mecA* and other PBP genes (129). In *B. subtilis*, resistance is lost in (p)ppGpp^0 cells treated with antibiotics tiamulin, lincomycin, and iboxamycin (130).

In *S. aureus*, acute amino acid starvation leads to increased tolerance to vancomycin (131). A clinical isolate of *Enterococcus faecium* with a constitutively active Rel enzyme showed higher multi-antibiotic tolerance and vancomycin resistance (132). *S. aureus* clinical isolates have also been found with mutations in *rel,* resulting in a hyperactive SYNTH domain, which provides multidrug tolerance (133). Furthermore, researchers have shown decreased tolerance when (p)ppGpp synthetases are mutated to become inactive or are blocked by small molecules in

Enterococcus faecalis (134), *Staphylococcus aureus* (135), *Clostridium difficile* (136), and *Bacillus subtilis* (137).

1.3.7 Single-cell heterogeneity in (p)ppGpp

Since (p)ppGpp plays a key role in downregulating many energy-consuming processes and upregulating stress response genes and pathways, understanding how (p)ppGpp levels vary within a population and how this variation affects bacterial physiology is crucial. Until recently, existing methods for (p)ppGpp detection, discussed in more detail in 1.4, were not suitable for assessing heterogeneity in (p)ppGpp levels within a population, creating a gap in knowledge. However, studies can suggest that (p)ppGpp varies among a population even if they cannot measure (p)ppGpp levels directly.

Libby *et al.* examined how specific cell wall stresses can lead to increased SAS expression in *B. subtilis* and found that a small population, less than 1%, had very high *sasA* expression (29). Using a fluorescent reporter, they sorted cells with high *sasA* expression through Fluorescence-Activated Cell Sorting (FACS) and treated them with ciprofloxacin. These cells showed increased tolerance to ciprofloxacin, suggesting that a small subpopulation might have higher synthetase levels and, therefore, more (p)ppGpp, which boosts tolerance. Diez *et al.* demonstrated that (p)ppGpp could influence protein synthesis heterogeneity in *B. subtilis* by using a fluorescent protein synthesis marker, O-propargyl puromycin (OPP) labeling. They observed a bimodal population with cells showing little to no protein synthesis and others with moderate to high synthesis during the late transition phase (71). This bimodal distribution resulted from epistatic interactions between *sasA* and *sasB*, indicating that finely tuned regulation of (p)ppGpp metabolism produces a heterogeneous and bimodal population (31).

Variation in (p)ppGpp levels among individual cells in *E. coli* has long been thought to contribute to differential antibiotic tolerance (138).

Could heterogeneity in (p)ppGpp levels contribute to the formation of different subpopulations, each with distinct characteristics? Although current technologies do not yet allow us to answer this question, some (p)ppGpp-dependent genes could be regulated differently in a population with single-cell heterogeneity in (p)ppGpp levels. For example, sporulation pathways might be activated in a subpopulation of cells with higher (p)ppGpp (139), leading to a group of cells that eventually become sporulating. This heterogeneity, resulting in a subpopulation with lower activity, has prompted research into what are known as "persister" cells—cells that exhibit increased antibiotic tolerance and cause persistent infections (140). While the role of (p)ppGpp in persister cell formation remains highly debated and contested (141–145), heterogeneity in this small signaling molecule could potentially influence their development.

1.4 Current methods of (p)ppGpp detection

1.4.1 Radiolabeling and thin-layer chromatography (TLC)

The earliest method for detecting (p)ppGpp dates back to the discovery of (p)ppGpp itself. Cashel and Gallant identified the magic spots using thin-layer chromatography (TLC) pulsed with radioactive isotope ^{32}P-phosphate (6), employing nucleotide separation methods described only a few years earlier by Randerath and Randerath (146). These methods allowed for the distinct separation of nucleotides by running the TLC in two dimensions. Since then, methods have been modified to enable separation and analysis in one dimension (147). When running in one dimension, conditions must be optimized to ensure separation between similar nucleotides.

For example, pGpp and GTP may migrate similarly on the TLC unless buffer conditions are adjusted to improve this separation.

Briefly, bacteria are fed with ^{32}P-phosphate-supplemented media, and nucleotides are harvested from the bacteria, usually through lysis and buffer reconstitution. The lysates are then run on TLC. TLC methods are also used to quantify (p)ppGpp production *in vitro* from biochemical assays, typically by isolating nucleotides from enzymes and quenching reactions with acetone. To visualize the TLC results from bacterial harvests and *in vitro* assays, researchers employ phosphor imaging screens, which often include quantification features in the software. TLC plates from pure *in vitro* assays can also be visualized simply with UV light.

1.4.2 High-performance liquid chromatography and mass spectrometry (HPLC-MS)

A powerful technique for analyzing and quantifying nucleotides from bacterial cultures is high-performance liquid chromatography (HPLC) combined with mass spectrometry (MS), often referred to as HPLC-MS. One initial challenge was that two different HPLC methods provided different advantages and costs: small-anion exchange (SAX) HPLC and ion-pair reverse-phase (IPRP) HPLC (148). Varik *et al.* optimized a combination of these two methods to enable the analysis, separation, and measurement of nucleotides (149). The technique was further improved when combined with HPLC-MS, using columns that offer even higher resolution, as shown by Zbornikova *et al.* (150).

A brief description of the experimental protocol involves growing a culture to the desired density or under specific conditions, followed by concentrating the cells on a cellulose acetate filter. The filter is then washed with lysis buffer containing an internal standard, lyophilized, and resuspended in water. The samples can be subsequently separated, validated, and quantified using HPLC-MS.

This method offers improved separation techniques but requires a more complex biochemical setup than is typically available in most bacteriology labs. It can also be relatively insensitive for (p)ppGpp detection, needing large culture volumes to reach detection limits or relying on amino acid starvation to produce high levels of nucleotides in smaller volumes.

1.4.3 A gap in our understanding

These two methods, described in 1.4.1 and 1.4.2, are the most reliable ways to detect (p)ppGpp in a culture. Each method has its own advantages and disadvantages. TLC is accessible but relies on radioactivity for sensitive detection. HPLC-MS provides better separation of nucleotides, but its readings are less sensitive.

Both methods tend to rely on artificial induction of the stringent response rather than measuring natural (p)ppGpp levels. Techniques for inducing the stringent response include amino acid starvation (118), blocking aminoacyl-tRNA charging with the isoleucyl-tRNA synthetase inhibitor mupirocin (151), and isoleucyl starvation caused by excessive valine, as shown by Cashel and Gallant (6). This causes a rapid, nonphysiological spike in (p)ppGpp compared to levels during normal growth (149). Not only does it produce a sharp increase in (p)ppGpp, but it also depletes other nucleotides, quickly exhausting the key building blocks of RNA (149). Additionally, culturing bacteria in low-phosphate media supplemented with ^{32}P-phosphate can induce osmotic stress and phosphorus starvation.

Dynamic sampling is difficult when measuring (p)ppGpp with HPLC-MS or TLC. The environment of a growing culture is constantly changing, and at any moment, cells might encounter a challenge that causes a spike in (p)ppGpp production.

Lastly, both methods provide useful information and can offer a quantitative measurement of (p)ppGpp detection, but that value represents the entire culture from which it is sampled.

Given the implications of heterogeneity on (p)ppGpp levels and its downstream effects, it would be highly valuable to gain single-cell insights into the variability of (p)ppGpp levels within a population. Overall, these limitations of the two methods reveal a gap in our understanding of the technology, preventing a full comprehension of the dynamic, biological, and variable nature of (p)ppGpp signaling.

1.5 Riboswitches

1.5.1 A primordial mode of gene regulation

Riboswitches are structured elements of noncoding RNA that bind metabolic ligands and regulate the expression of downstream genes in bacteria (152). The Breaker group identified a 5' untranslated sequence of mRNA in the *E. coli btuB* gene that can bind coenzyme B_{12} without protein assistance to regulate *btuB* expression, leading to the first discovery of a riboswitch (153). A riboswitch is typically located in the 5' untranslated region (UTR) of an mRNA, forming at least one ligand-binding aptamer domain that determines the expression platform. This platform contains an anti-terminator and a terminator that take different conformations depending on whether the ligand is present or absent. Alternative folding of the expression platform, driven by ligand binding to the aptamer, is used to regulate transcription, translation, or other gene expression processes (154, 155). Riboswitches are considered one of the oldest gene regulation mechanisms, existing in ancient organisms before the evolution and emergence of proteins (156–158).

Since their discovery in 2002, and with the help of improved bioinformatic analysis, the number of identified riboswitches has increased rapidly. Over 55 riboswitch classes, each defined by unique ligands, have been identified (159). Riboswitch experts believe that even more riboswitch classes are hidden within bacterial and eukaryotic genomes, waiting to be discovered

(160). Riboswitches are classified by the natural ligand they bind, and their type and subtype are based on differences in aptamer structure related to the same ligand (152). Some known riboswitch classes bind *S*-adenosyl methionine (SAM), Mn^{2+}, PRPP, c-di-GMP, and c-di-AMP, and these ligands often control the expression of metabolic pathways involved in ligand use or metabolism (159). Riboswitch gene regulation offers a valuable tool for researchers to easily detect ligand availability *in vivo* by placing these RNAs upstream of reporter genes, such as fluorescent proteins and β-galactosidase (161–163).

1.5.2 *ykkC* riboswitches

One of the most diverse groups of riboswitches is the *ykkC* class (164). Different *ykkC* riboswitch subclasses bind PRPP (165), guanidine (166), (deoxy)cytidine or adenosine diphosphate ((d)CDP/ADP) (167), and (p)ppGpp (168), which will be explained in more detail in 1.5.3. These subclasses share high sequence and structural similarity, making them difficult to distinguish and dependent on the genetic context.

The primary subtype of *ykkC* riboswitches, subtype 1, is guanidine-binding (166). However, during the initial study of these riboswitches, researchers found that certain *ykkC* motif RNAs (subtype 2) had specific mutations at nucleotide positions within the ligand-binding pocket, which were confirmed by structural studies (169). This subtype 2 classification can be further divided into 2a through 2d, based on the ligand it binds (164).

1.5.3 Discovery of (p)ppGpp binding riboswitches

When further characterizing *ykkC* subtype 2a riboswitches, Sherlock *et al.* noted that these riboswitches do not bind guanidine, unlike subtype 1, and are often located upstream of branched-chain amino acid (BCAA) biosynthetic genes (168). Because of this genetic context,

(p)ppGpp became a candidate ligand. After extensive bioinformatic analysis and *in vitro* testing, the first class of (p)ppGpp-binding riboswitches was discovered and validated (Figure 1.7A, B).

Sherlock *et al.* investigated a putative (p)ppGpp riboswitch in *the Desulfitobacterium hafniense* genome upstream of the *ilvE* operon ((168), Fig. 4). They reconstituted this riboswitch into an *in vitro* expression system. They monitored transcription in the presence of various concentrations of ppGpp. They found that when there was little to no ppGpp, the predominant transcript formed was a truncated transcript, likely due to termination. However, when the ppGpp concentration was high, the primary transcript was the full-length product (Figure 1.7C). From this, the researchers concluded that the *D. hafniense ilvE* riboswitch functions as a transcriptional terminator when ppGpp is not bound, allowing transcription to continue when the ligand is bound.

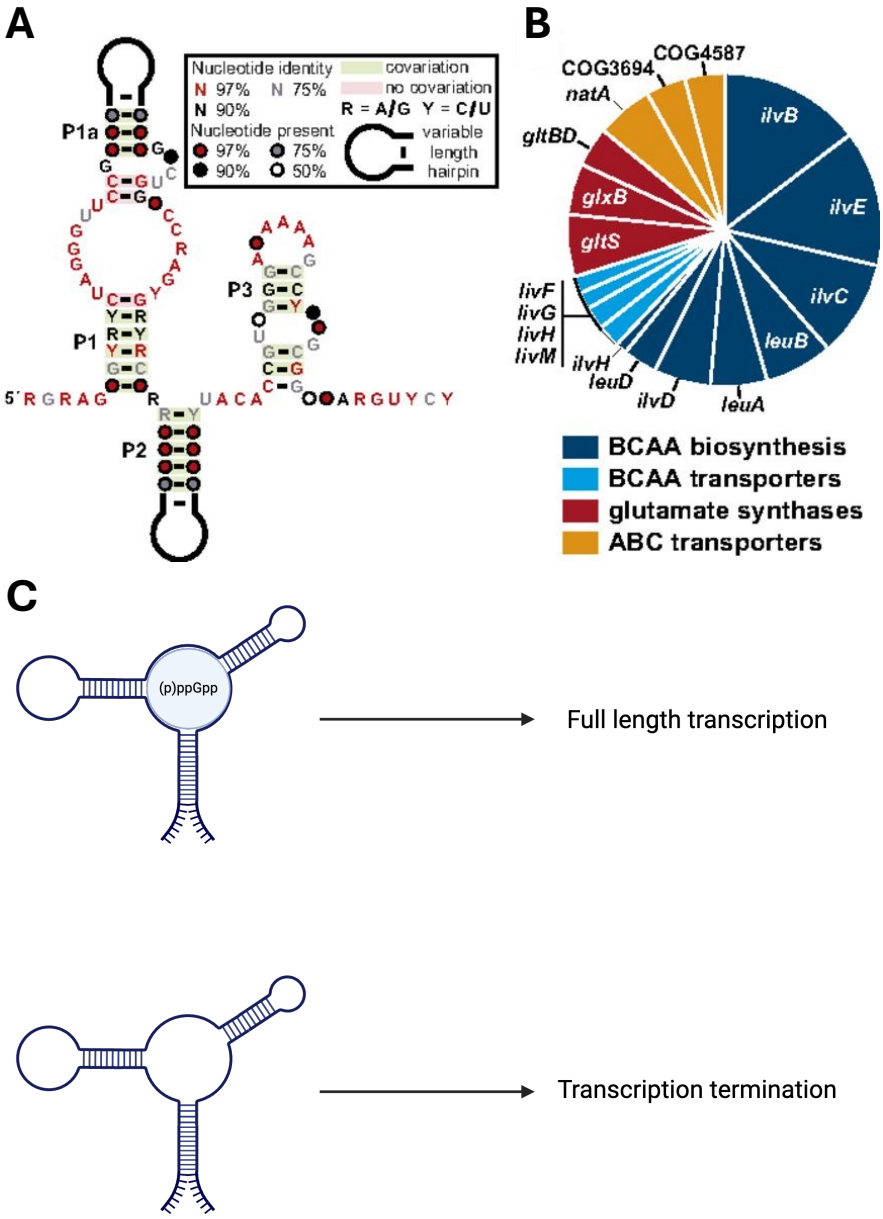

Figure 1.7 Discovery of a new class of (p)ppGpp binding riboswitches.
A) Consensus sequence of *ykkC* subtype 2a (p)ppGpp binding riboswitches, adapted from Sherlock *et al.* (2018). B) Genes predicted to be regulated by (p)ppGpp riboswitches, adapted from Sherlock *et al.* (2018). C) (p)ppGpp binding allows for downstream *D. hafniense ilvE* gene transcription, while little to no (p)ppGpp binding results in premature transcription termination.

Jagodnik *et al.* further examined these (p)ppGpp riboswitches and explored how they bind differently to pppGpp and ppGpp (170). In this study, they identified (p)ppGpp riboswitches that

attach to the penta- or tetraphosphate molecule in various ways. For example, the *Clostridiales bacterium natA* aptamer prefers pppGpp about 10 times more than ppGpp, while the *Oxobacter pfennigii livK* aptamer favors ppGpp roughly 6 times more than pppGpp. The *D. hafniense ilvE* riboswitch binds strongly to both pppGpp and ppGpp.

Taken together, these findings demonstrate the potential use of the *D. hafniense ilvE* riboswitch for research in (p)ppGpp detection. Hypothetically, there is no downstream reporter gene expression at low cellular (p)ppGpp levels, while reporter expression occurs when (p)ppGpp levels are elevated. Using this regulatory unit upstream of a reporter gene offers a new solution to the long-standing challenge of detecting (p)ppGpp. Other researchers are already exploring this approach (171). A riboswitch-based (p)ppGpp detection system allows for the rapid, sensitive, and comprehensive detection of the alarmone at both single-cell and population levels under natural growth conditions—without triggering a complete stringent response through acute starvation methods. This riboswitch-based (p)ppGpp detection method is the primary focus of this thesis. It will be further characterized, validated, and used in the upcoming chapters.

1.6 Scope of this thesis

In this thesis, I present a novel solution for detecting (p)ppGpp in bacteria and utilize this tool to characterize (p)ppGpp metabolism, triggers, heterogeneity, and physiological effects. I describe the development of an inducible luminescent (p)ppGpp reporter, RsFluc, in *B. subtilis*. I then detail RsFluc validation and characterization, both *in vitro* and *in vivo*. I utilize RsFluc to examine (p)ppGpp metabolism through mutations affecting synthetase catalysis and allosteric activation. I analyze RsFluc activity in response to environmental conditions and correlate the signal with growth arrest and reduced protein synthesis. I introduce a single-cell fluorescent

(p)ppGpp reporter, RsGFP, in *B. subtilis*, and use it to conclude heterogeneity in (p)ppGpp levels and how variation at the single-cell level relates to specific physiologies. I measure RsGFP fluorescence throughout growth and discuss how environmental factors contribute to heterogeneity and signal differences between exponential and transition phases. I investigate heterogeneity in bacterial transcriptomes at high (p)ppGpp levels and correlate (p)ppGpp with a subpopulation identified via single-cell RNA sequencing (scRNA-seq). I explore the links between heterogeneity in (p)ppGpp and bacterial growth, as well as antibiotic tolerance. I also describe collaborative efforts to develop a method that labels cells for protein synthesis via OPP incorporation while providing their transcriptomic profile. I introduce a methodology for gaining transcriptomic insights in conjunction with protein synthesis measurements. I validate this method by analyzing a regulon identified within a high-protein synthesis cluster. Finally, I summarize and discuss these findings, suggesting future research directions to expand this work.

Chapter 2

2 Development of a novel luminescent *in vivo* (p)ppGpp reporter in *B. subtilis*

This chapter has been adapted from Hydorn *et al.* 2025 (172).

2.1 Design of an inducible, luminescent (p)ppGpp reporter

In designing a (p)ppGpp reporter for use in living *B. subtilis*, I aimed for a tool that is accessible for researchers, tunable to optimize different conditions, and dynamic—providing real-time measurement of fluctuations in (p)ppGpp levels throughout growth. A previously published reporter gene with demonstrated dynamic readout is firefly luciferase (139). Mirouze *et al.* demonstrated that when fused downstream of promoter sequences, firefly luciferase provides a novel reporter system with enhanced temporal dynamics, accurately reflecting changes in transcription during growth. For adjusting expression levels, I chose the IPTG-inducible promoter, $P_{hyperspank}$, because it allows tunability between conditions to optimize the signal-to-noise ratio of a luminescent reporter. I inserted a sequence corresponding to the (p)ppGpp-sensitive riboswitch from the promoter of *Desulfitobacterium hafniense ilvE* (168) between an inducible promoter ($P_{hyperspank}$) and the *luc* gene encoding firefly luciferase (RsFluc; Figure 2.1). This construct was integrated at the *sacA* locus, and luminescence measurements were performed during growth in S7/glucose defined medium supplemented with casamino acids (S7+CAA), unless otherwise specified, using a microplate reader.

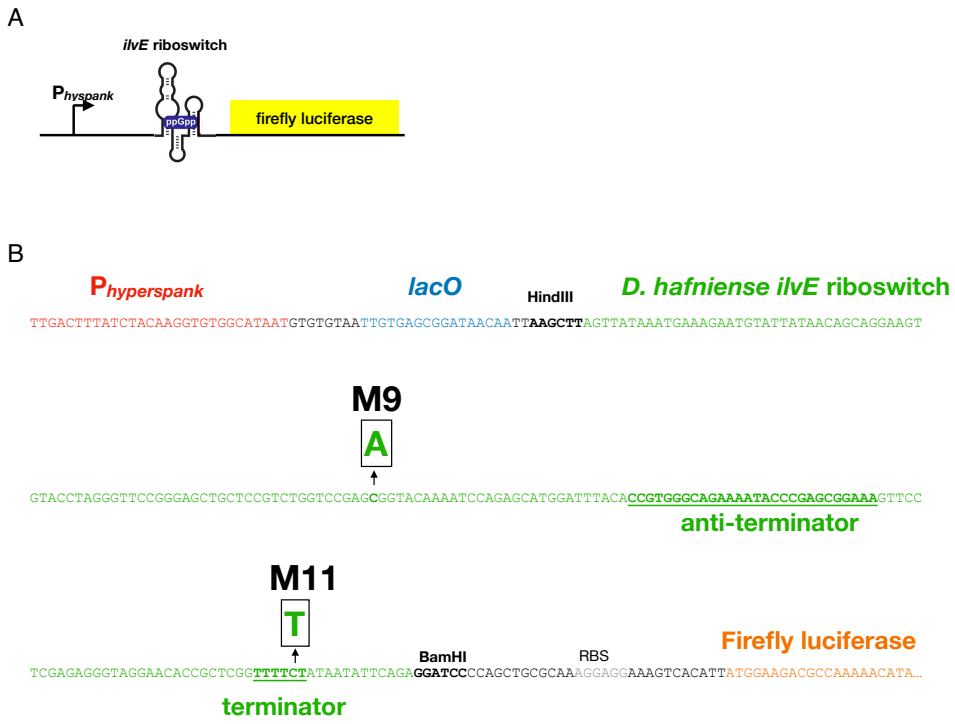

Figure 2.1 Luminescent (p)ppGpp reporter design in *B. subtilis*.
A) Schematic of the (p)ppGpp reporter RsFluc depicting the inducible promoter $P_{hyperspank}$ fused to the (p)ppGpp-sensitive riboswitch of *D. hafniense ilvE* followed by the gene encoding firefly luciferase. B) Shown is the $P_{hyperspank}$ promoter sequence (red), the *lac* operator binding sequence (blue), and the *D. hafniense ilvE* riboswitch gBlock sequence (green), with anti-terminator and terminator sequences bolded and underlined, and the M9 and M11 mutations from Sherlock *et al*. 2018 annotated. In gray, the Shine-Dalgarno ribosome binding sequence (RBS). In orange, the 5' end of the firefly luciferase gene. Restriction enzymes HindIII and BamHI sites are bolded.

Raw luminescence readings were normalized to OD_{600} (RLU/OD) (Figure 2.2, blue). I observed two waves of luminescence: one immediately after the start of growth and a second, larger one during the early transition phase, near the point when the growth rate slows down. Although the timing and size of the second wave (~220 min) were consistent across many biological replicates, the first wave was significantly more variable, possibly due to the proximity to the culture dilution performed at the experiment's start. Both waves depended on the presence of the riboswitch in the reporter construct, as a reporter ($RsFluc^0$) lacking the intervening riboswitch sequence showed significantly reduced luminescence (Figure 2.3A). The

remaining response suggests that (p)ppGpp might also stimulate transcription initiation from $P_{hyperspank}$.

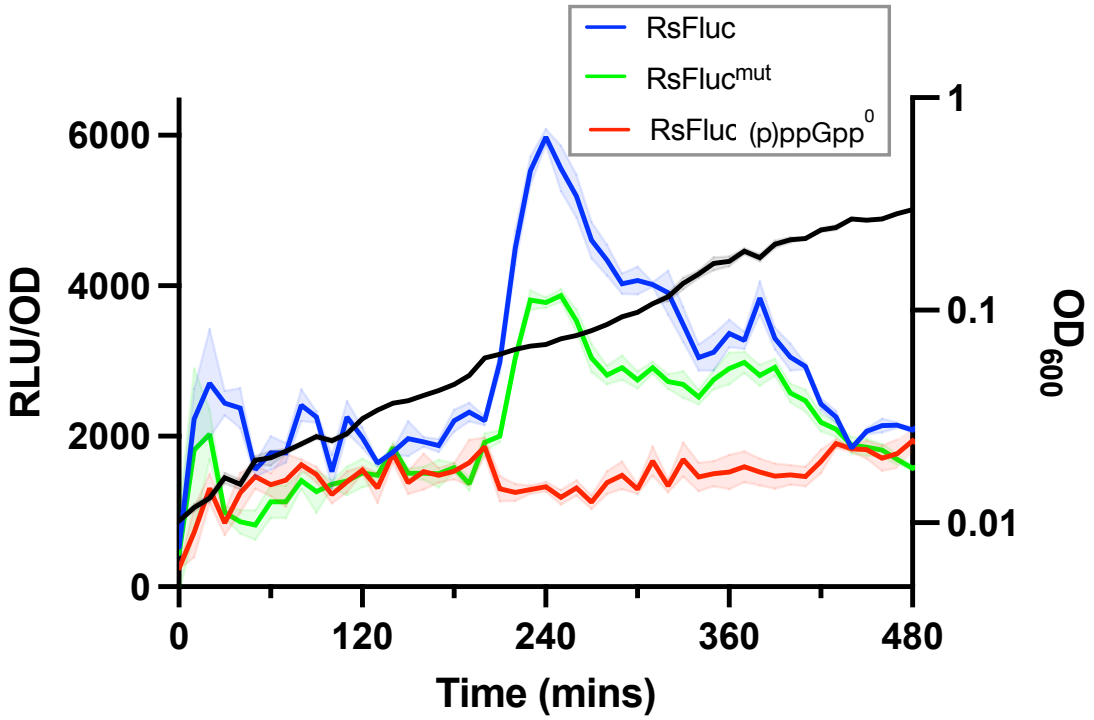

Figure 2.2 RsFluc (p)ppGpp reporter luminescence throughout growth. Luminescence (RLU/OD_{600}) of RsFluc (blue; JDB4496) and mutant $RsFluc^{mut}$ (green; JDB4631) in wildtype backgrounds and RsFluc in a Δ*relA*Δ*sasA*Δ*sasB* background (red; JDB4512). Growth (OD600) of RsFluc in wildtype background (black; JDB4496). Representative replicate in technical triplicate.

An RsFluc-expressing strain with deletions in the genes encoding all three *B. subtilis* (p)ppGpp synthetases (*relA*, *sasA*, *sasB*; $(p)ppGpp^0$) showed significantly reduced luminescence (Figure 2.2, red), aligning with the expectation that the signal reflects (p)ppGpp levels. Additionally, I built mutant RsFluc reporters incorporating two previously characterized riboswitch mutations (168): one that reduces sensitivity to (p)ppGpp by disrupting the binding pocket (M9, Figure 2.1B), and another that enhances termination (M11, Figure 2.1B), thereby increasing response specificity. Reporters with either mutation displayed lower luminescence (Figure 2.3B, C), and a reporter with both mutations ($RsFluc^{mut}$) was markedly diminished

(Figure 2.2, green). Since these mutations are not known to block (p)ppGpp binding entirely, their effects are less severe than in a (p)ppGpp^0 mutant strain, which may lead to secondary physiological effects due to the absence of the signaling molecule, particularly in transcription and translation (65, 67).

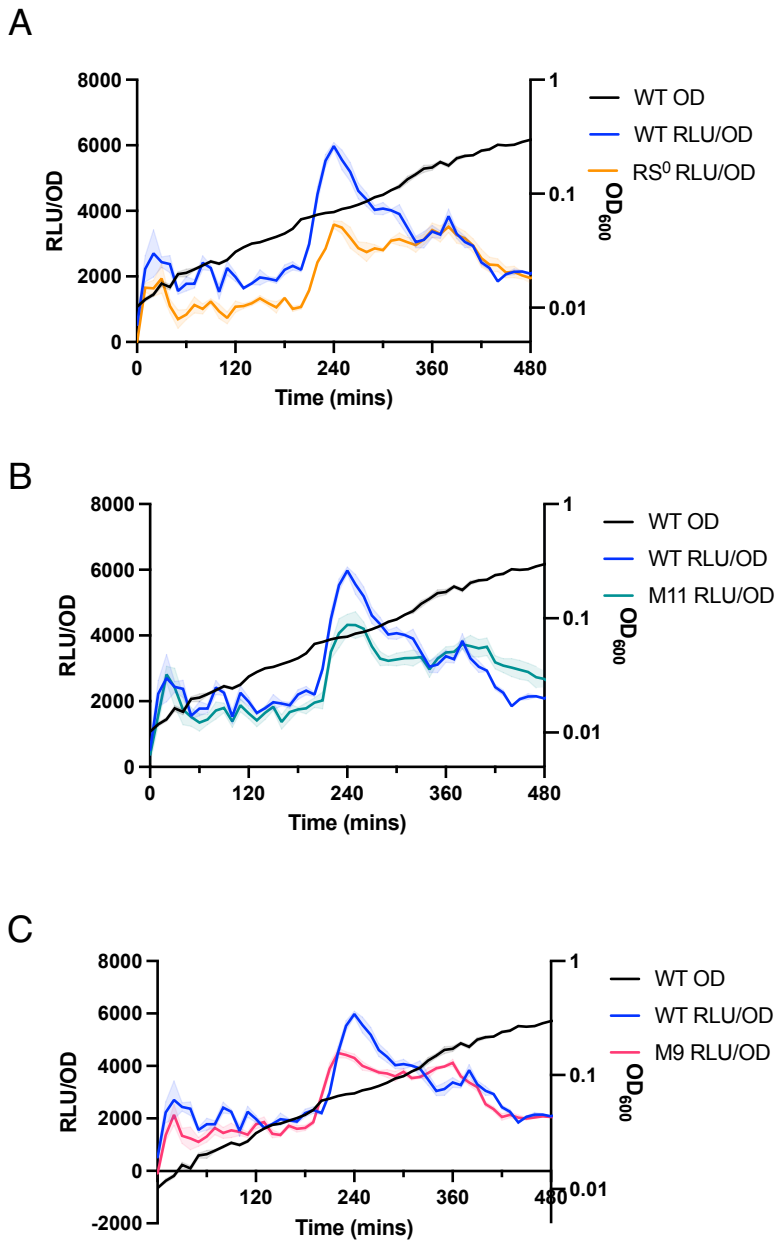

Figure 2.3 Luminescence activity of RsFluc reporter mutants.
Luminescence (RLU/OD_{600}) of: A) RsFluc (blue; JDB4496) and mutant RsFluc construct lacking a riboswitch sequence (orange, RS^0; JDB4524), B) RsFluc (blue) and M11 mutant RsFluc (green; JDB4522), and C) RsFluc (blue) and M9 mutant RsFluc (pink; JDB4599). Growth of RsFluc (OD_{600}) (black). Representative replicates in technical triplicates.

(p)ppGpp collectively refers to ppGpp and pppGpp. The *D. hafniense ilvE* riboswitch shows no preference in vitro for binding either pppGpp or ppGpp (170), indicating that RsFluc is

equally sensitive to both molecules *in vivo*. Aptamers with a preference for pppGpp or ppGpp have been identified (170). For example, the *Clostridiales bacterium natA* aptamer exhibits about a 10-fold preference for pppGpp compared to ppGpp, while the *Oxobacter pfennigii livK* aptamer shows roughly a 6-fold preference for ppGpp (170). I generated versions of the RsFluc reporter containing these aptamers instead of *D. hafniense ilvE*, named RsFluc^{natA} and RsFluc^{livK}, respectively. The similarity between RsFluc and the ppGpp-sensitive reporter RsFluc^{livK} (Figure 2.4, purple) aligns with previous findings that ppGpp levels are greater than those of pppGpp (173). Additionally, the pppGpp-sensitive reporter RsFluc^{natA} displayed a delayed expression compared to the other reporters (Figure 2.4, cyan).

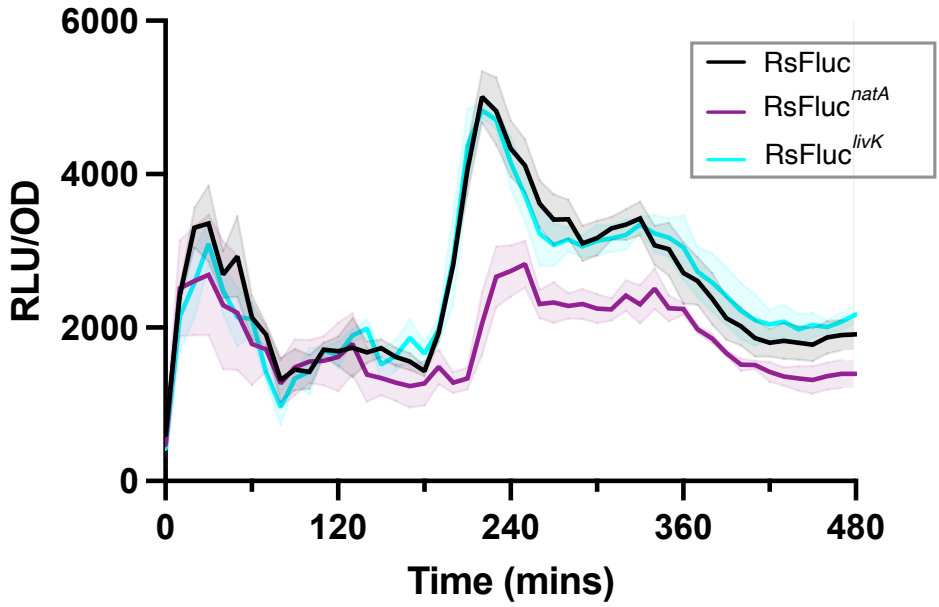

Figure 2.4 Luminescence of (p)ppGpp, pppGpp, and ppGpp RsFluc reporters. Luminescence (RLU/OD_{600}) of RsFluc (black; JDB4496), RsFluc^{natA} (purple; JDB4730), and RsFluc^{livK} (cyan; JDB4731). Representative replicate in technical triplicates.

2.2 Biochemical validation of (p)ppGpp reporter

To further confirm that (p)ppGpp luminescence activity was due to changes in (p)ppGpp levels, we measured (p)ppGpp using HPLC-MS at different points in the growth curve with

varying RsFluc activities. We selected early growth stages with low luminescence, the period of peak luminescence, and after the luminescence declined. This work was conducted in collaboration with Elizabeth Fones and Carrie Harwood. Values were normalized to OD_{600} and to a parallel measurement in a (p)ppGpp^0 strain, showing lower (p)ppGpp levels before and after the peak (Figure 2.5). The corrected luminescence data closely matched actual (p)ppGpp concentrations across sampling times, indicating that our (p)ppGpp reporter was both dynamic and accurate.

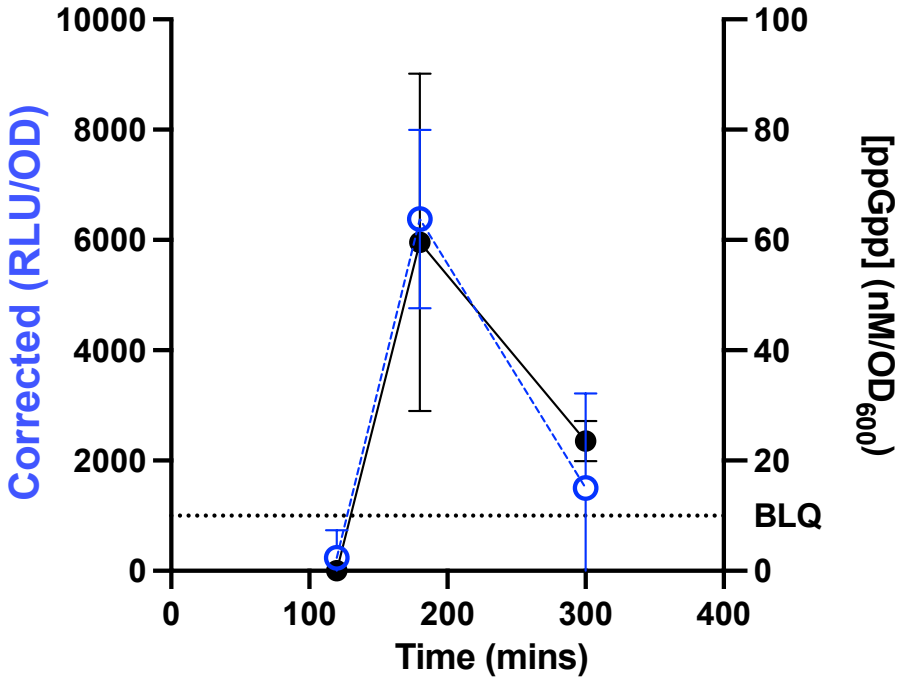

Figure 2.5 (p)ppGpp reporter luminescence reflects cellular ppGpp concentration. ppGpp concentration determined by HPLC-MS (black closed circles) and corresponding reporter (JDB4496) luminescence corrected for (p)ppGpp^0 (JDB4512) luminescence by subtraction (blue open circles). HPLC-MS experiments conducted by Elizabeth Fones under the support of Carrie Harwood. Representative replicate in technical triplicate.

Calculation of the absolute concentration of (p)ppGpp yielded an estimate of approximately 60 nM/OD_{600} (Figure 2.6A). Notably, we observed only modest declines in GTP in the wild-type strain (Figure 2.6B). During the spike in luminescence, ppGpp accounted for approximately 20%

of the guanosine nucleotide pool (Figure 2.6C). The HPLC-MS data indicated that ATP levels remained relatively constant throughout the sampling time points (Figure 2.6D).

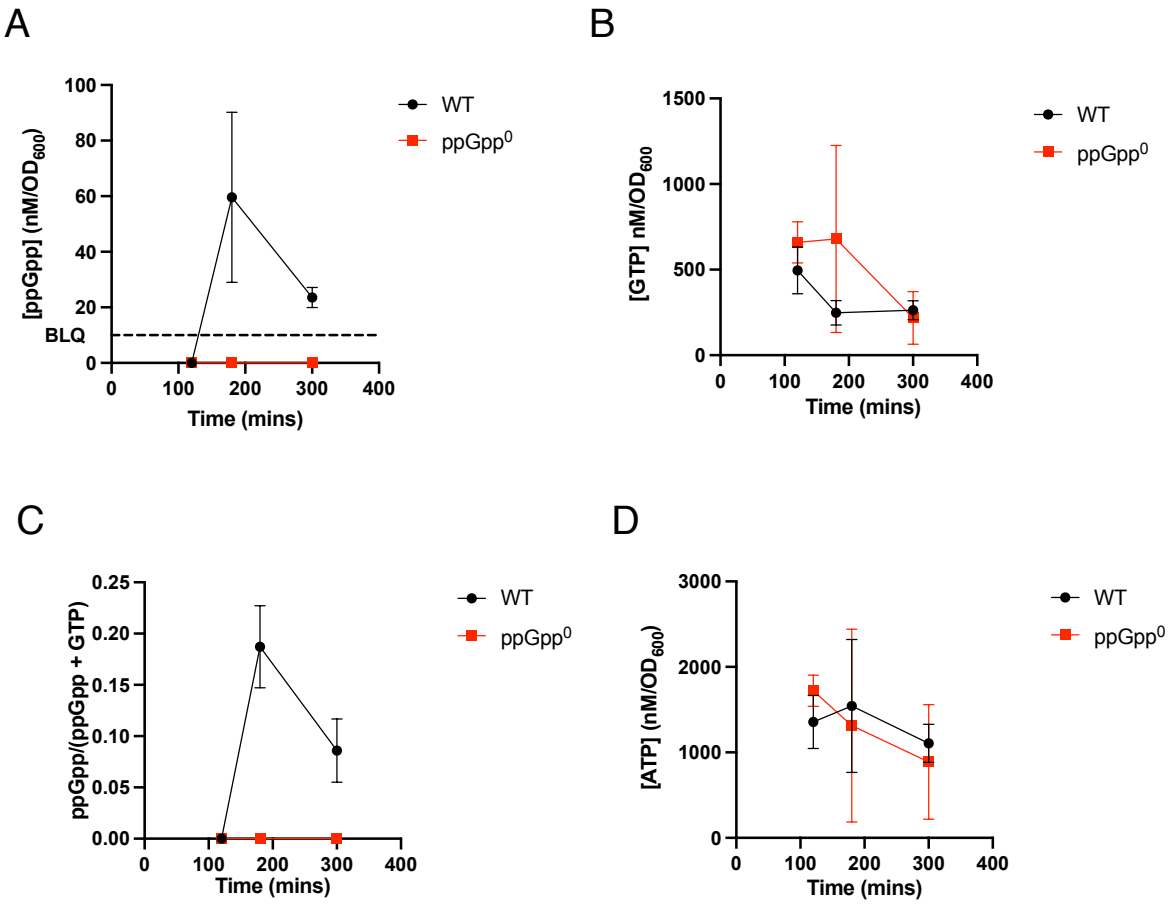

Figure 2.6 HPLC-MS quantification of nucleotide levels sampled during growth. Nucleotide quantifications in the WT (black, JDB4496) and a (p)ppGpp^0 background (red, JDB4512) of A) ppGpp, B) GTP, C) guanosine pools, and D) ATP, as analyzed via HPLC-MS collected at specified intervals. HPLC-MS experiments conducted by Elizabeth Fones under the support of Carrie Harwood. Representative replicate done in technical triplicates.

2.3 Physiological validation of (p)ppGpp reporter

2.3.1 Changes in luminescence levels reflect changes in reporter transcription

The RsFluc reporter depends on protein synthesis because luciferase is a protein reporter, and (p)ppGpp inhibits translation by binding (71). To confirm that changes in (p)ppGpp reporter luminescence truly reflect alterations in the full-length transcription of the firefly luciferase gene,

I used fluorescent *in situ* hybridization (FISH) microscopy with fluorescent probes that bind to mRNA inside the cell. The FISH probes were designed to hybridize to *yfp* mRNA, which was engineered downstream of $P_{hyperspank}$ and *D. hafniense ilvE* riboswitch at the *amyE* locus in the RsFluc background strain. I verified that the RsFluc reporter signal correlates with changes in transcriptional readthrough using FISH (Figure 2.7). About 10 minutes after the increase in reporter transcription observed at TP3 (Figure 2.7B), RsFluc luminescence peaks (Figure 2.7A). The transcription of the reporter then returns to baseline levels in subsequent time points (Figure 2.7B), and the RsFluc signal diminishes similarly (Figure 2.7A).

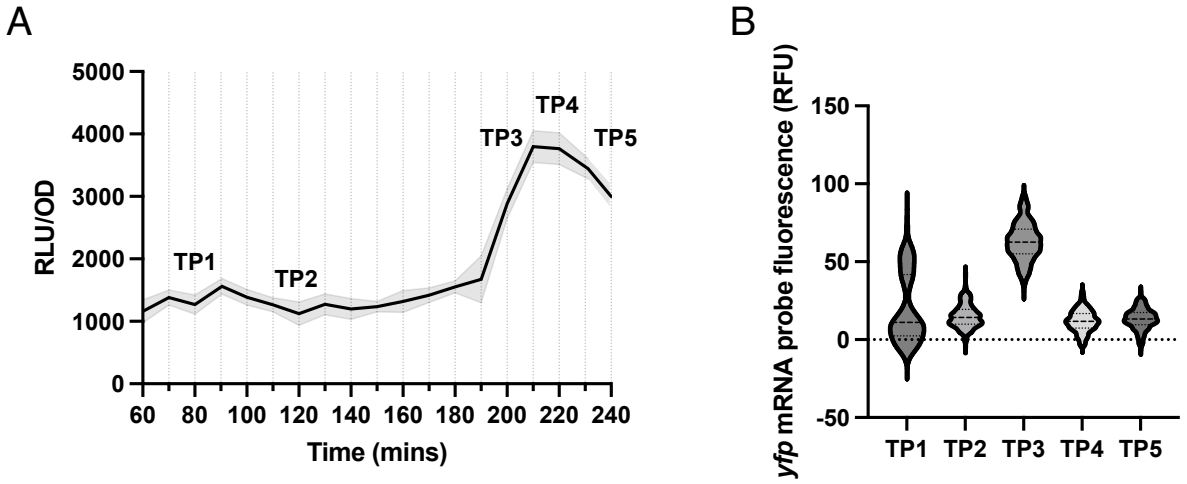

Figure 2.7 RsFluc transcriptional activity assayed by FISH.
A) Samples of a strain carrying both RSFluc and *ilvE-riboswitch*-YFP reporters (JDB4623) were collected and analyzed via FISH at specified time points (TP1-TP5: TP1 = 80, TP2 = 120, TP3 = 200, TP4 = 220, and TP5 = 240 mins) throughout the luminescence curve (RLU/OD_{600}) and imaged via fluorescent microscopy. B) The population distribution of single cell fluorescence at each time point (TP1, n = 202; TP2, n = 333; TP3, n = 481; TP4, n = 315; TP5, n = 197).

2.3.2 Reporter responds to acute amino acid starvation

I characterized how perturbations that stimulate *in vivo* (p)ppGpp synthesis affect RsFluc activity. Since uncharged tRNAs activate RelA-dependent (p)ppGpp synthesis (10), many such perturbations influence aminoacyl-tRNA charging. For example, a culture grown in amino acid-

rich medium that is shifted to a medium lacking amino acids exhibits decreased aminoacylation (174) that triggers (p)ppGpp synthesis (175). Consistently, a spike in RsFluc activity occurred shortly (~30 min) after the down-shift (Figure 2.8, black), and this response was reduced in a strain expressing the RsFluc^{mut} reporter (Figure 2.8, blue). The timing of this reaction highlights the temporal relationship between our reporter and (p)ppGpp levels. Amino acid starvation leads to a rapid decrease in tRNA charging (~5 min (176)) and an increase in ppGpp synthesis (~10-15 min (177)). The difference between these times and what I observe with RsFluc suggests that activation of the riboswitch and subsequent firefly luciferase expression occur in less than 20 minutes.

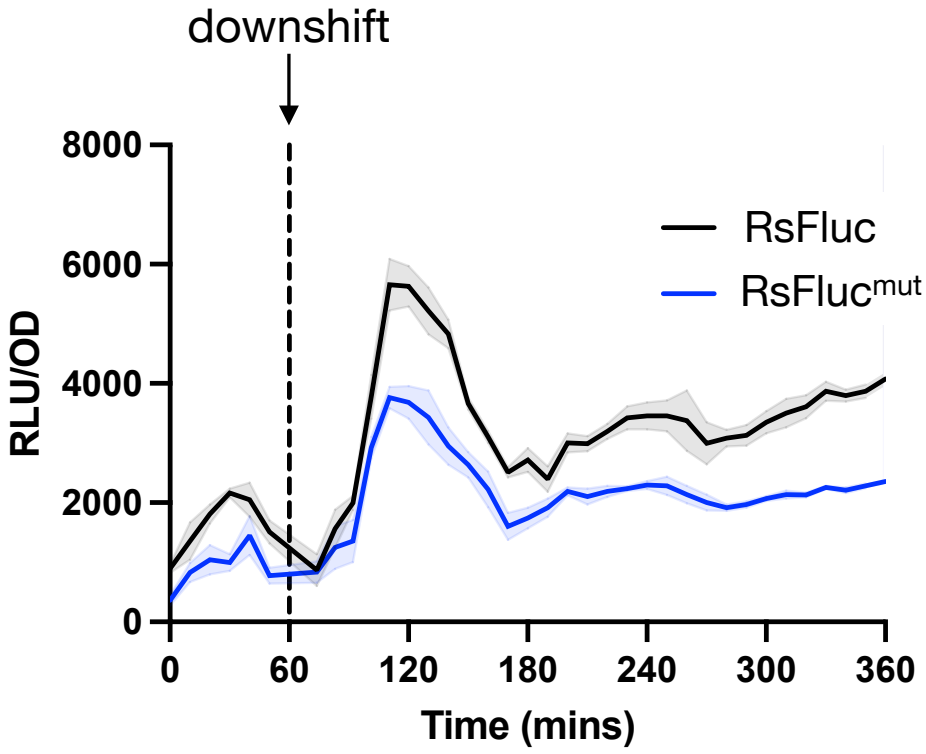

Figure 2.8 RsFluc reporter response to nutrient downshift.
Luminescence (RLU/OD_{600}) of RsFluc (black; JDB4496) and RsFluc^{mut} (blue; JDB4631) after amino acid downshift at T_{60} (dashed line). Representative replicate done in technical triplicate.

Inhibitors of tRNA synthetases offer an alternative means of controlling tRNA charging. For example, mupirocin, which inhibits isoleucyl-tRNA synthetase,(177) promotes (p)ppGpp synthesis (151). Consistently, cells expressing RsFluc treated with mupirocin showed a notable increase in luciferase production. This change was not observed in cells expressing the (p)ppGpp-insensitive RsFluc^{mut} reporter, indicating that the effect was specific to alterations in (p)ppGpp levFigure 2.9.

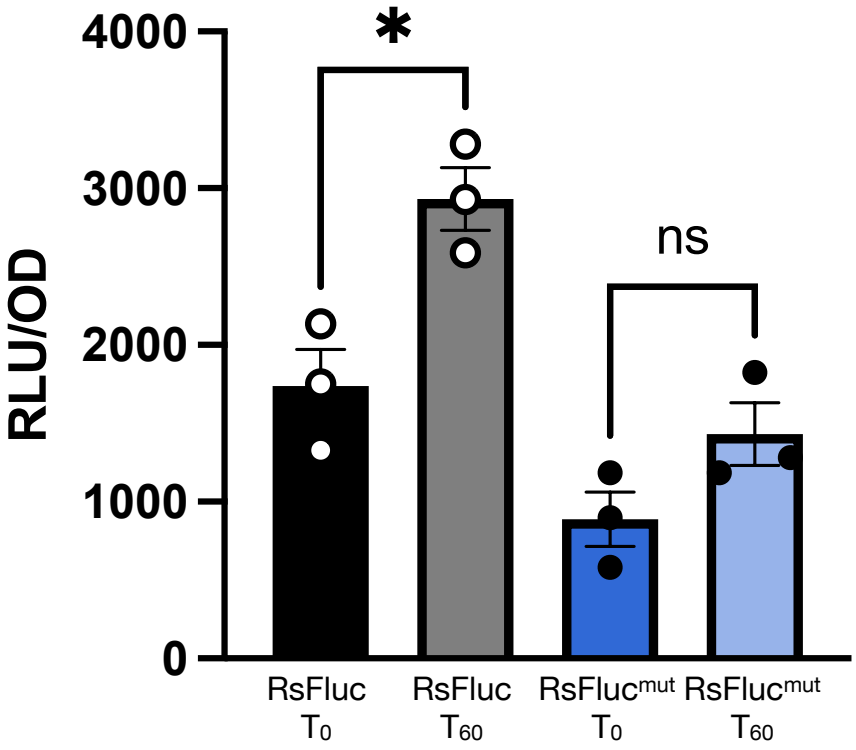

Figure 2.9 RsFluc response to mupirocin treatment.
Luminescence (RLU/OD_{600}) of RsFluc (black; JDB4496) and RsFluc^{mut} (blue; JDB4631) after 0 and 60 mins of 50 ng/mL mupirocin treatment. Significance was determined by a two-tailed t-test; p-value < 0.05 for RsFluc, with no significant difference for RsFluc^{mut}. Representative replicate done in technical triplicate.

I investigated the mupirocin concentration that causes the maximum stimulation of RsFluc activity, finding that 100 ng/ml was more effective than 50 ng/ml (Figure 2.10A). The significant reduction in growth with 100 ng/ml mupirocin (Figure 2.10B) indicates that at this concentration,

mupirocin likely exerts physiological effects beyond (p)ppGpp synthesis, such as directly inhibiting protein synthesis.

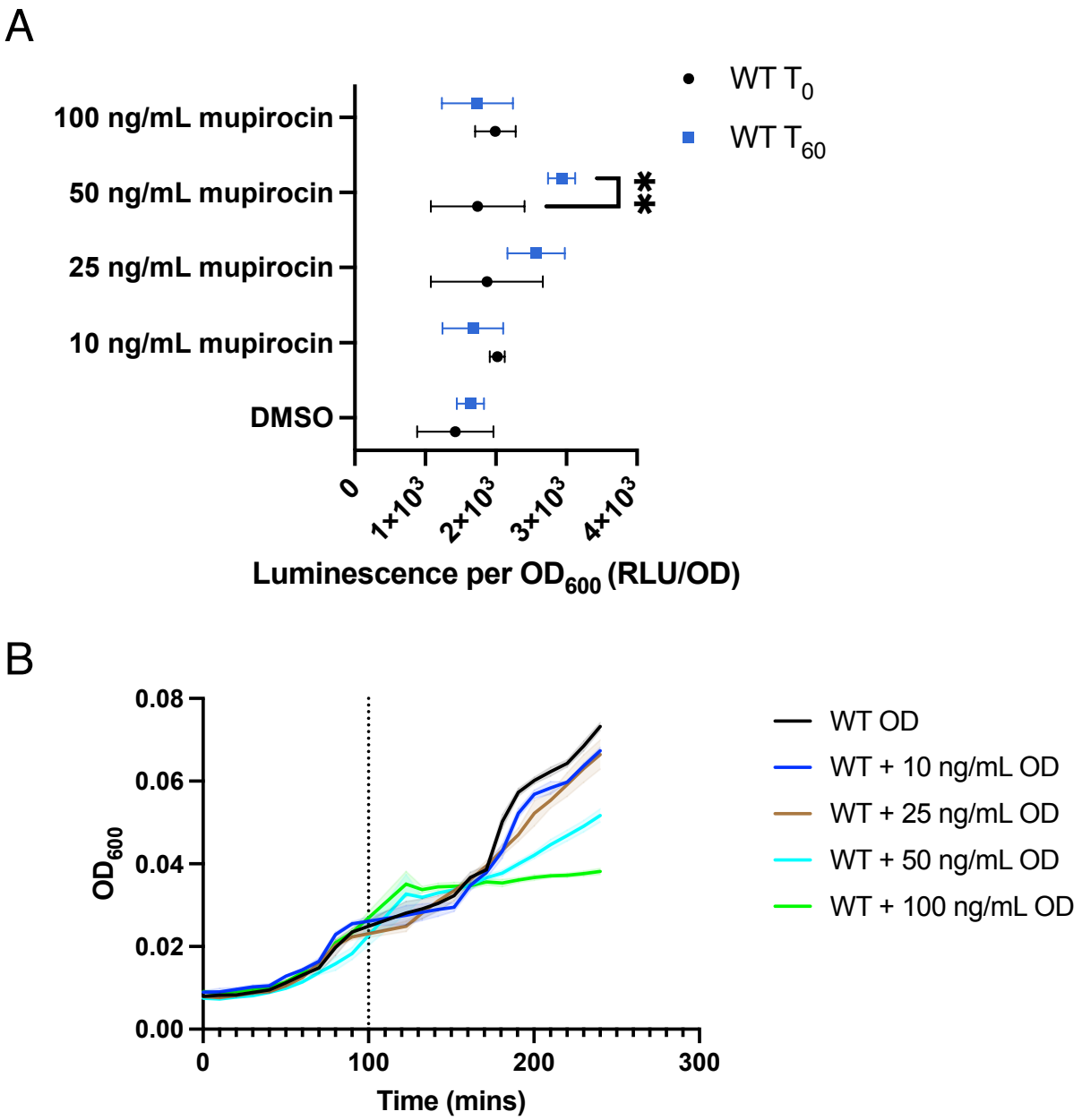

Figure 2.10 RsFluc response to mupirocin titration.
A) Luminescence (RLU/OD_{600}) of RsFluc (JDB4496) at start (T_0) of treatment (black) and after 60 mins of treatment, T_{60} (blue) with varying concentrations of mupirocin. Significance determined by two-way ANOVA with multiple comparison, comparing T_0 and T_{60} under each treatment. 50 ng/mL mupirocin (*) had a p-value of 0.0036 whereas other treatments were not significant. B) Growth (OD_{600}) of RsFluc before and after the time of mupirocin addition (dotted line) as treated with DMSO (black), 10 µg/mL (blue), 25 µg/mL (brown), 50 µg/mL (cyan), and 100 µg/mL (green) mupirocin. Representative replicate done in technical triplicates.

Both direct (^{32}P-radiolabeling) (178) and indirect (transcriptional profiling) (179) assays observe (p)ppGpp synthesis during a diauxic shift when bacteria adapt to grow on a secondary carbon source after glucose exhaustion. I measured RsFluc activity during a diauxic shift from glucose to arabinose as the sole carbon source (i.e., without amino acid supplementation), following a protocol (139) based on the original observations of Monod *and B. subtilis* (180). The transient flattening of the growth curve in the culture grown in 0.5 mg/ml glucose & 2.0 mg/ml arabinose is characteristic of a diauxic shift and is accompanied by a prominent spike in RsFluc activity at ~240 min, indicating a substantial increase in (p)ppGpp levels (Figure 2.11, blue). In contrast, growth in 2.5 mg/ml glucose (Figure 2.11, black) did not result in significant changes in either growth or luciferase activity.

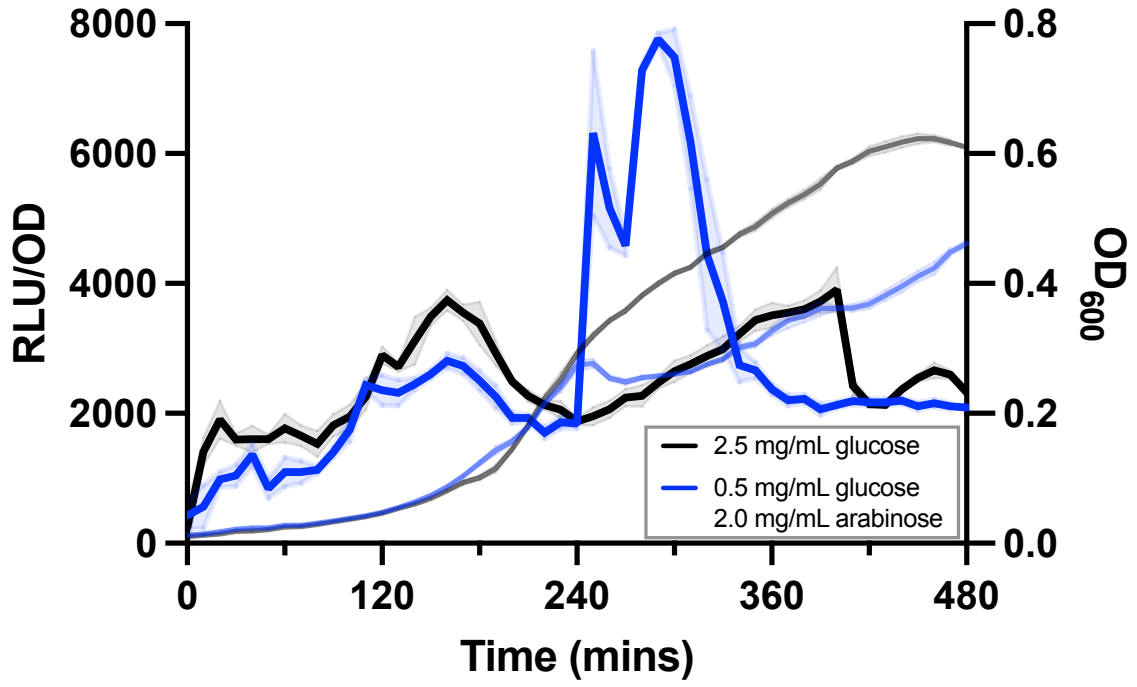

Figure 2.11 RsFluc response to diauxic shift.
Luminescence (RLU/OD_{600}) of RsFluc (JDB4496) grown in defined minimal media containing either 2.5 mg/mL of glucose (black) or 0.5 mg/mL glucose and 2.0 mg/mL arabinose (blue). Respective OD_{600} measurements are shown in grey and light blue, respectively. Representative replicate done in technical triplicate.

2.3.3 RsFluc signal attenuated by (p)ppGpp synthetase inhibitor

In addition to evaluating RsFluc response to (p)ppGpp induction, I examined how RsFluc reacts to (p)ppGpp inhibition. In personal communications with Frederico Gueiros-Filho, 2-aminoethoxydiphenyl borate (2APB) was identified as a potential (p)ppGpp synthetase inhibitor through high-throughput *in vitro* screening of compounds. I tested the effect of 2APB on the RsFluc signal. I cultured RsFluc with DMSO solvent and 2APB and observed that the RsFluc signal decreased when 2APB was added to the culture (Figure 2.12). This is consistent with the report by Gueiros-Filho, which indicates that 2APB inhibits (p)ppGpp synthetase.

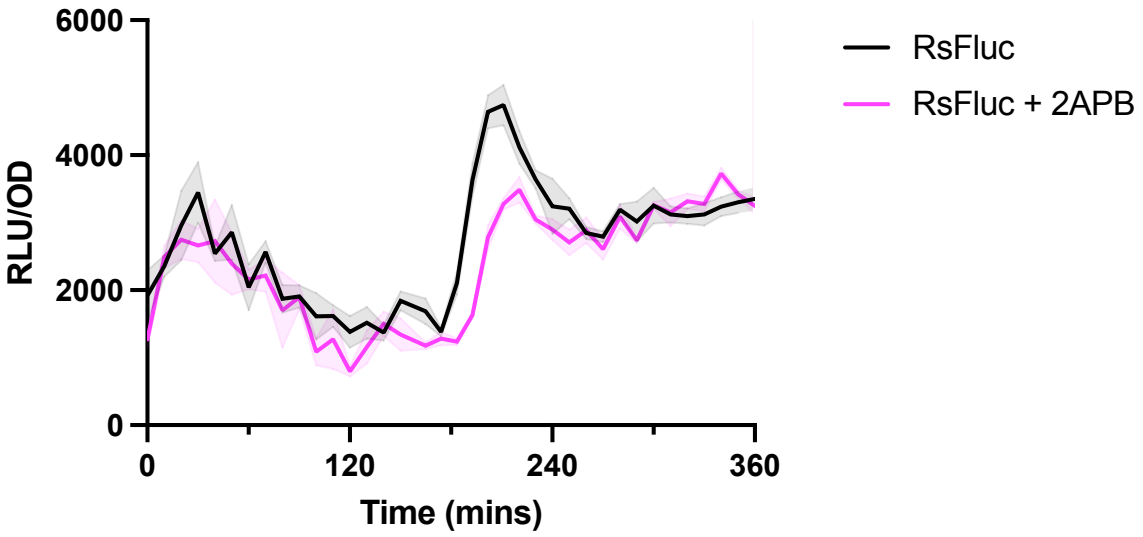

Figure 2.12 RsFluc response to 2APB.
Luminescence (RLU/OD_{600}) of RsFluc (black, JDB4496) and RsFluc + 40 µM 2APB (pink). Representative replicate done in technical triplicate.

2.3.4 Reporter coincides with known (p)ppGpp-dependent transcriptional pathways

To further confirm that RsFluc activity reflects (p)ppGpp levels, I measured the expression of a firefly luciferase fusion to the *purE* promoter, which is sensitive to (p)ppGpp concentrations (119), using strain construction with Sathya Nagarajan's assistance. Specifically, (p)ppGpp promotes PurR DNA binding, leading to increased repression of *purE* transcription.

Consistent with earlier findings (119), P_{purE}-luciferase activity was influenced by the absence of (p)ppGpp (Figure 2.13, compare orange and purple). I noted the lowest P_{purE}-luciferase activity (orange) around the same time RsFluc activity (black) rose (~180 min), with a subsequent increase in P_{purE} activity as RsFluc declined (Figure 2.13).

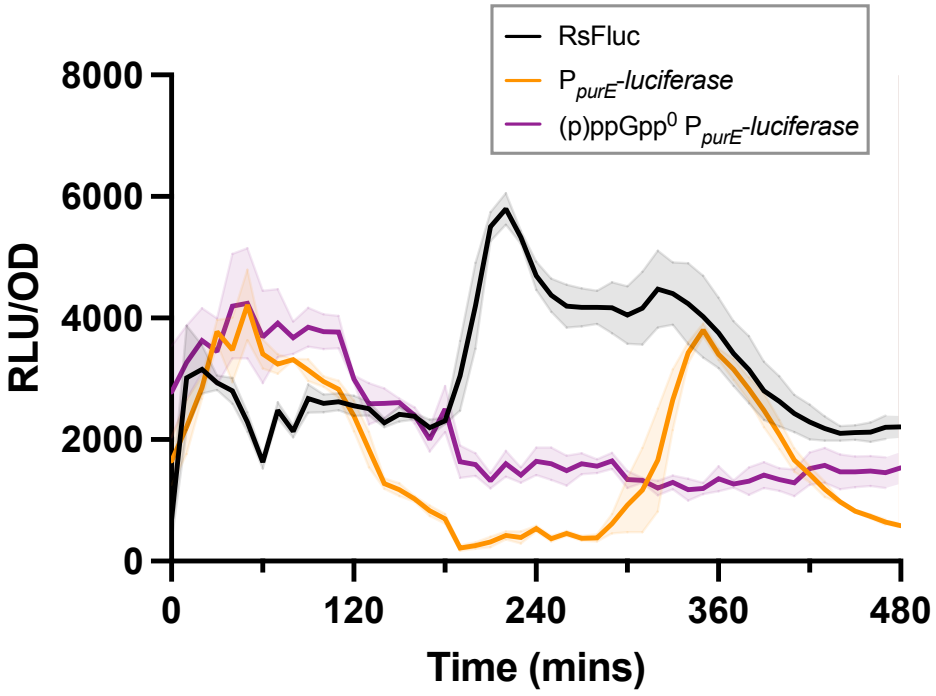

Figure 2.13 RsFluc activity coincides with known (p)ppGpp-dependent purine metabolism pathways.
Luminescence (RLU/OD_{600}) of RsFluc (black; JDB4496) and a P_{purE} luciferase promoter fusion in wildtype (orange; JDB4803) and (p)ppGpp^0 (purple; JDB4804) backgrounds. Representative replicate done in technical triplicate

2.4 Conclusions

I constructed and validated the RsFluc and RsFluc^{mut} reporters using both *in vitro* and *in vivo* assays. RsFluc^{mut} activity is not fully attenuated, which agrees with *in vitro* transcription data on individual M9 and M11 mutants ((168), Fig. 4). However, RsFluc^{mut} attenuation offers a control in a wild-type strain, unlike a (p)ppGpp^0 strain, which may show secondary effects due to the lack of synthetase activity (181). RsFluc accurately reflects nucleotide abundance as

measured by HPLC-MS, indicates changes in reporter transcription, responds to known (p)ppGpp inducers and inhibitors, and aligns with identified (p)ppGpp-dependent genetic pathways. Overall, these data support the conclusion that RsFluc activity reflects (p)ppGpp levels.

Chapter 3

3 Investigating (p)ppGpp metabolism and bacterial physiology in *B. subtilis* using a novel reporter

This work is adapted from Hydorn *et al.* 2025 (172). After validation and characterization, I employed RsFluc to investigate (p)ppGpp metabolic pathways. As discussed in 1.2, the metabolism of (p)ppGpp in *B. subtilis* has been well characterized through *in vitro* biochemical assays; however, the development of RsFluc enables *in vivo* exploration of metabolism with high temporal resolution. Additionally, I use RsFluc to study growth rate and protein synthesis by closely monitoring changes in (p)ppGpp levels and drawing conclusions about different physiological states at various points along the RsFluc curve.

3.1 Evaluating synthetase contributions to (p)ppGpp metabolism

3.1.1 Rel acts as the primary synthetase during natural growing conditions

I investigated the source of the (p)ppGpp responsible for the RsFluc signal during natural growth in S7+CAA medium. *B. subtilis* RelA, SasA (RelP), and SasB (RelQ) are the known (p)ppGpp biosynthetic enzymes (26, 182). Consistently, an RsFluc-expressing strain lacking all three proteins (Δ*relA*Δ*sasA*Δ*sasB*) shows significantly reduced luminescence compared to the wild-type parent (Figure 2.2). I examined the contributions of each protein to RsFluc activity by monitoring cells carrying single mutations in their respective genes during growth (Figure 3.1A; see Figure 3.1B for the corresponding growth curve). While all three mutations affected expression during growth, a strain lacking RelA synthetase activity due to an inactivating point mutation (D264G*)* in the synthetase domain (26) showed the most significant impact (blue, Figure 3.1A), nearly identical to the triple mutant Δ*relA*Δ*sasA*Δ*sasB* strain (red). In contrast,

single Δ*sasA* (green), Δ*sasB* (orange), or the combination Δ*sasA*Δ*sasB* (Figure 3.1C, brown) mutants displayed at most only modest delays in RsFluc signal.

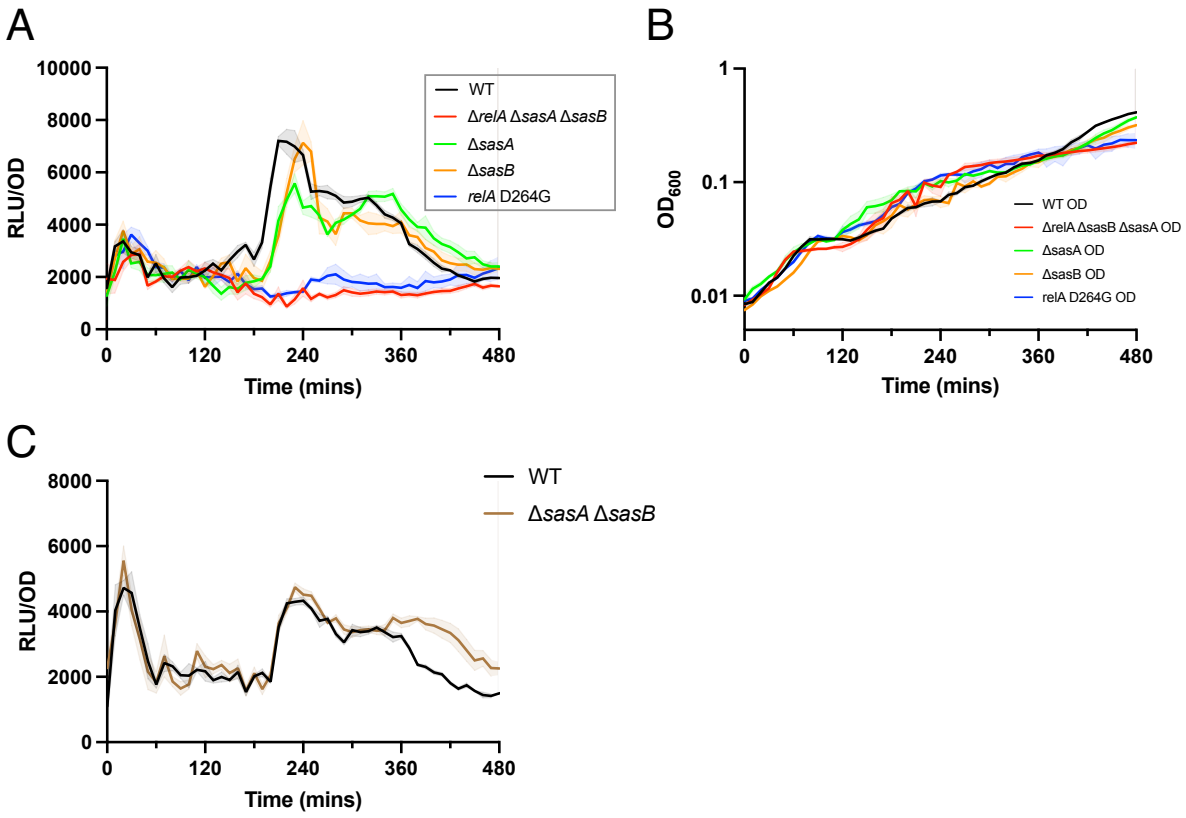

Figure 3.1 Relative contributions of (p)ppGpp synthetases to RsFluc activity during natural growth conditions.
Luminescence (RLU/OD_{600}) of A) RsFluc in wildtype (black; JDB4496), Δ*relA*Δ*sasA*Δ*sasB* (red; JDB4512), Δ*sasA* (green; JDB4515), Δ*sasB* (orange; JDB4516), and *relA-D264G* (blue; JDB4741), and C) Δ*sasA*Δ*sasB* (brown; JDB4511) backgrounds during growth in S7+CAA medium. B) Growth (OD_{600}) of RsFluc in wildtype (black), Δ*relA*Δ*sasA*Δ*sasB* (red), Δ*sasA* (green), Δ*sasB* (orange), and *relA-D264G* (blue) in S7+CAA medium. Representative replicate done in technical triplicate.

3.1.2 Rel and SasB allosteric activation are required to mount a full (p)ppGpp response

In vitro, both Rel (24) and SasB (30, 31) are allosterically activated by pppGpp, which is produced by Rel. SasB Phe-42 is a critical residue in this regulation, and a SasB mutant with an F42A substitution is no longer allosterically activated *in vitro* by pppGpp (30, 31). The RsFluc activity of a strain carrying a *chromosomal sasB-F42A* allele was delayed during growth (Figure

3.2A, blue; see B for the corresponding growth curve). Therefore, this delay results from the lack of SasB stimulation. Rel is also subject to allosteric regulation *in vitro* by pppGpp, with Tyr-200 being necessary for this effect (24). Introducing a Rel Y200A mutation into the chromosomal *rel* gene delayed the increase in RsFluc activity during growth compared to the wild-type parent strain (Figure 3.2A, purple; see B for the corresponding growth curve). Overall, these observations provide the first evidence of the *in vivo* role of allosteric regulation in (p)ppGpp metabolism during growth.

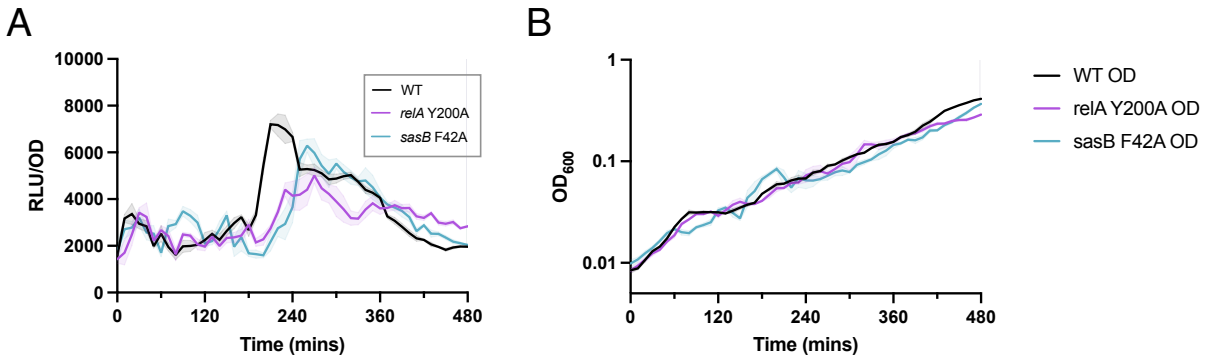

Figure 3.2 Allosteric activation of synthetases Rel and SasB necessary for full RsFluc activation.
A) Luminescence (RLU/OD_{600}) and B) growth (OD_{600}) of RsFluc in wildtype (black; JDB4496), *relA-Y200A* (purple; JDB4528), and *sasB-F42A* (blue; JDB4711) backgrounds in S7+CAA medium. Representative replicate done in technical triplicate.

3.1.3 Full synthetase activity necessary in response to acute starvation

I investigated the contributions of each protein to RsFluc activity by testing cells with single and combined mutations in synthetase genes during amino acid downshift, as described in Section 2.3.2. The (p)ppGpp^0 strain (Δ*relA*Δ*sasA*Δ*sasB*) cannot survive these conditions (101) and was therefore not included in these experiments. Individual Δ*sasA* and Δ*sasB* mutations caused delays in RsFluc activation after downshift (green, orange; Figure 3.3A, B). The *relA-D264G* strain was again severely affected, and under these conditions, the Δ*sasA*Δ*sasB* strain

was similarly impaired (blue, brown; Figure 3.3A, B), unlike during natural growth (Figure 3.1C).

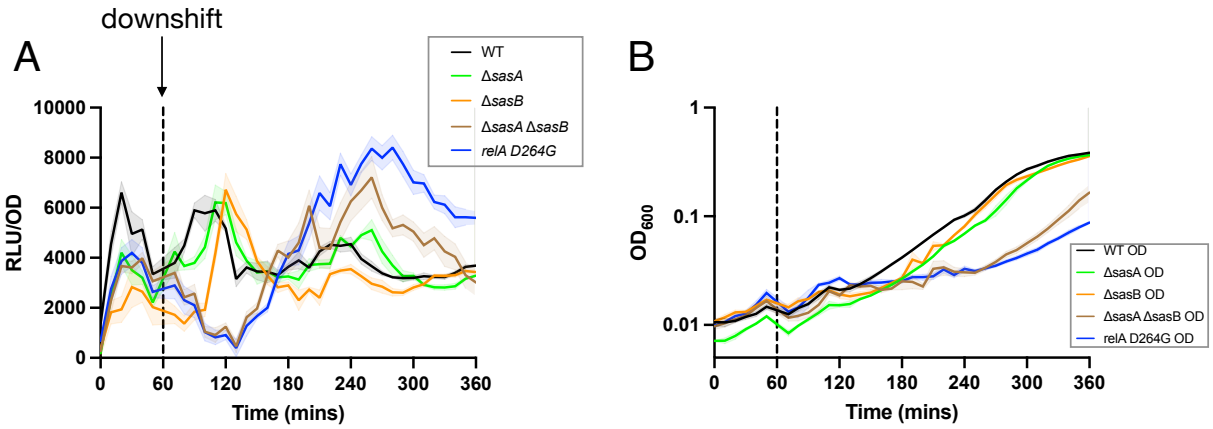

Figure 3.3 Contribution of (p)ppGpp synthetases to RsFluc acute amino acid starvation response.
A) Luminescence (RLU/OD_{600}) and B) growth (OD_{600}) of RsFluc in wildtype (black; JDB4496), Δ*sasA* (green; JDB4515), Δ*sasB* (orange; JDB4516), Δ*sasA*Δ*sasB* (brown; JDB4511), and *relA-D264G* (blue; JDB4741) backgrounds during amino acid downshift, indicated by the dashed line. Representative replicate in technical triplicate.

I also examined how allosteric activation of synthetase contributes to the rapid response to starvation by testing cells with single allosteric mutations in synthetase genes. Similar to what occurs during normal growth (Figure 3.2), mutations *relA-Y200A* and *sasB-F42A* both caused a delay in the RsFluc response to amino acid starvation (purple, blue; Figure 3.4A; see B for the growth curves). Interestingly, unlike during natural growth, RsFluc in the *relA-Y200A* background reaches full activation, albeit delayed, indicating that Rel does not require allosteric activation to produce a complete response during acute amino acid starvation. However, allosteric activation may still facilitate full activity during growth.

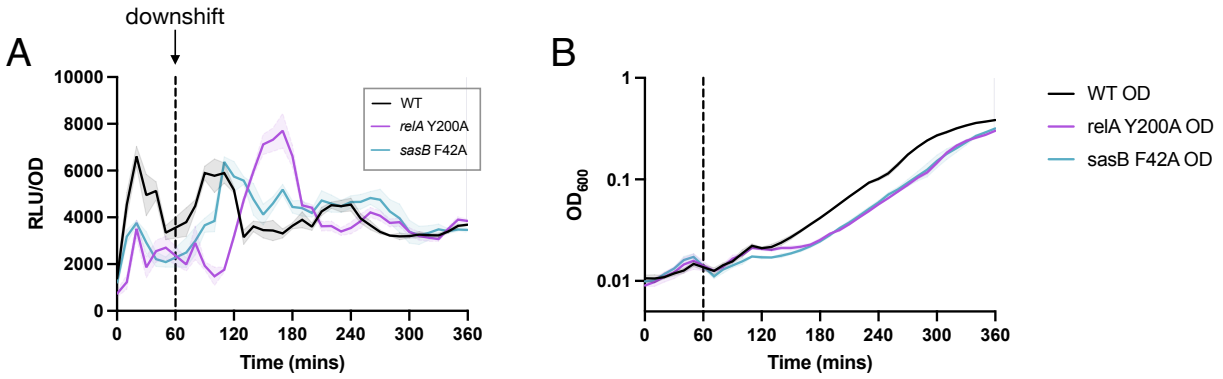

Figure 3.4 Contributions of allosteric activation of (p)ppGpp synthetases to RsFluc acute amino acid starvation response.
A) Luminescence (RLU/OD_{600}) and B) growth (OD_{600}) of RsFluc in wildtype (black; JDB4496), *relA-Y200A* (purple; JDB4528), and *sasB-F42A* (blue; JDB4711) backgrounds during amino acid downshift, indicated by the dashed line. Representative replicate done in technical triplicate.

3.2 Evaluating hydrolase contributions to (p)ppGpp metabolism

3.2.1 Rel hydrolase activity necessary to regulate (p)ppGpp synthesis and maintain cell viability

Regulation of RSH enzymes goes beyond directly affecting their biosynthetic activity, as many RSH enzymes, including Rel, also hydrolyze (p)ppGpp, indirectly opposing the synthetic process. Exploring the role of Rel-dependent (p)ppGpp hydrolysis in RsFluc expression is complex because of its essential role in the presence of any (p)ppGpp synthetases, including Rel itself (182). Inspired by a previous study (183), I developed a system that allows for the temporary expression of a mutant Rel protein lacking hydrolytic activity (D78A; (22)) controlled by the P_{liaI} bacitracin-inducible promoter (184) (Figure 3.5A). I first verified that expressing an inducible wild-type *relA* allele restored RsFluc activity in a (p)ppGpp^0 background (compare blue and gray; Figure 3.5B). Expression of the Rel-D78A mutant protein slowed growth (Figure 3.5C), consistent with increased (p)ppGpp levels, and caused a broadening of RsFluc activity peaks before and after those observed with wild-type Rel expression (Figure 3.5B, red).

Therefore, Rel hydrolase activity is essential for controlling the timing of (p)ppGpp production and keeping (p)ppGpp levels below those that are toxic to growth.

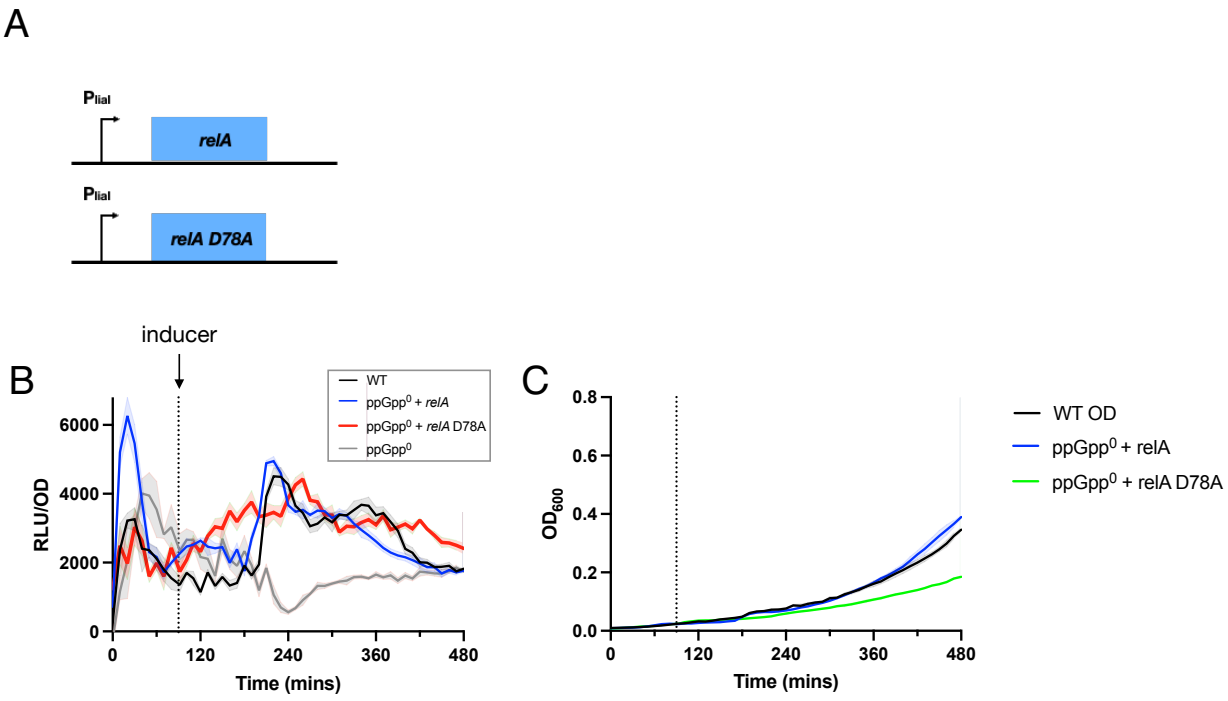

Figure 3.5 RelA hydrolase activity contributes to dynamics of RsFluc activity. A) Schematic of bacitracin-inducible *relA* constructs. B) Luminescence (RLU/OD_{600}) of RsFluc in wildtype (black, JDB4496), Δ*relA*Δ*sasA*Δ*sasB* with P_{lial}-*relA* (blue, JDB4675), Δ*relA*Δ*sasA*Δ*sasB* with P_{lial}-*relA-D78A* (red, JDB4676) and Δ*relA*Δ*sasA*Δ*sasB* (gray, JDB4512) strains. RelA expression induced by 5 µg/mL bacitracin at T_{90} (dashed line). C) Growth (OD_{600}) of RsFluc in wildtype (black), Δ*relA*Δ*sasA*Δ*sasB* with P_{lial}-*relA* (blue), and Δ*relA*Δ*sasA*Δ*sasB* with P_{lial}-*relA-D78A* (green) strain. RelA expression induced by 5 µg/mL bacitracin at T_{90} (dashed line). Representative replicate done in technical triplicate.

3.3 Assessing the role of nucleotide crosstalk in (p)ppGpp metabolism

3.3.1 Role of pGpp crosstalk in (p)ppGpp metabolism

As discussed in 1.2.3, pGpp is a smaller alarmone signaling nucleotide, previously thought to be another form of (p)ppGpp; however, recent studies on the target proteins of this molecule reveal that it may have distinct functions and should be regarded as a separate pathway (38, 39). pGpp has been shown to regulate the feedback mechanism of (p)ppGpp metabolism itself. It was

previously shown that when SasA was expressed in an otherwise (p)ppGpp^0 background, there was an accumulation of pGpp (39). However, this accumulation did not occur when cells were devoid of NahA through a Δ*nahA* mutation. This discovery later led to the identification of NahA as a pyrophosphohydrolase, which converts (p)ppGpp to pGpp by releasing a pyrophosphate or phosphate group (38). pGpp has since been shown to inhibit *B. subtilis* ppGpp synthetase SasB activity by competitively binding an allosteric site, which is stimulated by pppGpp binding (31). This introduces a negative feedback mechanism to control (p)ppGpp overaccumulation (Figure 1.5C).

To investigate how this feedback may influence RsFluc activity during natural growth in S7+CAA, I used an RsFluc assay in a strain with a single mutation in *nahA*, the gene encoding the NahA protein. Compared to the wildtype background, the Δ*nahA* mutation appeared to have little or no effect on RsFluc activity (Figure 3.6). Therefore, NahA's degradation of (p)ppGpp into pGpp does not significantly contribute to (p)ppGpp metabolism during natural growth in S7+CAA, in line with previous findings in LB (31).

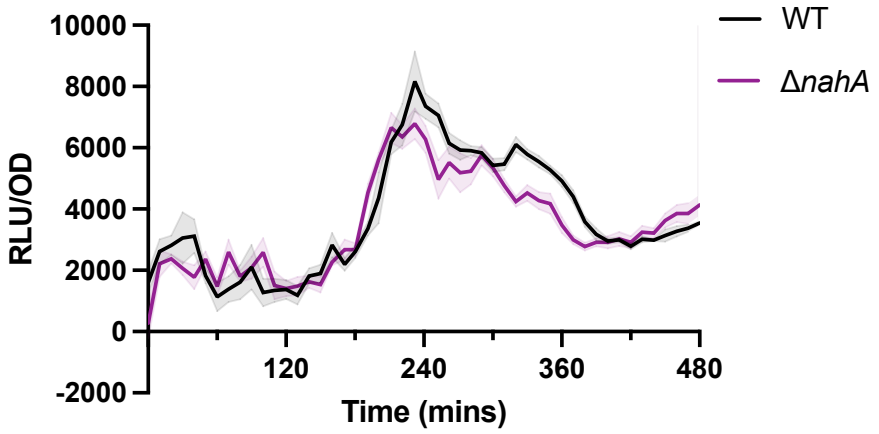

Figure 3.6 NahA contribution to RsFluc activity.
Luminescence (RLU/OD_{600}) of RsFluc in wildtype (black; JDB4496) and Δ*nahA* (purple; JDB4567) backgrounds. Representative replicate done in technical triplicate.

3.3.2 Role of c-di-AMP crosstalk in (p)ppGpp metabolism

As discussed in 1.2.3, crosstalk between c-di-AMP and (p)ppGpp occurs through allosteric regulation or, in some cases, direct inhibition of nucleotide metabolic enzymes. In *B. subtilis*, (p)ppGpp binds to c-di-AMP PDE to directly inhibit its breakdown, maintaining high c-di-AMP levels (59). Additionally, c-di-AMP has been shown to inhibit Rel activation via the c-di-AMP binding protein DarB (62). When DarB is in its apo form, it complexes with Rel to promote (p)ppGpp synthesis even without a stalled ribosome (Figure 1.5B). When c-di-AMP binds to DarB, the complex cannot form, resulting in no (p)ppGpp production.

To investigate if this crosstalk mechanism influences (p)ppGpp metabolism during natural growth in S7+CAA, I investigated RsFluc activity in a strain with a single mutation in *darB*, the gene encoding the DarB protein. Compared to a wild-type background, a Δ*darB* mutation appeared to have little to no effect on RsFluc activity (Figure 3.7). Therefore, DarB activity does not seem to significantly contribute to (p)ppGpp metabolism in *B. subtilis* during natural growth in S7+CAA.

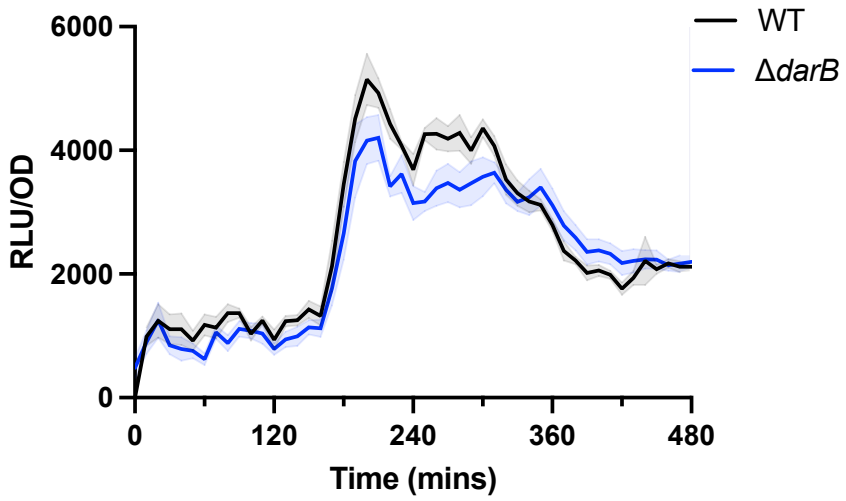

Figure 3.7 DarB contribution to RsFluc activity.
Luminescence (RLU/OD_{600}) of RsFluc in wildtype (black; JDB4496) and Δ*darB* (blue; JDB4568) backgrounds. Representative replicate done in technical triplicate.

3.4 Investigating (p)ppGpp production in variable environmental amino acid abundance

3.4.1 (p)ppGpp synthesized during amino acid starvation

The importance of Rel (p)ppGpp synthesis activity for RsFluc expression (Figure 3.1A) suggests that amino acid availability primarily drives (p)ppGpp production. To explore this idea, I examined how RsFluc activity relates to the levels of amino acids in the growth medium. Consistently, higher amounts of casamino acids (CAA) delay the peak of RsFluc activity (Figure 3.8A) without significantly impacting growth. When no amino acids are added, RsFluc activity drops notably, especially after exiting exponential growth (Figure 3.8B). This activity is higher than with the $RsFluc^{mut}$ (p)ppGpp-insensitive reporter (blue), indicating that it genuinely reflects (p)ppGpp levels.

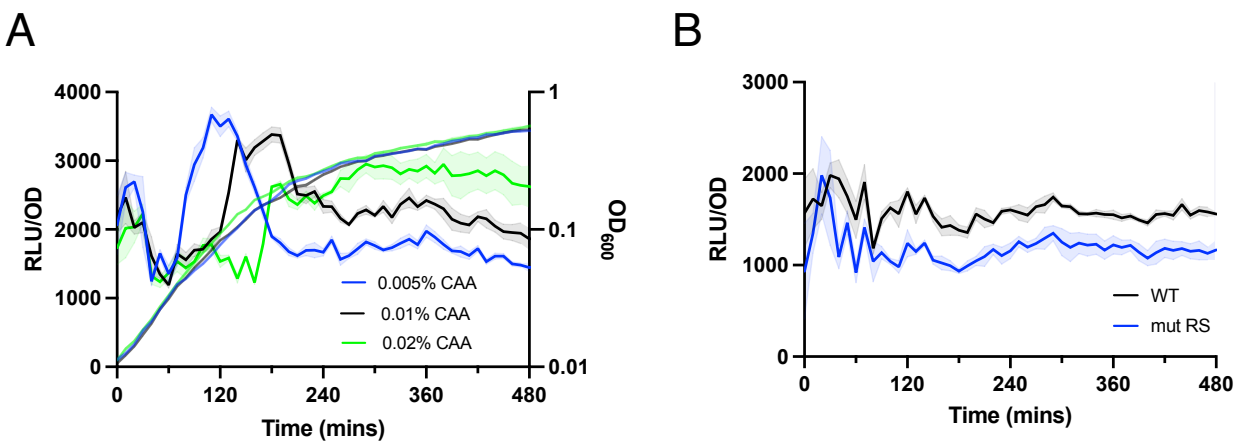

Figure 3.8 RsFluc activity and amino acid availability.
Luminescence (RLU/OD_{600}) of: A) RsFluc in prototroph (JDB4656) cultured in S7 supplemented with 0.005% (blue), 0.01% (black), and 0.02% (green) casamino acids, and B) RsFluc (black) and $RsFluc^{mut}$ (blue) in prototroph background without amino acid supplementation. Representative replicate done in technical triplicate.

3.4.2 Amino acid biosynthetic operons upregulated in response to amino acid starvation in a (p)ppGpp-dependent manner

I examined how changes in RsFluc activity correlate with well-known (p)ppGpp-dependent physiological events in *B. subtilis*, such as gene activation (101) and decreased protein synthesis (185). Specifically, inducing the stringent response with arginine hydroxamate results in (p)ppGpp-dependent activation of several amino acid biosynthetic genes (101). I developed firefly luciferase fusions to the promoters of three of these genes (P_{serA}-*luc*, P_{ilvB}-*luc*, P_{metE}-*luc*) and compared their timing with that of RsFluc activity. All reporters showed luciferase activity with very similar timing to RsFluc (Figure 3.9A). Consistent with earlier findings, a *relA-D264G* mutation significantly reduced activity of all reporters (Figure 3.9B) (101).

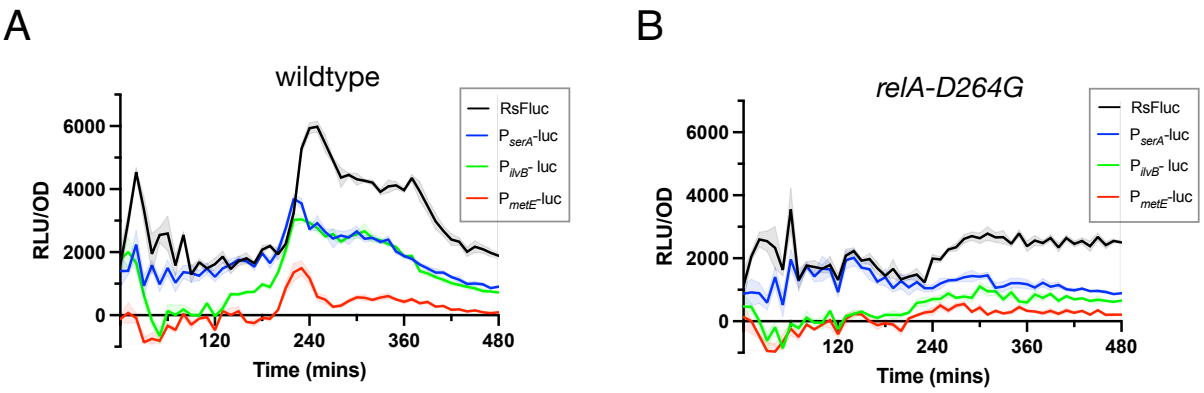

Figure 3.9 Correlation of amino acid biosynthetic gene expression and RsFluc activity.
Luminescence (RLU/OD_{600}) of: A) RsFluc (black, JDB4496), P_{serA}-luc reporter (blue, JDB4759), P_{ilvB}-luc reporter (green, JDB4792), and P_{metE}-luc reporter (red, JDB4798) in the wildtype background and B) reporters as A in the *relA-D264G* genetic background. Representative replicate done in technical triplicate.

3.5 (p)ppGpp and *B. subtilis* growth rates

3.5.1 (p)ppGpp production wave coincides with a decrease in growth rate

(p)ppGpp has been shown to regulate growth in *B. subtilis* by inhibiting transcription of rRNA and ribosomal proteins (185), global translation initiation (71), and DNA replication elongation (104, 105). A rise in (p)ppGpp levels should be accompanied by a decrease in growth in wild-type background cells. Interestingly, I observed that the spike in RsFluc activity, which occurs robustly around 220 minutes (Figure 2.2, blue), coincided with the transition from exponential to stationary phase growth (Figure 2.2, black). To explore this further, I visualized RsFluc activity alongside the growth rate, μ. The sharp increase in RsFluc activity (Figure 3.10, blue) aligns with a steep decline in the culture's growth rate (Figure 3.10, black). Therefore, the RsFluc reporter kinetics can effectively capture the (p)ppGpp signaling dynamics that lead to slowed growth.

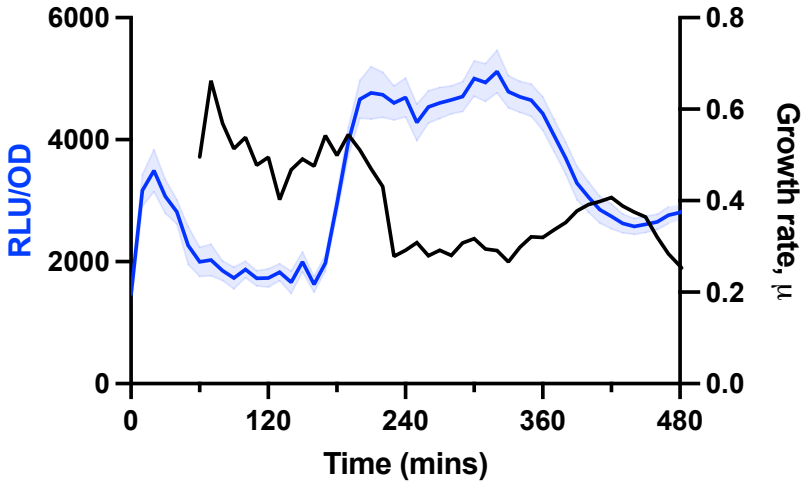

Figure 3.10 Temporal relationship between growth rate and RsFluc activity. Luminescence (RLU/OD_{600}) of RsFluc (blue, JDB4496) and growth rate (black). Growth rate/hr (μ) at a given time (t) is defined as $\ln[OD_{600}(t) - OD_{600}(t_{-60})]$. Representative replicate done in technical triplicate

3.5.2 Protein synthesis rates decline as (p)ppGpp is produced

The increase in RsFluc coincides with a sharp decrease in growth rate (Figure 3.10, black). The linear correlation between protein synthesis—especially ribosomal proteins—and growth rate (185) suggests that the rise in RsFluc is linked to reduced protein synthesis. To compare the timing of protein synthesis and (p)ppGpp changes, I added OPP (O-propargyl-puromycin) to cells before (Figure 3.11A, arrow "TP1") and during ("TP2") the increase in RsFluc. Click conjugation of OPP with a fluorophore (Figure 3.11B, 'wildtype') and subsequent measurement showed OPP labeling significantly decreased from TP1 to TP2 (Figure 3.11C). Because (p)ppGpp inhibits translation initiation (71), I investigated whether this change in OPP labeling depended on (p)ppGpp. I collected samples of (p)$ppGpp^0$ cells at the same time points and processed them similarly (Figure 3.11B, '(p)$ppGpp^0$'). Unlike wildtype cells, OPP labeling in $ppGpp^0$ cells did not decline between TP1 and TP2; in fact, it increased (Figure 3.11D), supporting the role of (p)ppGpp in reducing protein synthesis.

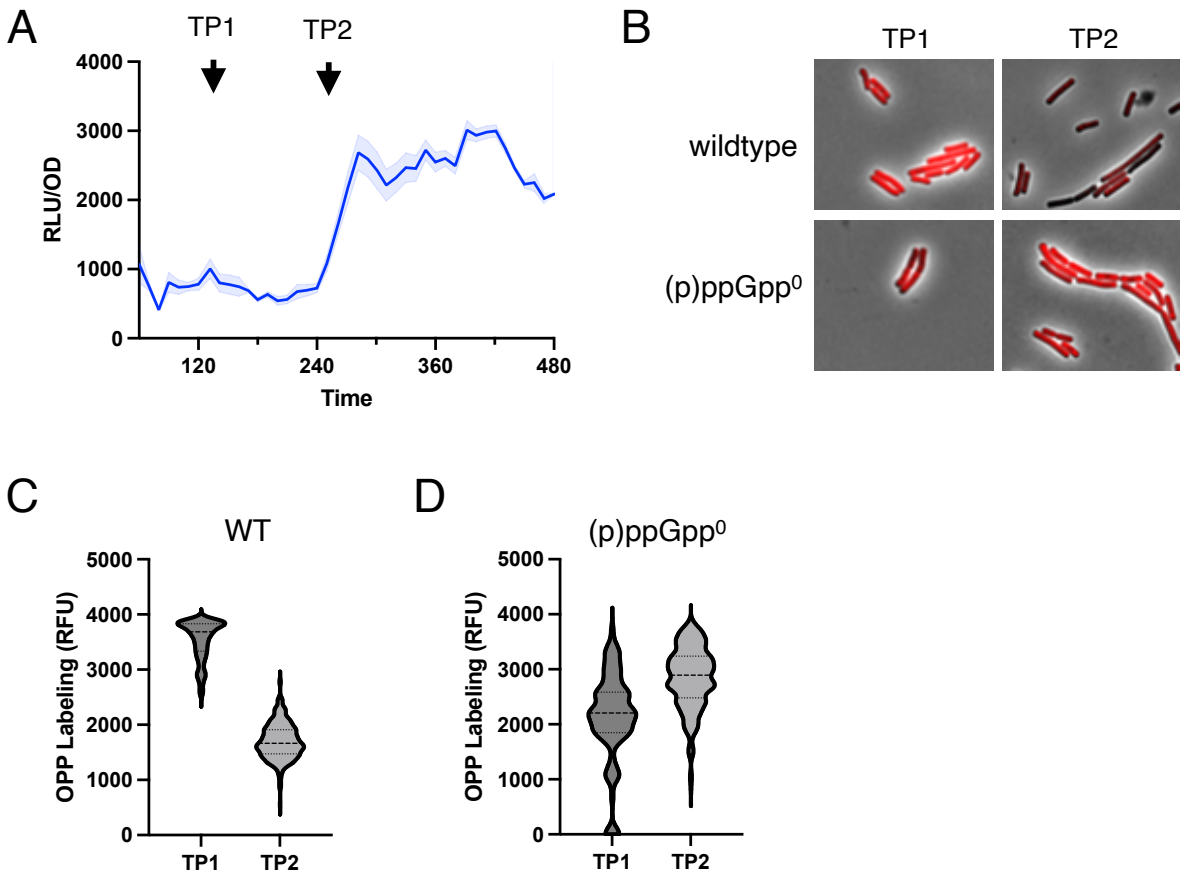

Figure 3.11 Temporal relationship between protein synthesis and RsFluc activity. A) Luminescence (RLU/OD_{600}) of RsFluc in wildtype (blue, JDB4496). Samples were taken at time points TP1 (120 min) and TP2 (240 min). B) Representative composite (fluorescent, phase) images of cells at TP1 and TP2 in either wildtype (JDB4496) or Δ*relA*Δ*sasA*Δ*sasB* ('(p)ppGpp^0'; JDB4512) backgrounds. C) and D) quantification of images from B. Representative replicate done in technical triplicate.

3.6 Conclusions

I used RsFluc to study (p)ppGpp metabolism during amino acid starvation, both during growth and after nutrient downshift. These results align with previous findings that Rel is the main synthetase of (p)ppGpp in *B. subtilis* (26). This research also allowed us to examine (p)ppGpp dynamics in a hydrolase mutant *of B. subtilis* for the first time, helping us better understand how biochemical characteristics relate to *in vivo* (p)ppGpp metabolism. I observed how RsFluc responded to different levels of amino acid supplementation, supporting the idea that

amino acid starvation is a key driver of (p)ppGpp production. I showed how RsFluc correlates with various physiological states related to growth and protein synthesis. These findings support earlier evidence that protein synthesis inhibition occurs via (p)ppGpp binding to IF2 (71).

Chapter 4

4 Assessing heterogeneity in (p)ppGpp and single-cell physiological variation

As discussed in 1.3.7, assessing single-cell variation in (p)ppGpp and its physiological consequences within a heterogeneous population could provide new insights into the fields of sporulation, competence, and persister cell formation. When designing a single-cell (p)ppGpp reporter for use in live *B. subtilis*, I drew inspiration from the design of RsFluc (Figure 2.1), which was extensively characterized and validated in Chapter 2. Although RsFluc offers numerous benefits for researchers, measuring luminescence at the single-cell level is a very challenging task. To create a single-cell (p)ppGpp reporter, I considered fluorescent protein reporters, as they can be measured with higher resolution using techniques like microscopy and flow cytometry. A fluorescent reporter for (p)ppGpp had previously been developed utilizing an RNA aptamer, Broccoli, engineered between the aptamer and the expression platform of a (p)ppGpp-binding riboswitch (171). However, this reporter was not as thoroughly characterized and validated as our own RsFluc system. A common protein used in gene reporter constructs in bacteria is green fluorescent protein (GFP), which is fused downstream of promoter sequences to produce a fluorescent output that quantifies gene expression levels (102). Using a fluorescent, single-cell reporter will enable investigations into heterogeneity in (p)ppGpp levels and the physiological effects of this variation.

4.1 Development of an inducible, fluorescent (p)ppGpp reporter

4.1.1 Designing a single-cell, fluorescent (p)ppGpp reporter

To construct our *in vivo* single-cell (p)ppGpp reporter, I inserted a sequence corresponding to the (p)ppGpp-sensitive riboswitch from the promoter of *Desulfitobacterium hafniense ilvE* (168) between an inducible promoter ($P_{hyperspank}$) and the *gfpmut2* gene, which encodes

GFPmut2, a bright and rapidly maturing GFP mutant (RsGFP; Figure 4.1). This construct was integrated at the *sacA* locus, and fluorescence measurements were taken during growth in S7/glucose defined medium (S7), unless otherwise noted, using single-cell microscopy imaging.

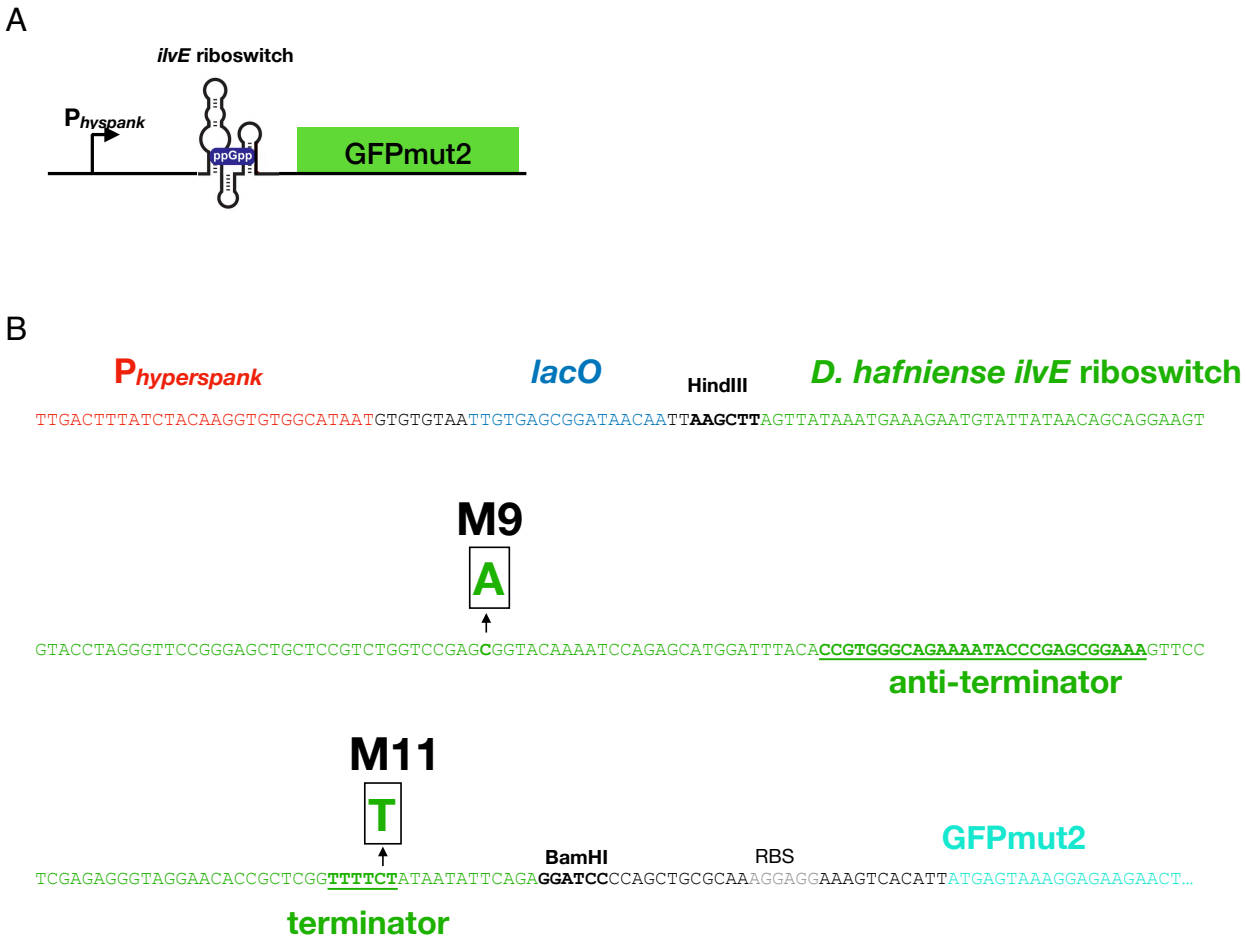

Figure 4.1 Fluorescent (p)ppGpp reporter design in *B. subtilis*.
A) Schematic of the (p)ppGpp reporter RsGFP depicting the inducible promoter $P_{hyperspank}$ fused to the (p)ppGpp-sensitive riboswitch of *D. hafniense ilvE* followed by the gene encoding GFPmut2. B) Shown is the $P_{hyperspank}$ promoter sequence (red), the *lac* operator binding sequence (blue), and the *D. hafniense ilvE* riboswitch gBlock sequence (green), with anti-terminator and terminator sequences bolded and underlined, and the M9 and M11 mutations from Sherlock *et al*. 2018 annotated. In gray, the Shine-Dalgarno ribosome binding sequence (RBS). In cyan, the 5' end of the GFPmut2 gene. Restriction enzymes HindIII and BamHI sites are bolded.

I also employed the M9 and M11 mutations identified by Sherlock *et al.* ((168), Fig. 4) and characterized as $RsFluc^{mut}$ in Chapter 2 to generate $RsGFP^{mut}$.

4.1.2 Heterogeneity in (p)ppGpp throughout growth

I measured RsGFP fluorescence signals throughout growth in wild-type *B. subtilis* cells using microscopy. As cells progress from the exponential to the transition phase of growth (Figure 4.2C), the fluorescence intensity of the RsGFP reporter increased (Figure 4.2A, 'RsGFP'). Quantifications of this microscopy show that the increase in fluorescence signal is heterogeneous within the population (Figure 4.2B). These measurements were background-subtracted for autofluorescence in the GFP channel. I also measured the RsGFP^{mut} reporter intensity throughout growth (Figure 4.2C). I observed that, while reporter intensity increased over time (Figure 4.2A, 'RsGFP^{mut}'), this increase was reduced and less heterogeneous compared to RsGFP (Figure 4.2B). Consistent with findings in RsFluc in 3.5.1, the increase in fluorescence occurs as the cells exit exponential growth and enter the transition phase, a period of slowed growth.

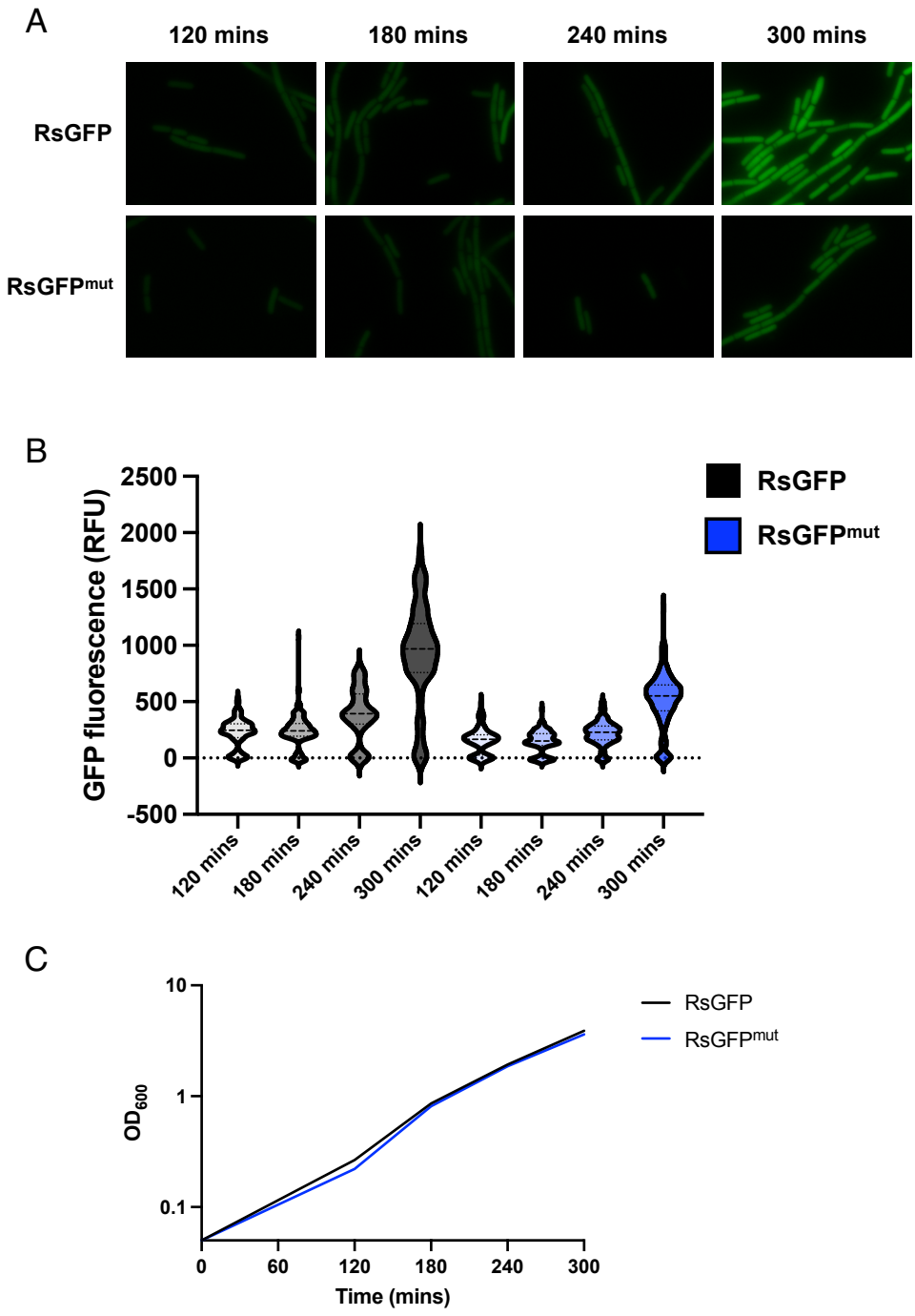

Figure 4.2 RsGFP fluorescence throughout growth.
A) Representative GFP fluorescent microscopy images of wildtype *B. subtilis* strains carrying RsGFP (JDB4632) and RsGFP^{mut} (JDB4661) reporters and B) violin plots of the quantification of microscopy images, background corrected for GFP autofluorescence (RsGFP: 120 mins, n = 131; 180 mins, n = 185; 240 mins, n = 103; 300 mins, n = 199, and RsGFP^{mut}: 120 mins, n = 71; 180 mins, n = 130; 240 mins, n = 244; 300 mins, n = 178) throughout different points along the C) growth curve in S7.

4.1.3 Role of environmental conditions in single-cell variation of (p)ppGpp

As found in 3.4.1 using RsFluc, environmental conditions significantly influence both amino acid starvation–induced (p)ppGpp production (Figure 3.8A) and basal (p)ppGpp levels (Figure 3.8B). To examine how environmental factors affect (p)ppGpp production and variation at the single-cell level, I used S7 media with different amino acid sources or no supplementation, as detailed in Appendix A: Materials and methods. I first measured RsGFP and RsGFP^{mut} signals during the exponential and transition phases of growth in S7. I observed that RsGFP fluorescence was reduced during exponential growth and increased significantly during the transition phase (Figure 4.3, 'RsGFP'). Similarly, the RsGFP^{mut} signal also increased, but the increase was less pronounced compared to the RsGFP (Figure 4.3, 'RsGFP^{mut}'). This suggests that the fluorescence increase is specifically linked to a rise in (p)ppGpp throughout growth in S7. This aligns with the higher luminescence observed in RsFluc compared to RsFluc^{mut} in S7 without supplementation (Figure 3.8B). Additionally, I noted that the fluorescence increase between the exponential and transition phases in RsGFP varied heterogeneously, as shown by the broad range and interquartile range (IQR) (Figure 4.3B, 'RsGFP').

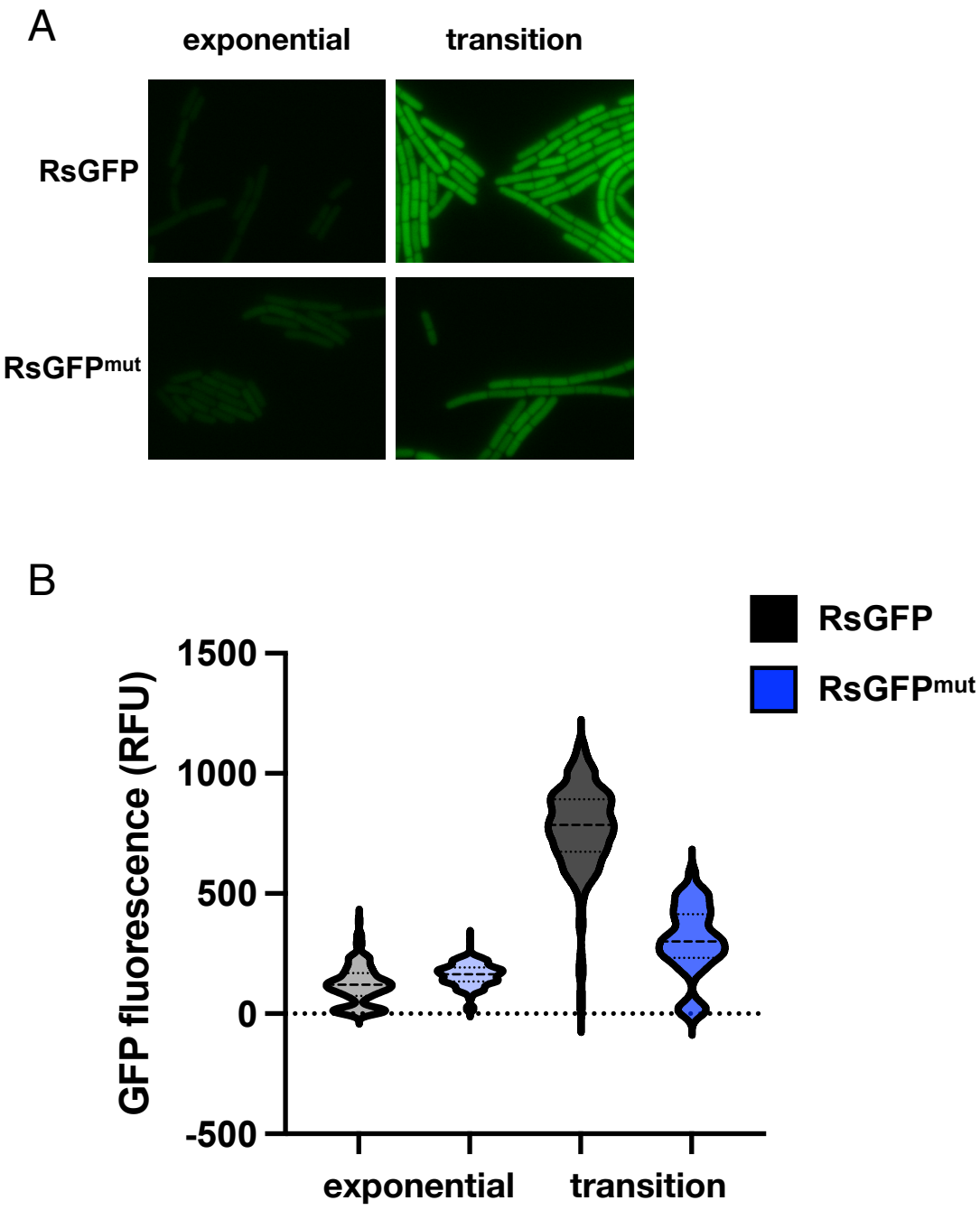

Figure 4.3 RsGFP fluorescent signal in S7.
A) Representative GFP fluorescent microscopy images of wild-type *B. subtilis* strains carrying RsGFP (JDB 4632) and RsGFP^{mut} (JDB4661) reporters and B) violin plots of the quantification of microscopy images (RsGFP: exponential, n = 134; transition, n = 180; and RsGFP^{mut}: exponential, n = 253; transition, n = 173) in exponential and transition phases of growth in S7, background corrected for GFP autofluorescence.

I then assessed RsGFP in a defined medium supplemented with amino acids, S7+CAA, which was used to characterize and validate RsFluc activity in Chapter 2 and is detailed in 0. I imaged RsGFP-containing *B. subtilis* cells during exponential and transition phases of growth in S7+CAA and observed that fluorescence intensity increased moderately (Figure 4.4, 'RsGFP'). I also noted that cells containing RsGFP^{mut} showed a moderate increase in signal throughout growth in S7+CAA, somewhat attenuated compared to RsGFP (Figure 4.4, 'RsGFP^{mut}'). This aligns with the modest attenuation seen in RsFluc^{mut} (Figure 2.2, green) compared to RsFluc (Figure 2.2, blue). The increase in fluorescence of RsGFP during growth in S7+CAA is modest but appears relatively heterogeneous, characterized by a wide range, IQR, and multimodality (Figure 4.4B, 'RsGFP'). However, RsGFP^{mut} also exhibits this same heterogeneity, indicating that it is not a result of single-cell variation in (p)ppGpp production (Figure 4.4B, 'RsGFP^{mut}').

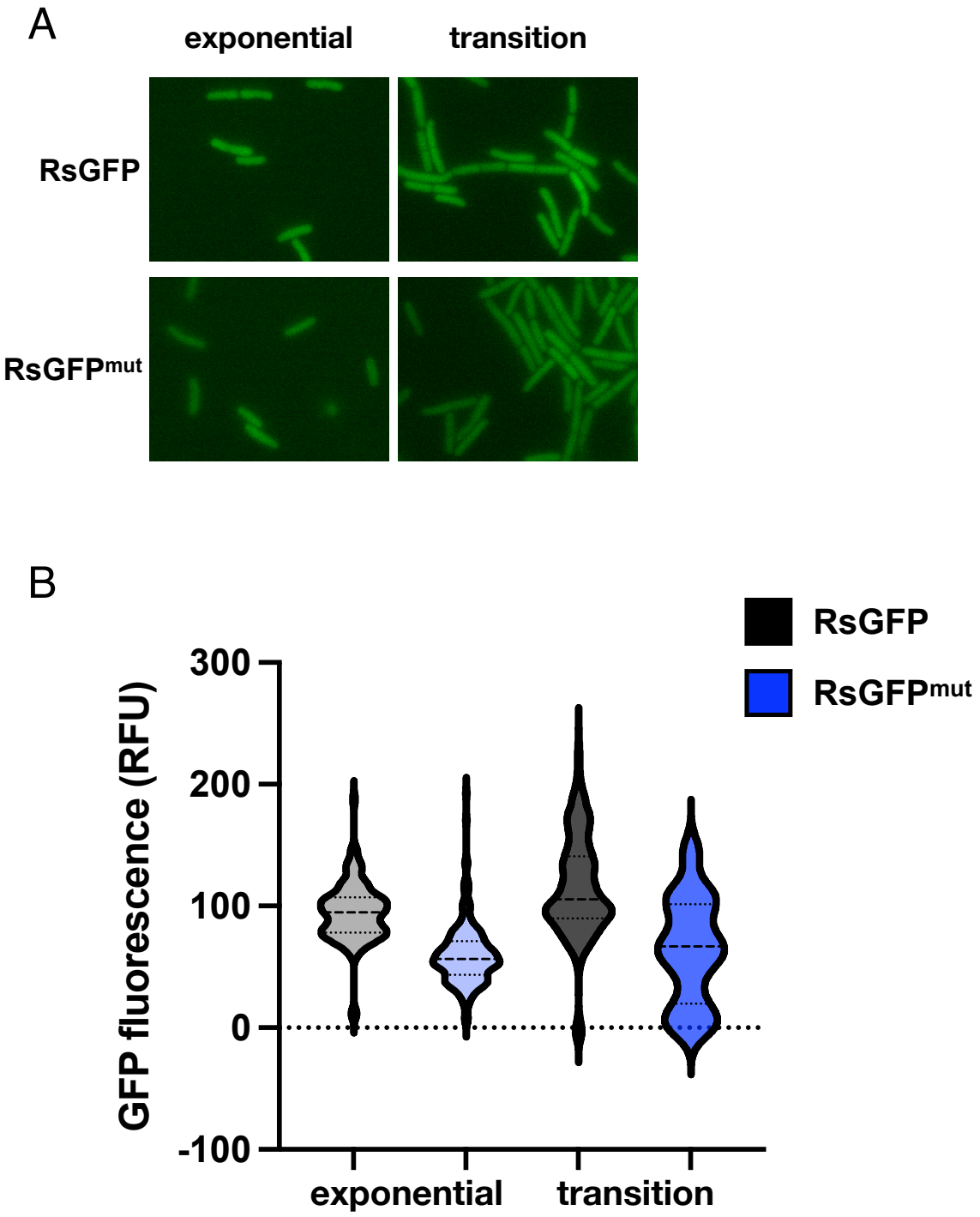

Figure 4.4 RsGFP fluorescent signal in S7+CAA.
A) Representative GFP fluorescent microscopy images of wildtype *B. subtilis* strains carrying RsGFP (JDB4632) and RsGFP^{mut} (JDB4661) reporters and B) violin plots of the quantification of microscopy images (RsGFP: exponential, n = 118; transition, n = 266; and RsGFP^{mut}: exponential, n = 210; transition, n = 41) in exponential and transition phases of growth in S7+CAA, background corrected for GFP autofluorescence.

Upon comparing these different media, I concluded that S7 medium without supplementation caused a significant increase in RsGFP compared to RsGFP^{mut} and exhibited a heterogeneous distribution as cells progressed from the exponential to the transition phase of growth (Figure 4.3). S7+CAA medium resulted in a lower induction of RsGFP (Figure 4.4) but produced a consistent and strong induction of RsFluc at around 220 minutes (Figure 2.2).

4.2 Heterogeneity in (p)ppGpp and bacterial physiology

4.2.1 Single-cell variation in (p)ppGpp and the *B. subtilis* transcriptome

Physiological and transcriptional heterogeneity exists within a bacterial population, leading to distinct clonal subpopulations that provide evolutionary and ecological advantages (71, 186–189). Many studies on heterogeneity have relied on fluorescent transcriptional reporters, which are typically limited to 4 or 5 spectrally distinct reporters at a time. However, recent advances in bacterial single-cell transcriptomics now enable the profiling of transcriptome-wide heterogeneity across thousands of cells (190–195). Recently, our collaborator Adam Rosenthal developed a technique for single-cell RNA sequencing (scRNA-seq) using transcriptome-wide probes (29,765 unique probes from the *B. subtilis* ProBac-seq probe set (190)) and ProBac-seq protocols (196). This ProBac-seq protocol isolates single cells via microfluidic droplets and hybridizes each cell with a unique probe set equipped with barcode identifiers and PCR handles for sequencing.

Together with Adam Rosenthal, we developed a method to analyze heterogeneity in (p)ppGpp and transcriptomes using the RsFluc reporter. Rosenthal designed probes compatible with the *luciferase* gene used in RsFluc. To examine heterogeneity in (p)ppGpp production, I sampled RsFluc in wild-type *B. subtilis* for scRNA-seq, probing for *luciferase* along with the 29,765 unique probes from the existing probe set. I sampled at 210 minutes during growth in

S7+CAA, when RsFluc was beginning to increase (Figure 4.5), as I anticipated a rise in reporter transcription shortly before reaching the maximum RsFluc signal in these conditions (Figure 2.7).

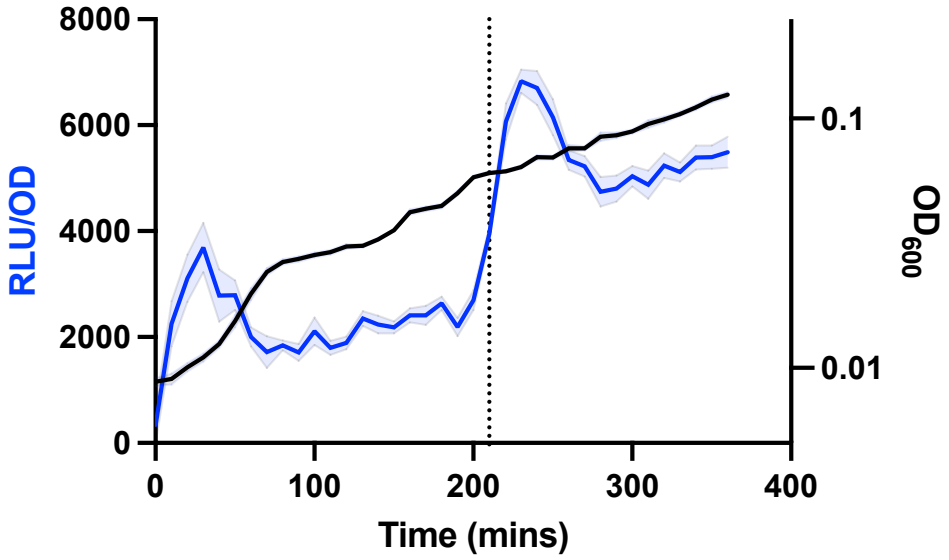

Figure 4.5 RsFluc sampled for scRNA-seq.
Luminescence (blue, RLU/OD_{600}) and growth (black, OD_{600}) of RsFluc (JDB4496) sampled for scRNA-seq at the time indicated by the dashed line, done in technical triplicate.

We discovered that shortly before the maximum RsFluc signal (Figure 4.5), the transcriptomes of the cells were distinct. Differential gene expression analysis identified eight separate cell clusters in the RsFluc sample (Figure 4.6A). We observed that the luciferase probes were present in a minimal number of cells and were differentially enriched in cluster 4 (Figure 4.6B). Analysis of the differentially expressed genes in cluster 4 showed that genes involved in sporulation, competence, polyketide synthesis, and extracellular polysaccharide production were upregulated (Figure 4.6C). Purine biosynthesis genes were downregulated (Figure 4.6C), consistent with previous findings that high (p)ppGpp anti-induces purine biosynthesis pathways (119). Additionally, genes related to DNA replication and cell division were found to be downregulated (Figure 4.6C).

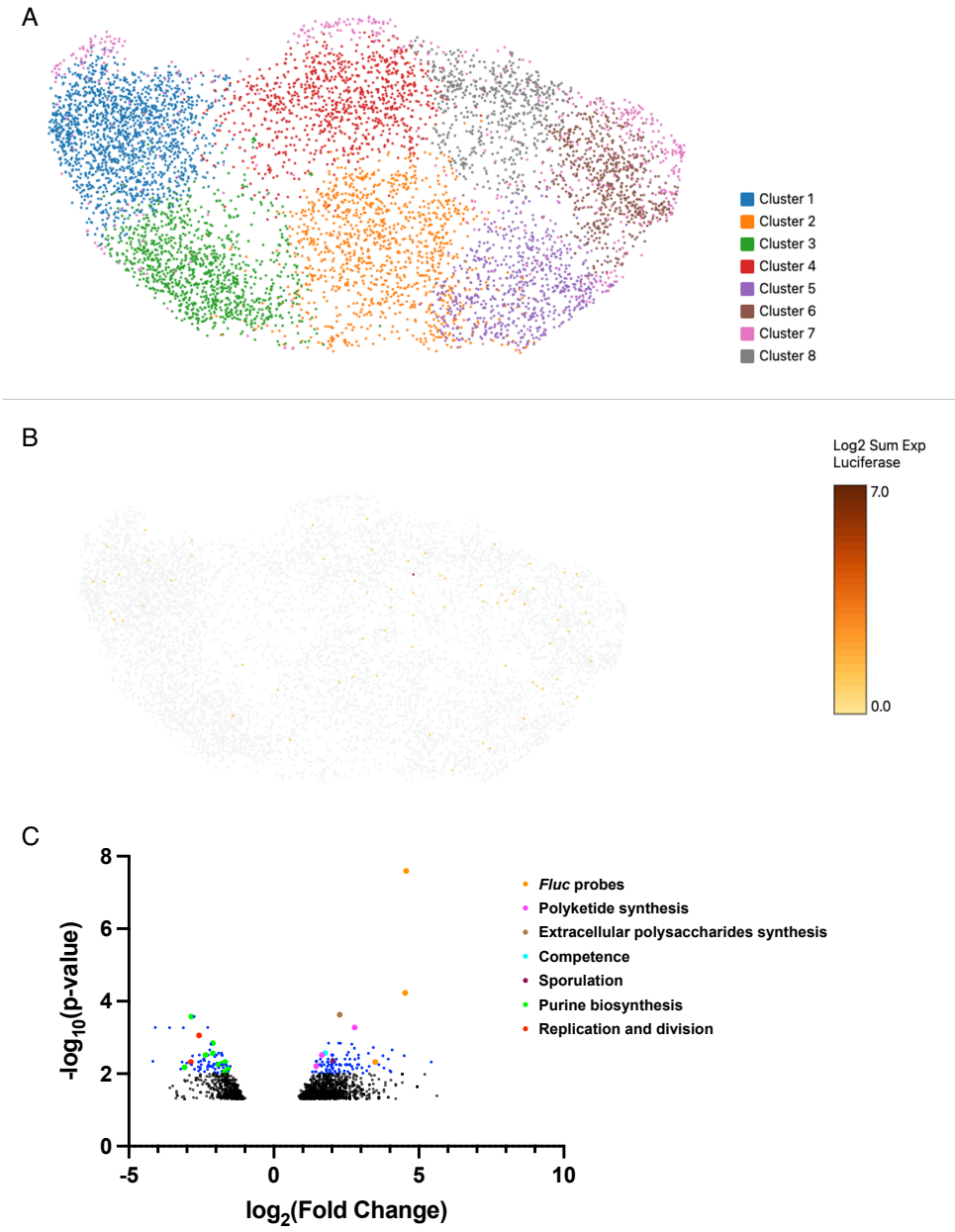

Figure 4.6 Heterogeneity in transcriptomes.
scRNA-seq experiments and analysis performed by Adam Rosenthal. A) UMAP two-dimensional representation of the cell clusters of scRNA-seq of wild-type *B. subtilis* cells containing RsFluc (JDB4496). B) *luciferase* transcripts are more frequent in cluster 4. C) Volcano plot of genes up- and down-regulated in cluster 4. Black dots represent probes with a significant p-value<0.05, and blue dots represent probes with a significant p-value<0.01. Fluc probes in orange, polyketide synthesis in magenta, EPS in brown, competence in cyan, sporulation in maroon, purine biosynthesis in green, replication and division in red.

4.2.2 Assessing regrowth in a subpopulation of cells high in (p)ppGpp

(p)ppGpp slows growth by inhibiting translation, replication, and rRNA transcription, as discussed in 1.3. Growth laws indicate a positive correlation between nutrient availability, growth, and the RNA:protein ratio, which reflects an increase in rRNA content (197). This RNA:protein ratio is tightly regulated in growing bacteria through (p)ppGpp signaling to optimize ribosomal biogenesis efficiency (198). It is possible that in a population with variable (p)ppGpp levels, there is also variability in growth among individual cells. This growth variability was studied recently using scRNA-seq techniques to analyze growth law patterns and transcriptional profiles in *B. subtilis*. The study found that a slow-growing subpopulation was enriched with stress response genes, which may indicate higher (p)ppGpp levels compared to the overall population (199).

To examine the relationship between (p)ppGpp and regrowth using our RsGFP reporter, I employed fluorescence-activated cell sorting (FACS) to isolate a highly fluorescent RsGFP population, $RsGFP^{high}$, and compared it to a simple random sampling (SRS) of the RsGFP population, $RsGFP^{SRS}$. The cells were grown to the transition phase in S7, where we expect a bright RsGFP signal and a heterogeneous population (Figure 4.3). The cells were diluted to an optimal density in S7 and analyzed using flow cytometry on the cell sorter, utilizing forward scatter and the FITC channel laser for GFP fluorescence (Figure 4.7A). After establishing a population distribution, I selected 20,000 cells from the top 5% of GFP fluorescence, of a specific size. I sorted this as the $RsGFP^{high}$ group, which likely exhibits elevated (p)ppGpp signaling throughout growth. I also randomly selected 20,000 cells of similar size, without specifying for GFP fluorescence, and sorted these as the $RsGFP^{SRS}$ group. Following sorting, the cells recovered in S7 were plated to determine the colony-forming units (CFU) per given volume

(CFU/mL). The CFU/mL was then measured every 30 minutes, with the increase normalized to the initial cell concentration post-recovery at 0 minutes. I observed that the RsGFP^{high} subpopulation modestly increased in cell count over time, rising by 65% in the 90 minutes after recovery (Figure 4.7B, black). The RsGFP^{SRS} subpopulation showed a more significant increase of 141%, more than doubling the cell count (Figure 4.7B, blue). These two subpopulations exhibited different patterns of recovery and regrowth after FACS, suggesting that heterogeneity in (p)ppGpp levels correlates with heterogeneity in growth within the population.

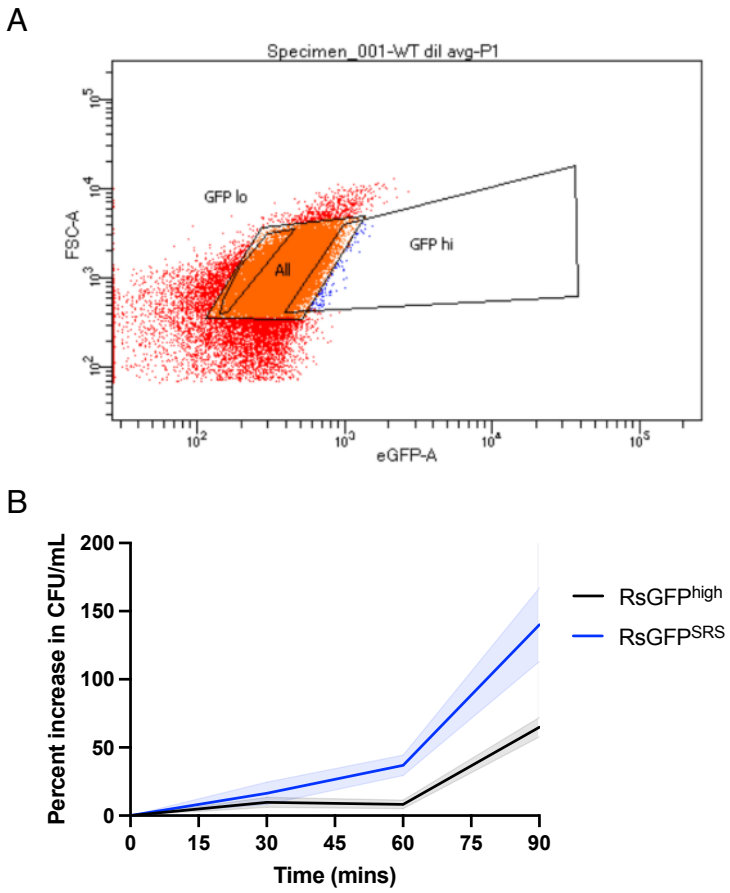

Figure 4.7 FACS and regrowth assay of RsGFP subpopulations.
A) Forward scatter and GFP plot of wildtype *B. subtilis* cells containing RsGFP (JDB4841). 'GFP hi' grouping represents the top 5% fluorescing cells of a given size sorted as RsGFP^{high}. 'All' grouping represents a simple random sample (SRS) of all cells of a given size sorted as RsGFP^{SRS}. B) Percent increase in CFU/mL count over time after sorting, normalized to CFU/mL at T_0 in RsGFP^{high} (black) and RsGFP^{SRS} (blue). Biological triplicates.

4.2.3 Assessing antibiotic tolerance in a subpopulation of cells high in (p)ppGpp

Cell-to-cell variability has been proposed as a potential source of persister cell formation in both Gram-positive and Gram-negative organisms (29, 143, 200, 201). Recently, Fung *et al.* investigated how single-cell heterogeneity in a shared (p)ppGpp-GTP switch resulted in different survival outcomes after antibiotic treatment (202). I aimed to explore how variations in (p)ppGpp levels at the single-cell level might influence survival after antibiotic exposure. To do this, I used FACS to sort a highly fluorescent RsGFP population, $RsGFP^{high}$, and compared it to the SRS of the RsGFP population, $RsGFP^{SRS}$. The cells were grown to the transition phase in S7, as I expected a bright RsGFP signal and a heterogeneous population (Figure 4.3). The cells were diluted to an optimal density in S7 and analyzed by flow cytometry on the cell sorter, using forward scatter and FITC channel laser for GFP fluorescence (Figure 4.8A). After establishing the population distribution, I selected 20,000 cells from the top 5% of GFP fluorescence within a specific size range. I sorted them as the $RsGFP^{high}$ group, which is likely to exhibit elevated (p)ppGpp signaling throughout growth. Additionally, I randomly selected 20,000 cells of similar size without selecting for GFP fluorescence and sorted them as the $RsGFP^{SRS}$ group. After sorting, the cells recovered in S7 were plated for CFU/mL counts. The cells were then treated with ciprofloxacin, an antibiotic that inhibits DNA gyrase as used previously (29), and plated for CFU/mL at regular intervals after treatment. I observed that the survival percentage of the $RsGFP^{high}$ population showed a biphasic killing curve following ciprofloxacin treatment (Figure 4.8B), a shape consistent with a persister population (140). In contrast, the survival percentage of the $RsGFP^{SRS}$ population rapidly declined after ciprofloxacin exposure (Figure 4.8B). I also noted that the variability between replicates in the $RsGFP^{high}$ group was substantial (Figure 4.8B), which warrants further investigation.

A

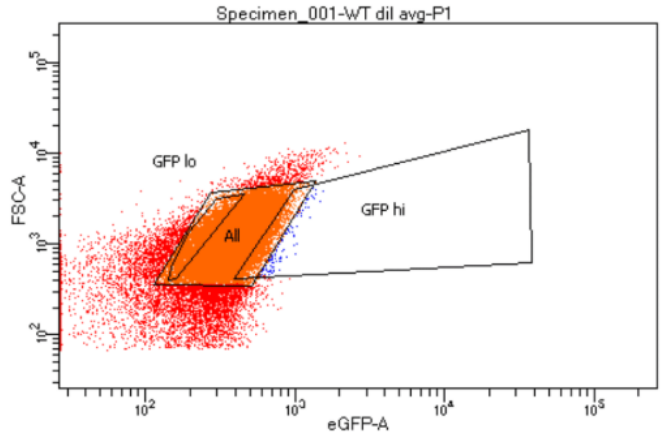

B

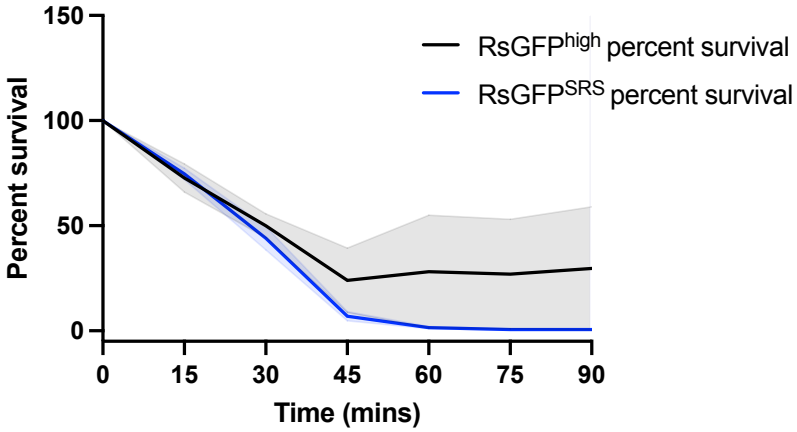

Figure 4.8 FACS and ciprofloxacin survival assay of RsGFP subpopulations. A) Forward scatter and GFP plot of wildtype *B. subtilis* cells containing RsGFP (JDB4841). 'GFP hi' grouping represents the top 5% fluorescing cells of a given size sorted as RsGFP^{high}. 'All' grouping represents a simple random sample (SRS) of all cells of a given size sorted as RsGFP^{SRS}. B) Percent survival over time after treatment with 1 µg/mL ciprofloxacin normalized to CFU/mL at T_0 in the RsGFP^{high} (black) and RsGFP^{SRS} (blue) groups. Biological triplicates.

4.3 Conclusions

RsGFP offers a valuable tool for examining heterogeneity in (p)ppGpp within a population. Here, I demonstrated how RsGFP can be used to analyze environmental factors that contribute to heterogeneity and various physiological responses, including transcriptional differences, growth,

and antibiotic tolerance. RsGFP can be applied in future studies to explore the sources of heterogeneity in (p)ppGpp, other physiological effects, or systems where luminescence measurements are not suitable.

Chapter 5

5 Validation of a clickable oligo for scRNA-seq

The work described in this chapter of the thesis is a result of a collaborative effort between Jonathan Dworkin, Christopher Baumann, Adam Rosenthal, and me. This chapter is adapted from Baumann, Hydorn, *et al.*, in revision (203). My contributions to this work are described in 5.2.2, and the findings from Baumann and Rosenthal are detailed in 5.1 and 5.2.1.

As discussed in Section 4.2.1, scRNA-seq can be a powerful tool for gaining insight into the heterogeneity of transcription profiles within bacterial populations. However, the transcriptome at any given moment may not accurately reflect the cell's current activity. Because single-cell RNA sequencing (scRNA-seq) measurements provide only a snapshot in time (204, 205), it is challenging to infer a cell's physiological state from just an inventory of transcripts. We focused on combining scRNA-seq techniques with physiological state labels, particularly using the protein synthesis marker OPP in *B. subtilis*, to better understand the connection between transcriptome heterogeneity and physiological states.

5.1 Assessing the relationship between single-cell variation in protein synthesis and the *B. subtilis* transcriptome

To develop a technique that links each cell's translation rate measurement, we reasoned that replacing the incorporation of fluorophores during OPP labeling protocols for microscopy with the incorporation of a user-defined oligonucleotide would provide a sequencing-based signal detectable via single-cell methods. To accomplish this, we adapted the OPP labeling method to include an oligonucleotide probe ($oligo^{synth}$) dual labeled with a click-chemistry azide molecule on the 3' end and a PCR handle for sequencing on the 5' end, compatible with the probe-based bacterial scRNA-seq method (196) (Figure 5.1A, B).

We then obtained combined single-cell signals of transcription and translation at a specific point during the transition phase of the growth curve (300 minutes, Figure 5.1C). Cells were exposed to OPP for 20 minutes, fixed in formaldehyde, and treated with the oligo^{synth} according to our optimized protocols. After click-incorporation, an aliquot of the cells was imaged, confirming single-cell suspension and heterogeneity in translation rates (Figure 5.1D). The remaining cell sample was then incubated with transcriptome-wide probes (29,765 unique probes from the *B. subtilis* ProBac-seq probe-set (190)) and a probe complementary to oligo^{synth,} processed using ProBac-seq protocols (196) with slight modifications. When overlaying the signal from the OPP probe onto the cells, a significant enrichment of the OPP signal is observed in cluster 4 (Figure 5.1F), indicating that this cell population exhibits higher translational activity, consistent with the fluorescence observation of bright cells (Figure 5.1D).

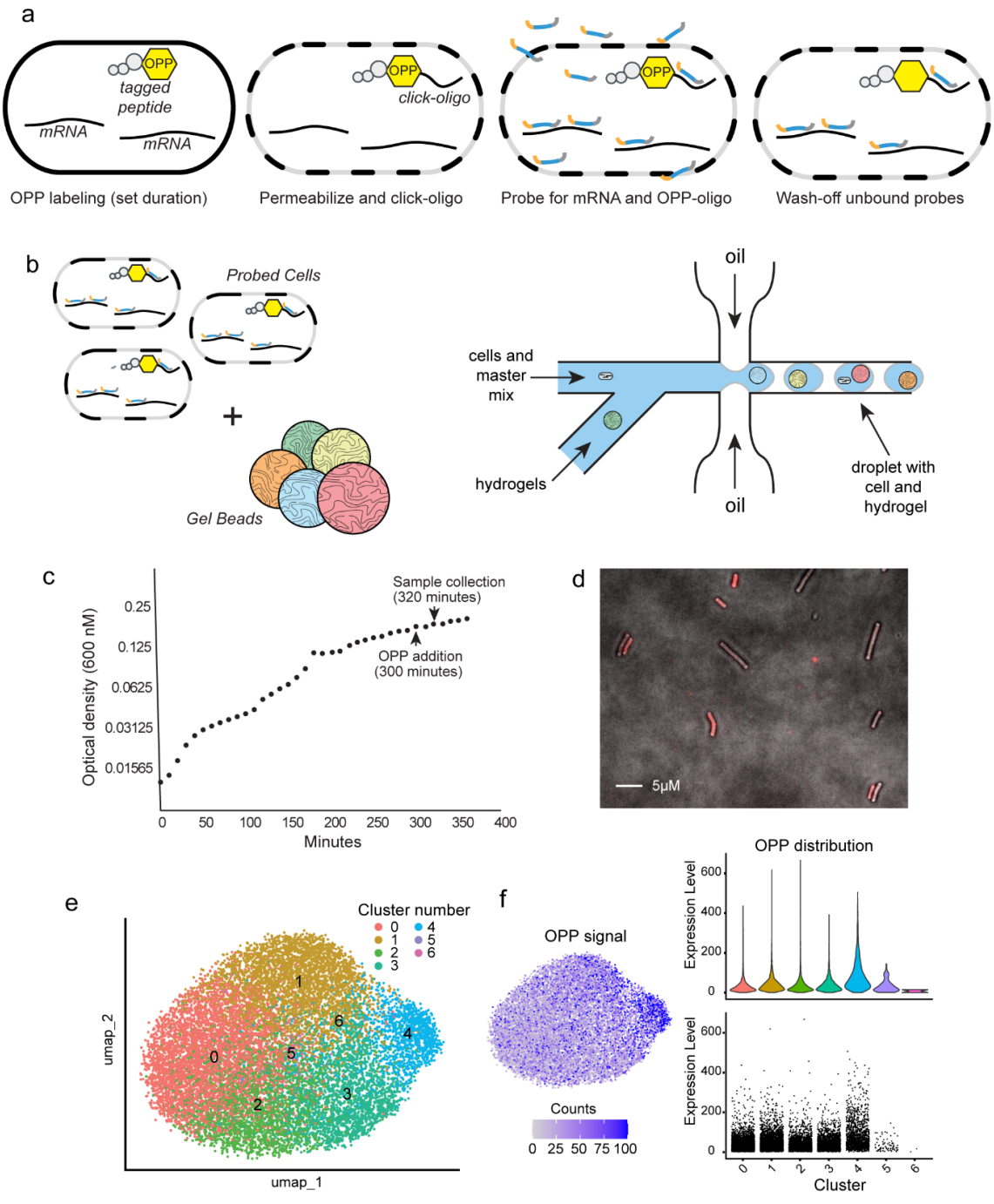

Figure 5.1 Single-cell RaTe Sequencing provides a tandem measurement of RNA and translation in single cells.

Adapted from Chris Baumann and Adam Rosenthal. a. Cells are incubated with OPP for a given duration of time, then fixed, permeabilized, and conjugated with azide+fluorophore-containing DNA oligonucleotide. OPP-labeled cells are then hybridized with probe sets complementary to the mRNA and OPP oligo sequences. Unbound probes are thoroughly washed to prepare labeled cells for single-cell encapsulation. b. Cells and barcoded beads are separated into single-cell emulsions using

microfluidic single-cell encapsulation. c. OPP was added to cells at 300 minutes, during the transition stage of growth, and a sample for analysis was harvested and fixed 20 minutes after the addition of OPP. d. A representative image from the sample after Azide+Fluorophore DNA oligonucleotide conjugation. e. UMAP two-dimensional representation of the cell clusters f. **The OPP signal is higher in cluster 4, as seen when the single-cell signal from the OPP probe is projected onto** the UMAP. OPP distribution signal in each cluster is displayed in both a violin plot (top) and a corresponding cell plot (bottom)

5.2 Investigating the role of increased translation of transcriptional activator AlsR in the high *alsSD*-expressing subpopulation

5.2.1 The high OPP oligo cluster also exhibited increased *ALS-SD* transcription.

Differential gene expression revealed several transcriptomic signatures that differentiate cell clusters (Figure 5.2A). Cluster 4, associated with high translational activity, contains cells overexpressing genes involved in arginine synthesis, acetoin synthesis, and proton motive force, among other processes (Figure 5.2A). In the context of *Bacillus subtilis* physiology, several of these processes were previously identified as heterogeneous by our groups and others, both in the transition growth phase (188, 190) and in biofilms (206, 207). Besides the enrichment of these functional genes, gene-set enrichment analysis also implicates a transcriptional repressor (Rex) and a transcriptional activator (AlsR) as potential genetic regulators of gene expression in this cell cluster (Figure 5.2A). Two of the most differentially expressed genes in this cluster, *alsS* and *alsD*, encode components needed for acetoin biosynthesis, a key overflow metabolite produced by *B. subtilis* during the transition phase of growth and in biofilms. Rosenthal previously found these genes to be heterogeneous during the transition phase of growth using a different growth medium (188). By using a fluorescent reporter for the promoter of the *alsSD* operon, they confirmed the heterogeneity of these genes under our culture conditions (Figure 5.2B).

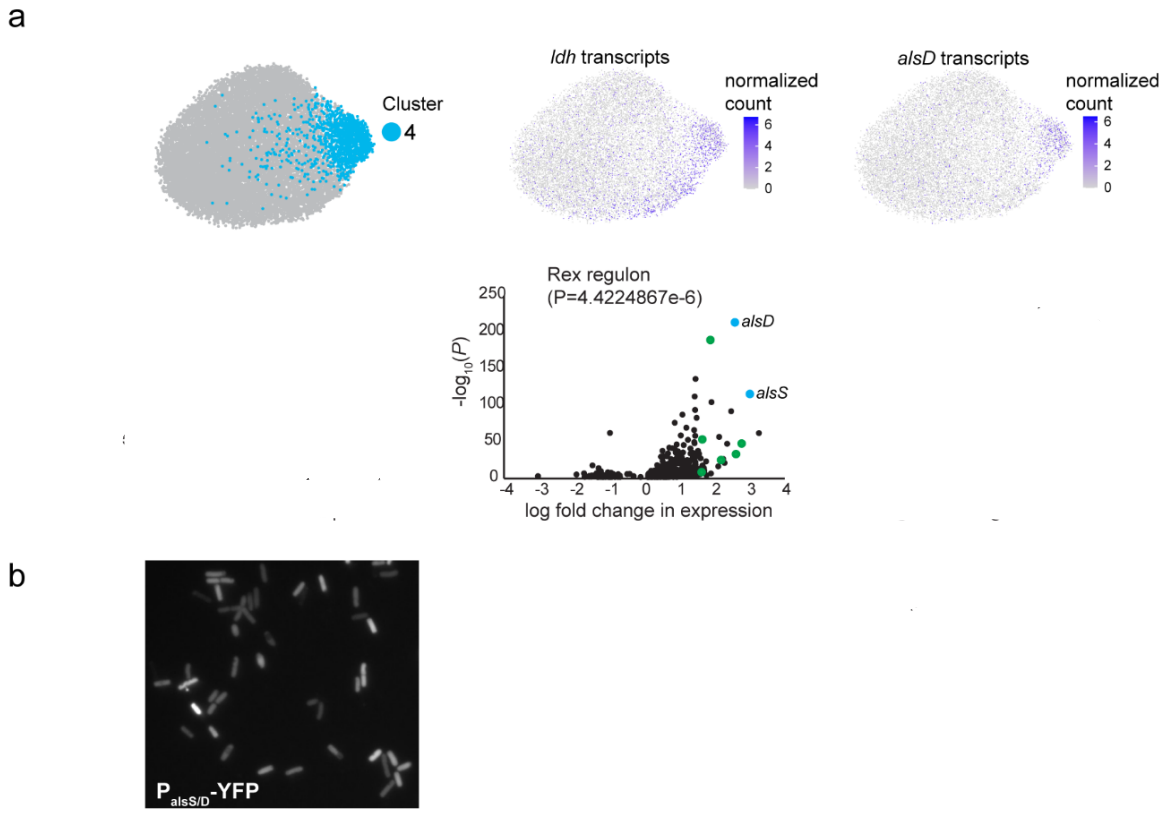

Figure 5.2 Distinct transcriptomic profiles and specific genetic regulators correlate with high translation rates in single cells.
Adapted from Chris Baumann and Adam Rosenthal. a. Top panels display the cells in cluster 4 and normalized single-cell expression of *alsD* and *ldh* transcripts, upregulated in cluster 4. The middle panel displays volcano plots of gene sets enriched in cluster 4, specifically the Rex regulon. The *alsS* and *alsD* values in the Rex volcano plot are colored in blue because the *alsSD* promoter has an imperfect Rex consensus motif with low binding affinity. Overexpressed genes verified in these gene sets are colored green; *alsS* and *alsD* are putative Rex-regulated genes and are colored in blue. b. A YFP reporter for the alsSD promoter is heterogeneous in S7+CAA media.

5.2.2 Increased protein synthesis correlated with increased AlsR protein levels

Heterogeneity in *alsS* expression could result from differences in levels of AlsR, the transcriptional activator of the *alsSD* operon (208). Specifically, cells enriched in acetoin biosynthesis genes also show higher OPP probe signals (Figure 5.1F and Figure 5.2A), indicating that variations in translation rates influence heterogeneity in AlsR protein levels and, consequently, differential expression of *alsS*. To explore this possibility and measure AlsR levels

in single cells, I engineered a strain expressing an AlsR-GFP fusion at the native locus. This construct restores AlsR function, as the activity of the PalsS-firefly luciferase transcriptional reporter was similar in strains expressing AlsR and AlsR-GFP (Figure 5.3).

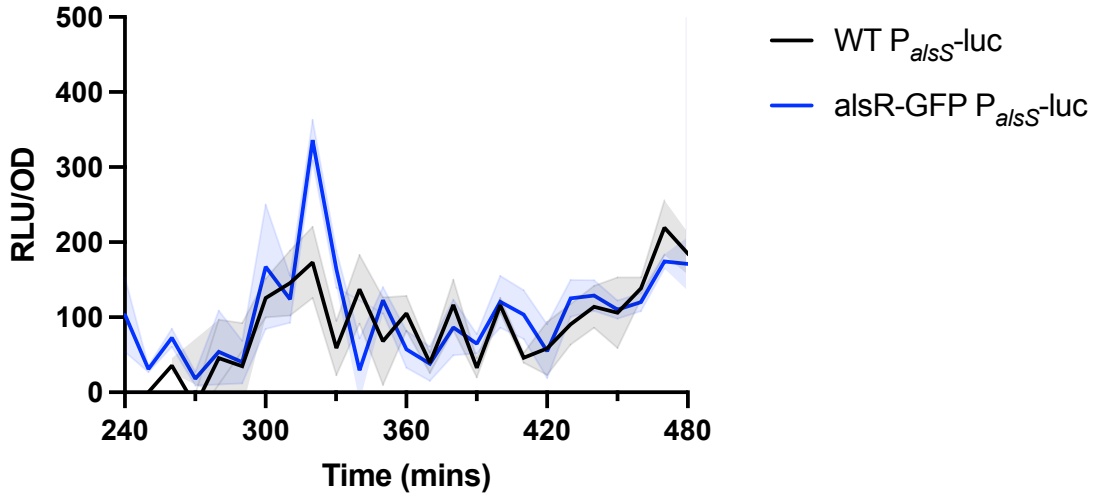

Figure 5.3 AlsR-GFP complements AlsR in regulating transcription of *alsS*. Luminescence (RLU/OD_{600}) of P_{alsS}-*firefly luciferase* (JDB4784, black) and *alsR*:: *alsR-GFP* P_{alsS}-*firefly luciferase* (JDB4787, blue). Representative replicate done in technical triplicate.

I incubated the AlsR-GFP strain with OPP and labeled it with the Click-iT AlexaFluor 594 picolyl azide. After imaging (Figure 5.4A) and analysis, I identified the top 25% of OPP-labeled cells as the "high protein synthesis" (HPS) group (Figure 5.4B). I also took a random sample of the entire population, of equal size (n = 298), which I refer to as "random sampling" (RS) (Figure 5.4B). Comparing the two groups showed that the HPS had significantly higher AlsR-GFP fluorescence than the RS group, indicating higher AlsR protein levels (Figure 5.4B). I then examined the correlation between AlsR-GFP and OPP signals in individual cells, finding a positive correlation ($R^2 = 0.5571$) between protein synthesis rates (OPP labeling) and GFP (AlsR-GFP) protein levels (Figure 5.4C). Therefore, differences in protein synthesis likely explain the heterogeneity in *alsS* transcription. While heterogeneity in alsSD operon expression

may be driven by differences in *alsR* transcription, the *alsR* gene does not show significant differential expression between clusters observed in scRNA-seq (Figure 5.4D).

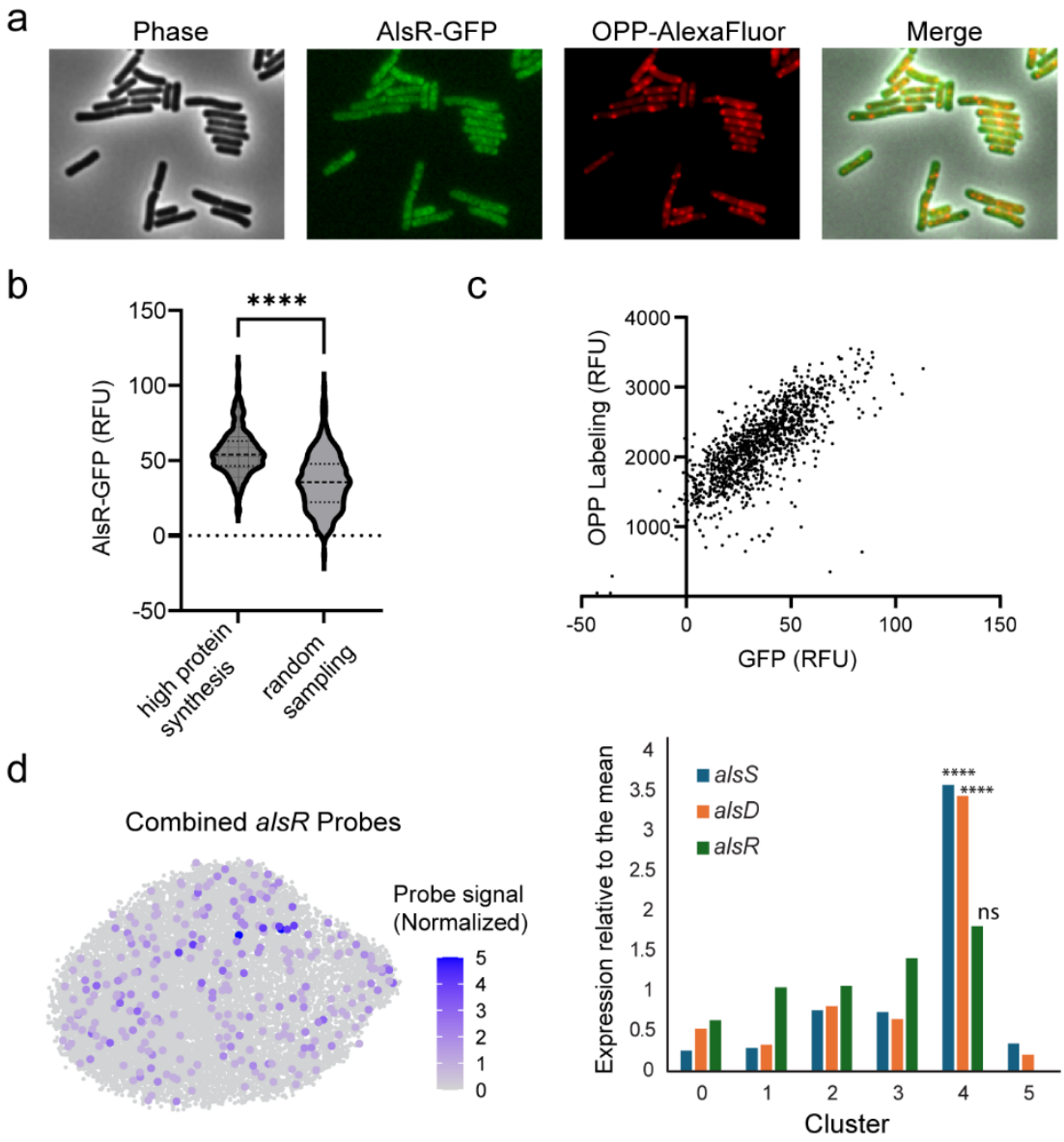

Figure 5.4 High protein synthesis rates account for increased AlsR protein levels. Prepared with Chris Baumann and Adam Rosenthal. a. AlsR-GFP expressing cells (JDB4786) after OPP incorporation and AlexaFluor™ labeling, shown in phase, GFP, mCherry, and merged channels. b. AlsR-GFP signal distribution in high protein synthesis cells (n = 298), defined by taking the top quartile of OPP-AlexaFluor fluorescing cells, and in a simple random sample (SRS, n = 298), background corrected for autofluorescence. ****, $p < 0.0001$ (Mann-Whitney U test). c. AlsR-GFP signal (x-axis) and OPP-AlexaFluor signal (y-axis) for all cells in population (n = 1195). Linear regression analysis **yielded a line of best fit with the following parameters: y = 20.02x + 1421, R^2** = 0.5571. d. The combined single-cell probe signal from all *alsR* probes is highlighted on the UMAP. ****Bonferroni corrected P value: *alsS* cluster 4 = 1.46E-11.

alsD cluster 4 =1.37E-209. *alsR* signal is not statistically differentially abundant in cluster 4.

5.3 Conclusions

Here I introduce a method for measuring bacterial transcriptomes and protein synthesis at the single-cell level, thereby connecting a cell's physiological state with its underlying gene expression. Our findings reveal a subpopulation of cells that exhibit higher protein synthesis rates and overexpress genes associated with overflow metabolism. I also demonstrate that the protein levels of AlsR, a crucial regulatory protein for key genes in this subpopulation, increase, despite its transcription not being significantly elevated, thereby establishing a link between regulator protein abundance and the transcription of its downstream targets. Additionally, I demonstrate a new technique further to explore the relationship between physiological state and transcriptomic profiles.

Chapter 6

6 Conclusions and Future Directions

6.1 Conclusions

6.1.1 Development, characterization, and validation of a novel luminescent (p)ppGpp reporter

In Chapter 2 of this thesis, I developed, characterized, and validated a novel tool for investigating (p)ppGpp dynamics in *B. subtilis*, referred to as RsFluc. I examined the effect of point mutations in the *D. hafniense ilvE* riboswitch on luminescent signals (Figure 2.2, Figure 2.3). I created pppGpp- and ppGpp-specific RsFluc candidates (Figure 2.4). Together with collaborators, I characterized RsFluc activity throughout growth. I measured absolute (p)ppGpp concentrations in the population using HPLC-MS techniques (Figure 2.5), as well as ATP and GTP levels (Figure 2.6). I confirmed that fluctuations in luminescent signals accurately reflected transcriptional changes of the reporter gene (Figure 2.7). I tested the RsFluc and RsFluc^{mut} responses to known and well-characterized amino acid starvation triggers, such as nutrient downshift (Figure 2.8), mupirocin treatment (Figure 2.9, Figure 2.10), and diauxic shift (Figure 2.11). Finally, I tracked RsFluc activity alongside transcriptional reporter assays of genes known to be anti-induced by (p)ppGpp (Figure 2.13).

(p)ppGpp has well-characterized global effects (25) that could influence RsFluc expression, extending beyond the riboswitch element, making it more challenging to interpret RsFluc activity. However, this is unlikely for two reasons. First, the activity of the RsFluc^{mut} reporter, which contains a mutation in the *ilvE* riboswitch that reduces its in vitro sensitivity to (p)ppGpp (168) is diminished compared to the wild-type RsFluc reporter (Figure 2.2). This reduction is similar to what is seen with the mutant RsFluc reporter lacking the entire RS element (RS^{0},

Figure 2.3A). Therefore, these findings in a wild-type background indicate that a significant effect on luciferase activity can be detected even in a strain that can produce (p)ppGpp. Second, although (p)ppGpp clearly inhibits overall protein synthesis (71), this inhibition would likely suppress the response of a reporter like luciferase, thereby reducing the observed (p)ppGpp-dependent increase in RsFluc activity. As a result, this increase is probably underestimated compared to the actual effect, due to the compensatory inhibition of (p)ppGpp on luciferase synthesis.

It's a long-standing belief that the effect of (p)ppGpp on bacterial physiology in *B. subtilis* primarily occurs through reductions in GTP levels and GTP dysregulation during high (p)ppGpp states (101). However, my analysis of GTP levels during peak (p)ppGpp shows that GTP is only slightly decreased (Figure 2.6B). This inconsistency may be due to a missing crucial time point in our sampling, where GTP levels could have been significantly dysregulated, and homeostatic mechanisms had already been activated. It may also result from the acute starvation methods often used to study (p)ppGpp, rather than natural growth conditions of gradual nutrient limitation (209).

Treatment with a small molecule that decreases tRNA aminoacylation, such as mupirocin, an isoleucyl-tRNA synthetase inhibitor, is a standard laboratory method to induce (p)ppGpp synthesis (177). I observe that mupirocin increases RsFluc expression (Figure 2.9), but the response is not linear; 50 ng/mL mupirocin causes a greater increase than 25 ng/mL, but less than 100 ng/mL (Figure 2.10A). Since higher mupirocin levels decrease tRNA charging, which itself inhibits protein synthesis, 100 ng/mL mupirocin could impair protein synthesis enough to affect the expression of the luciferase reporter. The fact that 100 ng/mL mupirocin has a significantly greater impact on growth than 50 ng/mL (Figure 2.10B) supports this explanation.

Therefore, interpreting the effects of 100 ng/mL mupirocin is complicated by the role of (p)ppGpp in inhibiting protein synthesis (71). Similar issues may arise with other molecules that induce (p)ppGpp synthesis by affecting tRNA charging, suggesting that careful titration may be necessary to properly account for indirect effects on protein synthesis (209).

6.1.2 Comprehensive evaluation of (p)ppGpp synthetase and hydrolase contributions to (p)ppGpp metabolism

In Chapter 3, I used the carefully characterized and validated RsFluc (p)ppGpp reporter to assess the contributions of various (p)ppGpp synthetases, hydrolases, and crosstalk effectors on (p)ppGpp metabolism in *B. subtilis* during growth in S7+CAA. I demonstrated that Rel is the primary (p)ppGpp synthetase during normal development (Figure 3.1). I showed that mutations to residues identified as allosteric activation sites in Rel and SasB reduced (p)ppGpp production and affected temporal regulation (Figure 3.2). I found that full synthetase activity is necessary for a timely and scaled response to nutrient downshift (Figure 3.3, Figure 3.4). I characterized the role of Rel as the primary (p)ppGpp hydrolase (Figure 3.5). I investigated the role of pGpp crosstalk with (p)ppGpp metabolism via NahA pyrophosphohydrolase activity (Figure 3.6). Finally, I examined c-di-AMP crosstalk mechanisms with (p)ppGpp metabolism through DarB activation of Rel (Figure 3.7).

When comparing the contributions of Rel, SasA, and SasB to (p)ppGpp metabolism during growth, it was clear that Rel was the primary synthetase of (p)ppGpp under these conditions (Figure 3.1A). Mutations Δ*sasA*, Δ*sasB*, and Δ*sasA*Δ*sasB* (Figure 3.1C) had minimal to no impact on (p)ppGpp metabolism. This suggests that the primary mechanism for (p)ppGpp production in this context is through amino acid starvation, rather than transcriptional changes (32) or cell wall stress (29), which primarily regulate SasB and SasA activity and expression,

respectively. The removal of allosteric activation in Rel significantly affected (p)ppGpp metabolism (Figure 3.2A). This suggests that auto-allostery activation is crucial for initiating a comprehensive (p)ppGpp response, consistent with the notion that auto-allostery has evolved to coordinate various Rel proteins within a cell, thereby slowing growth and protein synthesis (24).

I demonstrated that, unlike in natural growth conditions, all (p)ppGpp synthetases (Figure 3.3) and full activity (Figure 3.4) are necessary for temporal regulation and a complete (p)ppGpp response after downshift. This suggests that these SAS enzymes and allosteric activation may have evolved to support survival during acute starvation. This study provides a new *in vivo* context for the *B. subtilis* (p)ppGpp synthetase and its allosteric network (Figure 6.1). In summary, Rel functions as the main synthetase during natural growth and acute starvation. Auto-allosteric activation of Rel is essential for synthetase activity in both conditions. Both SAS enzymes are required for acute amino acid starvation, with allosteric activation of SasB being critical for this activity.

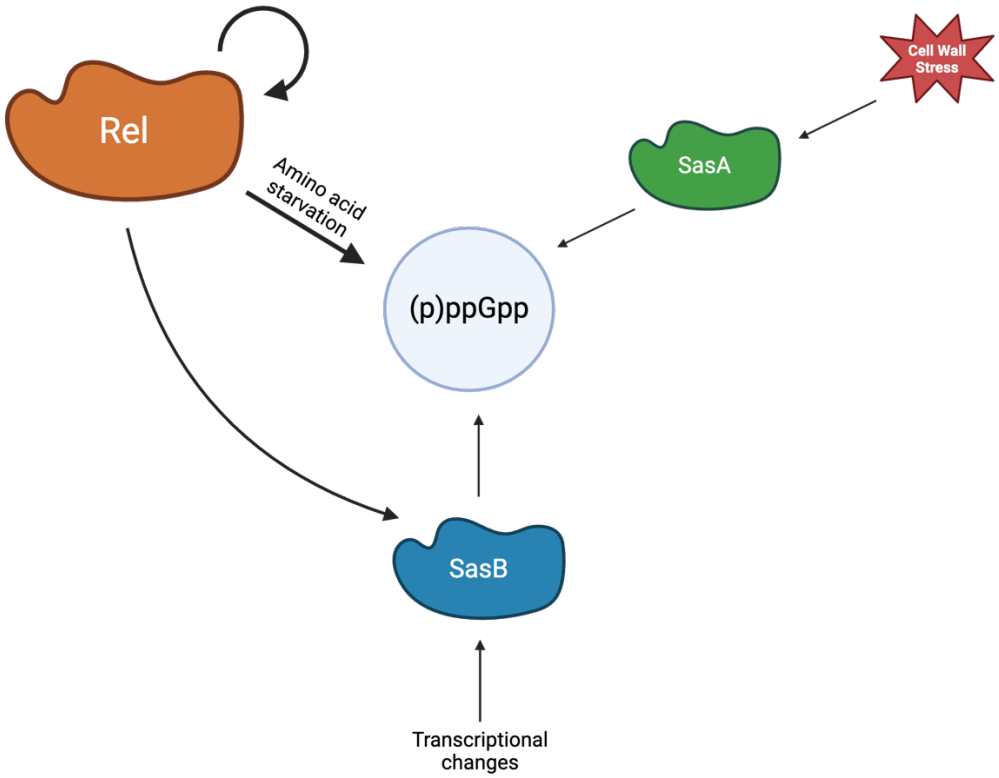

Figure 6.1 Schematic of (p)ppGpp synthetase allosteric network in *B. subtilis*. (p)ppGpp is mainly produced by the RSH enzyme Rel in *B. subtilis*. Rel exhibits auto-allostery to stimulate a positive feedback loop. SasB, whose expression and activity are thought to be regulated by transcriptional changes, is allosterically stimulated by pppGpp produced from Rel to synthesize (p)ppGpp. SasA is believed to be expressed in response to cell wall stress and remains active to create (p)ppGpp.

The RsFluc reporter offers a new technique for analyzing (p)ppGpp metabolism; however, studying (p)ppGpp hydrolysis is particularly challenging. Hydrolysis activity is crucial when synthetases are present. It is helpful to understand the role of hydrolysis in (p)ppGpp metabolism, as it is thought to regulate basal, homeostatic (p)ppGpp levels (20). Using the methods I developed in this thesis, I introduced a powerful new tool for assessing how hydrolysis affects (p)ppGpp dynamics. We observed that after inducing a Rel hydrolase mutant in a (p)ppGpp^0 background, (p)ppGpp quickly accumulated (Figure 3.5). This indicates that hydrolysis activity is crucial for regulating Rel and maintaining (p)ppGpp levels over time. We

observed a spike in RsFluc activity (Figure 2.2), and in a hydrolase mutant strain, the shape of that spike is lost (Figure 3.5). This study provides an *in vivo* context for previously established *in vitro* data.

Both pGpp (31, 39) and c-di-AMP (62) have been shown to interact with (p)ppGpp metabolic pathways in *B. subtilis*. With the RsFluc, I set out to investigate how these crosstalk mechanisms may affect (p)ppGpp metabolism. I found that neither NahA (Figure 3.6) nor DarB (Figure 3.7) activity affects (p)ppGpp metabolism, contrary to previous findings. However, these crosstalk mechanisms may still operate under different conditions. Researchers studied the crosstalk between pGpp and (p)ppGpp during sharp induction of (p)ppGpp (39). C-di-AMP and (p)ppGpp crosstalk was examined during low potassium conditions (62). Although I was unable to observe an effect, RsFluc can be used to explore other conditions for a more comprehensive investigation of crosstalk.

6.1.3 Assessing the environmental factors that contribute to (p)ppGpp synthesis

In 3.4, I examined how environmental conditions influence (p)ppGpp metabolism and response. I evaluated RsFluc under different levels of amino acid supplementation (Figure 3.8). Then, I analyzed the relationship between RsFluc activity and luciferase-based transcriptional reporters of amino acid biosynthetic genes (Figure 3.9).

Since it was clear that Rel was the main synthetase during growth in S7+CAA, I reasoned that the primary factor affecting the RsFluc signal was the amino acid limitation the population faced as it exhausted the supplemented amino acids. I hypothesized that lowering the amino acid concentration would cause an earlier peak in RsFluc compared to the 0.01% casamino acids (CAA) used in other assays. Conversely, increasing amino acids should delay the RsFluc peak. This pattern appeared when I conducted the assay (Figure 3.8A). By the same reasoning, I

expected no amino acid supplementation to lead to even higher RsFluc levels, but surprisingly, RsFluc activity remained relatively stable and low (Figure 3.8B). However, compared to the RsFluc^{mut} signal, RsFluc levels are higher (Figure 3.8B), indicating that basal (p)ppGpp levels are elevated under these conditions, and the population is well adapted to synthesize amino acids from S7 nutrients without supplementation.

The hypothesis that increased (p)ppGpp levels contribute to higher amino acid biosynthesis is further supported by the observation that RsFluc activity closely correlates with amino acid biosynthetic reporters in a (p)ppGpp-dependent way (Figure 3.9). When the RsFluc activity spikes, the transcriptional reporters for *the serA*, *ilvB*, and *metE* genes also increase, and this does not happen in a *relA-D264G* background strain. This suggests that elevated (p)ppGpp levels during growth in media without amino acid supplements enhance amino acid biosynthesis gene expression, allowing cells to adapt to the environment without exhausting external amino acids. Therefore, the RsFluc signal in media without supplementation remains high and doesn't exhibit a spike, unlike in media with supplements.

6.1.4 (p)ppGpp and growth arrest

In 3.5, I showed that the rise in RsFluc coincides with a sharp decline in the growth rate (Figure 3.10). I demonstrated that the increase in RsFluc coincides with a decrease in protein synthesis, as measured by OPP labeling, in a (p)ppGpp-dependent manner (Figure 3.11). Previous studies have demonstrated that (p)ppGpp directly inhibits protein synthesis by preventing the translation initiation factor IF2 from binding (71). One of the significant determinants of growth rates in the regulation of protein synthesis is that protein synthesis and growth rates are positively correlated (210).

I hypothesized that the population-level OPP labeling would decrease as RsFluc activity increased due to higher (p)ppGpp levels and the resulting inhibition of protein synthesis caused by this increase in (p)ppGpp. I then proposed that this regulation of protein synthesis would be absent in a (p)ppGpp^0 background, since these cells do not produce (p)ppGpp to inhibit IF2 activity. This pattern was observed in my experiments (Figure 3.11). Notably, this same time point corresponds to a sharp decline in growth rate (Figure 3.10). It is likely that the increase in (p)ppGpp, indicated by higher RsFluc, not only coincides with the decrease in growth, but also directly affects growth mechanisms such as 1.3protein synthesis, DNA replication, and cell division, leading to the overall decline in population growth rate.

6.1.5 Development and characterization of a fluorescent (p)ppGpp reporter

In 4.1.1 and 4.1.2, I discuss the development of a fluorescent *in vivo* riboswitch-based reporter, called RsGFP (Figure 4.1). I then characterized the RsGFP fluorescence throughout growth in S7 and observed that the signal intensified as the cells progressed from the early exponential phase to the transition phase (Figure 4.2). I also noticed that the fluorescence of RsGFP was heterogeneous within the population (Figure 4.2B), indicating variation in (p)ppGpp levels at the single-cell level.

Creating a tool to assess single-cell variation in (p)ppGpp was a top priority when starting this work. Previous research in the lab found that mutations in (p)ppGpp synthetases reduce heterogeneity in protein synthesis rates within the population (71). Other experiments showed that about 1% of cells within a population exhibit high expression of (p)ppGpp synthetase, SasA, and this elevated SasA expression leads to increased antibiotic tolerance (29). At the time of these studies, it was not possible to directly measure (p)ppGpp levels in living cells or at the single-cell level, which would allow testing whether (p)ppGpp levels are linked to heterogeneity

in protein synthesis or increased antibiotic tolerance. Since then, a fluorescent (p)ppGpp reporter has been developed, utilizing a fluorophore-binding RNA motif constructed between the aptamer and the expression platform of the *T. oceani 112 ilvE* riboswitch (171). In this study, variants of the riboswitch with different insertions were characterized to optimize fluorescence signal and ligand specificity *in vitro* and *in vivo*, but some key experiments were missing, such as correlating fluorescence with nucleotide abundance and investigating the mechanism of termination (transcriptional, translational, or otherwise). Because I established these experiments using the RsFluc reporter in Chapter 2, I utilized those findings to develop the RsGFP for assessing (p)ppGpp at the single-cell level. While RsGFP offers clear advantages as a reporter for single-cell studies, it is worth noting that the half-life of GFP is significantly longer than that of luciferase or RNA. The half-life of luciferase in *B. subtilis* is approximately 5 minutes (139). Although mRNA half-lives vary considerably, they are generally less than 7 minutes (211). GFP half-lives have been reported to range from 2 hours (212) to 5.6 hours (213). This complicates the interpretation of the RsGFP signal, as it reflects total (p)ppGpp signaling in a cell rather than the current (p)ppGpp level. Nonetheless, RsGFP fluorescence still provides valuable insights into how (p)ppGpp may influence cell physiology.

6.1.6 Evaluating environmental factors' contribution to heterogeneity in (p)ppGpp within a population

In 4.1.3, I examined how environmental factors, particularly amino acid supplementation in the media, affected the RsGFP signal. I tested RsGFP and RsGFP^{mut} in S7 without supplementation. I observed that the fluorescence intensity of RsGFP increased significantly, varying between the exponential and transition phases in a (p)ppGpp-dependent manner (Figure 4.3). I also tested RsGFP and RsGFP^{mut} in S7+CAA and found that the fluorescence intensity of

RsGFP modestly increased between the exponential and transition phases in a (p)ppGpp-dependent manner (Figure 4.4).

This work was motivated by findings in 3.4.1 that amino acid supplementation in the media affected the kinetics of (p)ppGpp signaling, and that S7 medium without supplementation showed basal, elevated production of RsFluc and thus higher (p)ppGpp levels. Using RsGFP to assess basal, homeostatic (p)ppGpp signaling is particularly helpful due to its increased half-life, as mentioned in Section 6.1.5. While the RsFluc signal does not show significant fluctuations or disruptions to (p)ppGpp production (Figure 3.8B), it's clear that these cells are producing higher amounts of (p)ppGpp, indicated by a substantial increase in RsGFP signal (Figure 4.3). The modest rise in RsGFP fluorescence in S7+CAA was surprising, given the results observed with RsFluc activity (Figure 2.2). This might be due to differences in maturation time between luciferase and GFP. Luminescence increased about 10 minutes after RsFluc transcription (Figure 2.7), suggesting the luciferase protein matures in less than 10 minutes. GFP maturation has been reported to take around 30 minutes (214). Since the RsFluc spike occurs very close to the decline in growth rate that marks the transition phase, sampling RsGFP at this transition may miss increases in fluorescence.

6.1.7 Heterogeneity in transcription profile and (p)ppGpp levels

In 4.2.1, alongside Adam Rosenthal, I examined heterogeneity in (p)ppGpp and transcriptomes in *B. subtilis* using RsFluc reporter sampled for scRNA-seq at the time point before the spike in luminescence in S7+CAA. We showed that at this time point, as determined by FISH assays (Figure 2.7, Figure 4.6), the population divided into distinct subpopulations with different transcriptional signatures (Figure 4.6A). We found that the RsFluc reporter grouped separately in cluster 4 (Figure 4.6B). Cluster 4 was upregulated in specific stress response genes,

including those involved in polyketide synthesis, EPS genes, and genes related to sporulation, competence, and the (p)ppGpp reporter itself (Figure 4.6C). Conversely, cluster 4 was downregulated in genes involved in purine biosynthesis, DNA replication, and cell division (Figure 4.6C).

This collaboration led to the development of a new technique to investigate both (p)ppGpp levels and transcriptional profiles. As detailed in 1.3.2, (p)ppGpp regulates transcription through several mechanisms in bacteria. In *B. subtilis,* this regulation mainly occurs via drops in GTP levels, which affect G start transcripts and alter CodY repression (181). Our assay could offer new insights into novel mechanisms of (p)ppGpp-dependent transcriptional regulation. Additionally, our observations support that (p)ppGpp anti-induces PurR repression of the *purEKBCSQLFMNHD* operon (119), as we saw these genes downregulated in the cluster with high (p)ppGpp (Figure 4.6C), providing new context that this regulation happens at the single-cell level rather than just at the population level, as seen in previous assays.

6.1.8 Single-cell regrowth variation

In 4.2.2, I investigated differential regrowth and (p)ppGpp within a population using the RsGFP reporter and FACS. I observed that the $RsGFP^{high}$ subpopulation experiences slower regrowth after sorting compared to a $RsGFP^{SRS}$ subpopulation (Figure 4.7).

It has long been established that (p)ppGpp inhibits growth by affecting translation, replication, and rRNA transcription, as discussed in 1.3. Growth laws demonstrate a positive correlation between nutrient availability, growth, and the RNA:protein ratio, which is indicative of increased rRNA content (197). This RNA:protein ratio is precisely controlled in growing bacteria through (p)ppGpp signaling to optimize ribosomal biogenesis (198). Some evidence suggests that growth rates can vary significantly within a population (199). Due to limitations in

(p)ppGpp detection methods, directly measuring how heterogeneity in (p)ppGpp contributes to single-cell growth variability was challenging. Using RsGFP and FACS provides a way to test this idea. I demonstrated for the first time that differences in (p)ppGpp levels within a population are linked to differences in regrowth.

6.1.9 Single-cell antibiotic tolerance variation

In 4.2.3, I examined the relationship between antibiotic tolerance and heterogeneity in (p)ppGpp within a population using the RsGFP reporter and FACS. I observed that the $RsGFP^{high}$ subpopulation did not have significantly higher antibiotic tolerance to ciprofloxacin treatment, characterized by a biphasic killing curve, compared to the $RsGFP^{SRS}$ subpopulation (Figure 4.8).

As discussed in 1.3.7, it has often been hypothesized that heterogeneity in (p)ppGpp contributes to the formation of a subpopulation of cells characterized by increased antibiotic tolerance, known as "persisters" (143). Previous methods could not directly assay heterogeneity in (p)ppGpp in single cells, which is necessary to test this hypothesis. Recently, a study found that a shared GTP-(p)ppGpp switch correlates with increased antibiotic tolerance to vancomycin (202). Another study focused on characterizing persisters and found that their transcriptome was consistent with a low protein synthesis group (201), as would be expected in a high (p)ppGpp subpopulation. However, neither of these studies directly assayed (p)ppGpp. The development of the RsGFP reporter offers a solution to this problem and provides a new approach to investigating these hypotheses. I showed that the $RsGFP^{high}$ subpopulation exhibited increased antibiotic tolerance compared to the $RsGFP^{SRS}$ subpopulation, and this $RsGFP^{high}$ also displayed a biphasic killing curve consistent with persister populations (127). This was the first direct demonstration that elevated (p)ppGpp levels are linked to increased antibiotic tolerance. Much

remains to be investigated to fully understand this tolerance, which will be discussed in Section 6.2.5.

6.1.10 Development of a novel technique for labeling cells for protein synthesis and transcriptomics

In Chapter 5, we developed a novel technique, in collaboration with Christopher Baumann and Adam Rosenthal, for studying both transcriptional profiles and physiological states, particularly protein synthesis. We validated this technique by discovering new biology related to AlsR regulation by protein synthesis levels. We demonstrated that when cells were labeled with OPP and a clickable oligo to measure protein synthesis, along with probes for the *B. subtilis* genome, the labeling was differentially enriched in one cluster (Figure 5.1). We then showed that the high OPP cluster also had increased levels of *alsSD* transcripts (Figure 5.2B), which are regulated by the transcriptional activator AlsR (208). Using a functional AlsR-GFP fusion protein (Figure 5.3), I then demonstrated that higher protein synthesis levels were associated with increased AlsR protein levels (Figure 5.4).

This was the first demonstration of a technique that directly links transcriptomic data with physiological states. Additionally, this work uncovered a novel mechanism of transcriptional regulation through variations in protein synthesis rates. We demonstrated that higher protein synthesis rates are associated with increased AlsR, which presumably supports increased *alsSD* transcription. This illustrates transcriptional regulation via differential protein synthesis. Recent studies have shown another example of this regulation in a (p)ppGpp-dependent manner (102).

6.2 Future Directions

6.2.1 Effect of (p)ppGpp on transcriptome in *B. subtilis*

Through the work presented in 4.2.1, (p)ppGpp heterogeneity is shown to be linked to heterogeneity in transcriptomes within a population. Work presented in 5.2.2 demonstrated that heterogeneity in protein synthesis levels leads to heterogeneity in transcriptomes. Recent studies have shown that (p)ppGpp-dependent regulation of protein synthesis affects the transcription of specific genes (102). The heterogeneity observed in (p)ppGpp drives heterogeneity in transcriptomes, rather than merely correlating with it, but the mechanisms underlying this process have yet to be uncovered.

One possible new mechanism demonstrated in this work and others (102) is the regulation of transcriptional activators or repressors through protein synthesis. Another mechanism yet to be investigated involves differential RNA stability in the presence or absence of (p)ppGpp. Recently, a group discovered that NahA, the enzyme that hydrolyzes (p)ppGpp to pGpp, also functions to hydrolyze the 5' cap of mRNAs from tri- ('5-ppp) to monophosphate (5'-p) (40). This 5'-ppp cap is believed to protect mRNAs from RNase degradation (215). Interestingly, *B. subtilis* possesses an additional enzyme that performs this degradation (216) and exhibits a sequence preference for guanosine nucleotide in the second position (217). Due to the structural similarities between the 5'-ppp mRNA and (p)ppGpp molecule, enzyme pyrophosphohydrolase activity on mRNA may be inhibited by (p)ppGpp binding. RsFluc, RsGFP, and other tools and methods explored in this work could facilitate investigations into (p)ppGpp-dependent mechanisms of mRNA stability, which could significantly alter the transcriptomes of cells within a population.

6.2.2 (p)ppGpp triggers in a variety of environmental conditions

Many of these studies discussed in previous sections aimed to investigate (p)ppGpp during natural growth or acute starvation conditions, but many researchers are also interested in the role

of (p)ppGpp across different stresses, such as heat (183) and cold (218) shock responses, osmotic stress (62), and acidic stress (219). RsFluc is a powerful and high-throughput tool that can be used to assess (p)ppGpp signaling in various conditions, including the stressors mentioned or even different nutrient sources.

6.2.3 Exploration of the correlation between RsGFP and similarly clustered genes at the single-cell level

Transcriptomic analysis of a strain containing RsFluc reveals a cluster of cells within the population that are differentially overexpressing the RsFluc reporter gene, as well as a variety of other genes that are differentially regulated. However, it remains unclear whether these genes are being up- or downregulated in a (p)ppGpp-dependent manner. These results warrant further investigation into the role of (p)ppGpp in the differentially regulated genes, such as those involved in sporulation, competence, EPS, and polyketide synthesis, which are upregulated, as well as the DNA replication and cell division genes, which are downregulated (Figure 4.6C).

6.2.4 Investigating the sources of heterogeneity in (p)ppGpp within a population

The mechanisms that cause heterogeneity in RsGFP and consequently in (p)ppGpp production within a population are still unknown. It could result from intrinsic noise or external environmental stimuli. To better understand heterogeneity in a bacterial population and to develop effective therapeutics, researchers should explore the sources driving this variability in (p)ppGpp production. I observed that strains grown in S7 without amino acid supplementation showed high heterogeneity, suggesting that noise in (p)ppGpp production or amino acid biosynthesis could be responsible for the variation. This needs further investigation and should be a focus of future research.

6.2.5 Investigating single-cell variation in (p)ppGpp and antibiotic tolerance

This work demonstrated that a subpopulation of cells expressing high levels of RsGFP was not significantly more tolerant to ciprofloxacin exposure than the overall population. However, these results warrant further investigation to conclusively determine whether heterogeneity in (p)ppGpp drives a subpopulation with increased antibiotic tolerance. First, it is essential to assess the experimental factors that contribute to variability between replicates. There is considerable variability and a high standard deviation across repeats (**Error! Reference source not found.**B), making it necessary to identify the sources of this variation to draw stronger conclusions. Second, some controls are needed for these experiments. It would be especially informative to see whether this pattern persists or disappears in RsGFP^{mut} and RS^{0}-GFP strains, which would help determine if (p)ppGpp signaling causes increased RsGFP or if a less specific mechanism is involved. Lastly, understanding how (p)ppGpp might enhance antibiotic tolerance requires further investigation. Transcriptomic data could identify genes involved in (p)ppGpp-dependent regulatory pathways that lead to increased survival. Alternatively, because (p)ppGpp inhibits replication, ciprofloxacin may be less effective as an antibiotic, as it targets DNA gyrase activity. All of these topics are potential subjects for future research.

6.2.6 Expanding novel click-oligo technique for additional assays

This work introduced a method to measure translation rates and transcriptomes in single cells; however, several other click-chemistry-based labeling assays exist and could be adapted to incorporate specific oligonucleotide probes for multiomic rate-based measurements. A recent study employed click-based oligonucleotide attachment to measure nascent RNA in single eukaryotic cells, utilizing an adapted GRO-seq run-on transcription assay that labeled newly synthesized transcripts with a click moiety (220). In addition to these examples, standard click-chemistry-based EdU assay kits could be adapted to link DNA synthesis rates to single-cell

transcriptomics, and a click-based TUNEL staining kit can be used to measure DNA nicks and free 3’ ends. Together, these physiological measurements can provide context to transcriptomic signatures, which can be challenging to interpret due to dynamic factors such as burst kinetics. Use of these different labels in transcriptomic data should be further explored, similar to the OPP-based translational labeling examined in this work.

References

1. Sands MK, Roberts RB. THE EFFECTS OF A TRYPTOPHAN-HISTIDINE DEFICIENCY IN A MUTANT OF ESCHERICHIA COLI. J Bacteriol. 1952 Apr;63(4):505–511. PMCID: PMC169301
2. Fangman WL, Neidhardt FC. PROTEIN AND RIBONUCLEIC ACID SYNTHESIS IN A MUTANT OF ESCHERICHIA COLI WITH AN ALTERED AMINOACYL RIBONUCLEIC ACID SYNTHETASE. J Biol Chem. 1964 June;239:1844–1847. PMID: 14213363
3. Neidhardt FC. Roles of amino acid activating enzymes in cellular physiology. Bacteriol Rev. 1966 Dec;30(4):701–719. PMCID: PMC441010
4. Gale EF, Folkes JP. The assimilation of amino-acids by bacteria. 15. Actions of antibiotics on nucleic acid and protein synthesis in Staphylococcus aureus. Biochem J. 1953 Feb;53(3):493–498. PMCID: PMC1198178
5. Pardee AB, Prestidge LS. The dependence of nucleic acid synthesis on the presence of amino acids in Escherichia coli. J Bacteriol. 1956 June;71(6):677–683. PMCID: PMC314583
6. Cashel M, Gallant J. Two compounds implicated in the function of the RC gene of Escherichia coli. Nature. 1969 Mar 1;221(5183):838–841. PMID: 4885263
7. Stent GS, Brenner S. A GENETIC LOCUS FOR THE REGULATION OF RIBONUCLEIC ACID SYNTHESIS. Proc Natl Acad Sci U S A. 1961 Dec;47(12):2005–2014. PMCID: PMC223254
8. Cashel M, Kalbacher B. The control of ribonucleic acid synthesis in Escherichia coli. V. Characterization of a nucleotide associated with the stringent response. J Biol Chem. 1970 May 10;245(9):2309–2318. PMID: 4315151
9. Sy J, Lipmann F. Identification of the synthesis of guanosine tetraphosphate (MS I) as insertion of a pyrophosphoryl group into the 3’-position in guanosine 5’-diphosphate. Proc Natl Acad Sci U S A. 1973 Feb;70(2):306–309. PMCID: PMC433245
10. Haseltine WA, Block R. Synthesis of guanosine tetra- and pentaphosphate requires the presence of a codon-specific, uncharged transfer ribonucleic acid in the acceptor site of ribosomes. Proc Natl Acad Sci U S A. 1973 May;70(5):1564–1568. PMCID: PMC433543
11. Rhaese HJ, Dichtelmüller H, Giesel F. Unusual phosphorylated substances associated with sporulation. Spore. 1972;V:174–179.
12. Rhaese HJ, Dichtelmüller H, Grade R. Studies on the control of development. Accumulation of guanosine tetraphosphate and pentaphosphate in response to inhibition of protein synthesis in Bacillus subtilis. Eur J Biochem. 1975 Aug 15;56(2):385–392. PMID: 809277
13. Mittenhuber G. Comparative genomics and evolution of genes encoding bacterial (p)ppGpp synthetases/hydrolases (the Rel, RelA and SpoT proteins). J Mol Microbiol Biotechnol. 2001 Oct;3(4):585–600. PMID: 11545276
14. Atkinson GC, Tenson T, Hauryliuk V. The RelA/SpoT homolog (RSH) superfamily: distribution and functional evolution of ppGpp synthetases and hydrolases across the tree of life. PloS One. 2011;6(8):e23479. PMCID: PMC3153485
15. Heinemeyer EA, Richter D. Mechanism of the in vitro breakdown of guanosine 5’-diphosphate 3’-diphosphate in Escherichia coli. Proc Natl Acad Sci U S A. 1978 Sept;75(9):4180–4183. PMCID: PMC336075

16. Xiao H, Kalman M, Ikehara K, Zemel S, Glaser G, Cashel M. Residual guanosine 3',5'-bispyrophosphate synthetic activity of relA null mutants can be eliminated by spoT null mutations. J Biol Chem. 1991 Mar 25;266(9):5980–5990. PMID: 2005134
17. Wendrich TM, Blaha G, Wilson DN, Marahiel MA, Nierhaus KH. Dissection of the mechanism for the stringent factor RelA. Mol Cell. 2002 Oct;10(4):779–788. PMID: 12419222
18. Loveland AB, Bah E, Madireddy R, Zhang Y, Brilot AF, Grigorieff N, Korostelev AA. Ribosome•RelA structures reveal the mechanism of stringent response activation. eLife. 2016 July 19;5:e17029. PMCID: PMC4974054
19. Hogg T, Mechold U, Malke H, Cashel M, Hilgenfeld R. Conformational antagonism between opposing active sites in a bifunctional RelA/SpoT homolog modulates (p)ppGpp metabolism during the stringent response [corrected]. Cell. 2004 Apr 2;117(1):57–68. PMID: 15066282
20. Takada H, Roghanian M, Murina V, Dzhygyr I, Murayama R, Akanuma G, Atkinson GC, Garcia-Pino A, Hauryliuk V. The C-Terminal RRM/ACT Domain Is Crucial for Fine-Tuning the Activation of "Long" RelA-SpoT Homolog Enzymes by Ribosomal Complexes. Front Microbiol. 2020;11:277. PMCID: PMC7058999
21. Takada H, Roghanian M, Caballero-Montes J, Van Nerom K, Jimmy S, Kudrin P, Trebini F, Murayama R, Akanuma G, Garcia-Pino A, Hauryliuk V. Ribosome association primes the stringent factor Rel for tRNA-dependent locking in the A-site and activation of (p)ppGpp synthesis. Nucleic Acids Res. 2021 Jan 11;49(1):444–457. PMCID: PMC7797070
22. Pausch P, Abdelshahid M, Steinchen W, Schäfer H, Gratani FL, Freibert SA, Wolz C, Turgay K, Wilson DN, Bange G. Structural Basis for Regulation of the Opposing (p)ppGpp Synthetase and Hydrolase within the Stringent Response Orchestrator Rel. Cell Rep. 2020 Sept 15;32(11):108157. PMID: 32937119
23. Shyp V, Tankov S, Ermakov A, Kudrin P, English BP, Ehrenberg M, Tenson T, Elf J, Hauryliuk V. Positive allosteric feedback regulation of the stringent response enzyme RelA by its product. EMBO Rep. 2012 Sept;13(9):835–839. PMCID: PMC3432798
24. Roghanian M, Van Nerom K, Takada H, Caballero-Montes J, Tamman H, Kudrin P, Talavera A, Dzhygyr I, Ekström S, Atkinson GC, Garcia-Pino A, Hauryliuk V. (p)ppGpp controls stringent factors by exploiting antagonistic allosteric coupling between catalytic domains. Mol Cell. 2021 Aug 19;81(16):3310-3322.e6. PMID: 34416138
25. Liu K, Bittner AN, Wang JD. Diversity in (p)ppGpp metabolism and effectors. Curr Opin Microbiol. 2015 Apr;24:72–79. PMCID: PMC4380541
26. Nanamiya H, Kasai K, Nozawa A, Yun CS, Narisawa T, Murakami K, Natori Y, Kawamura F, Tozawa Y. Identification and functional analysis of novel (p)ppGpp synthetase genes in Bacillus subtilis. Mol Microbiol. 2008 Jan;67(2):291–304. PMID: 18067544
27. Eiamphungporn W, Helmann JD. The Bacillus subtilis sigma(M) regulon and its contribution to cell envelope stress responses. Mol Microbiol. 2008 Feb;67(4):830–848. PMCID: PMC3025603
28. D'Elia MA, Millar KE, Bhavsar AP, Tomljenovic AM, Hutter B, Schaab C, Moreno-Hagelsieb G, Brown ED. Probing teichoic acid genetics with bioactive molecules reveals new interactions among diverse processes in bacterial cell wall biogenesis. Chem Biol. 2009 May 29;16(5):548–556. PMID: 19477419

29. Libby EA, Reuveni S, Dworkin J. Multisite phosphorylation drives phenotypic variation in (p)ppGpp synthetase-dependent antibiotic tolerance. Nat Commun. 2019 Nov 13;10(1):5133. PMCID: PMC6853874
30. Steinchen W, Schuhmacher JS, Altegoer F, Fage CD, Srinivasan V, Linne U, Marahiel MA, Bange G. Catalytic mechanism and allosteric regulation of an oligomeric (p)ppGpp synthetase by an alarmone. Proc Natl Acad Sci U S A. 2015 Oct 27;112(43):13348–13353. PMCID: PMC4629338
31. Diez S, Hydorn M, Whalen A, Dworkin J. Crosstalk between guanosine nucleotides regulates cellular heterogeneity in protein synthesis during nutrient limitation. PLoS Genet. 2022 May 20;18(5):e1009957. PMCID: PMC9173625
32. Beljantseva J, Kudrin P, Andresen L, Shingler V, Atkinson GC, Tenson T, Hauryliuk V. Negative allosteric regulation of Enterococcus faecalis small alarmone synthetase RelQ by single-stranded RNA. Proc Natl Acad Sci U S A. 2017 Apr 4;114(14):3726–3731. PMCID: PMC5389274
33. Chen Y, Boggess EE, Ocasio ER, Warner A, Kerns L, Drapal V, Gossling C, Ross W, Gourse RL, Shao Z, Dickerson J, Mansell TJ, Jarboe LR. Reverse engineering of fatty acid-tolerant Escherichia coli identifies design strategies for robust microbial cell factories. Metab Eng. 2020 Sept;61:120–130. PMCID: PMC7501233
34. Roghanian M, Semsey S, Løbner-Olesen A, Jalalvand F. (p)ppGpp-mediated stress response induced by defects in outer membrane biogenesis and ATP production promotes survival in Escherichia coli. Sci Rep. 2019 Feb 27;9(1):2934. PMCID: PMC6393671
35. Potrykus K, Murphy H, Philippe N, Cashel M. ppGpp is the major source of growth rate control in E. coli. Environ Microbiol. 2011 Mar;13(3):563–575. PMCID: PMC4556285
36. Fernández-Coll L, Maciag-Dorszynska M, Tailor K, Vadia S, Levin PA, Szalewska-Palasz A, Cashel M. The Absence of (p)ppGpp Renders Initiation of Escherichia coli Chromosomal DNA Synthesis Independent of Growth Rates. mBio. 2020 Mar 10;11(2):e03223-19. PMCID: PMC7064777
37. Kriel A, Bittner AN, Kim SH, Liu K, Tehranchi AK, Zou WY, Rendon S, Chen R, Tu BP, Wang JD. Direct regulation of GTP homeostasis by (p)ppGpp: a critical component of viability and stress resistance. Mol Cell. 2012 Oct 26;48(2):231–241. PMCID: PMC3483369
38. Yang J, Anderson BW, Turdiev A, Turdiev H, Stevenson DM, Amador-Noguez D, Lee VT, Wang JD. The nucleotide pGpp acts as a third alarmone in Bacillus, with functions distinct from those of (p) ppGpp. Nat Commun. 2020 Oct 23;11(1):5388. PMCID: PMC7584652
39. Fung DK, Yang J, Stevenson DM, Amador-Noguez D, Wang JD. Small Alarmone Synthetase SasA Expression Leads to Concomitant Accumulation of pGpp, ppApp, and AppppA in Bacillus subtilis. Front Microbiol. 2020;11:2083. PMCID: PMC7492591
40. Frindert J, Kahloon MA, Zhang Y, Ahmed YL, Sinning I, Jäschke A. YvcI from Bacillus subtilis has in vitro RNA pyrophosphohydrolase activity. J Biol Chem. 2019 Dec 27;294(52):19967–19977. PMCID: PMC6937576
41. Makman RS, Sutherland EW. ADENOSINE 3',5'-PHOSPHATE IN ESCHERICHIA COLI. J Biol Chem. 1965 Mar;240:1309–1314. PMID: 14284741
42. Ross P, Weinhouse H, Aloni Y, Michaeli D, Weinberger-Ohana P, Mayer R, Braun S, de Vroom E, van der Marel GA, van Boom JH, Benziman M. Regulation of cellulose synthesis in Acetobacter xylinum by cyclic diguanylic acid. Nature. 1987 Jan 15;325(6101):279–281. PMID: 18990795

43. Witte G, Hartung S, Büttner K, Hopfner KP. Structural biochemistry of a bacterial checkpoint protein reveals diadenylate cyclase activity regulated by DNA recombination intermediates. Mol Cell. 2008 Apr 25;30(2):167–178. PMID: 18439896
44. Bochner BR, Lee PC, Wilson SW, Cutler CW, Ames BN. AppppA and related adenylylated nucleotides are synthesized as a consequence of oxidation stress. Cell. 1984 May;37(1):225–232. PMID: 6373012
45. Fung DK, Trinquier AE, Wang JD. Crosstalk between (p)ppGpp and other nucleotide second messengers. Curr Opin Microbiol. 2023 Dec;76:102398. PMCID: PMC10842992
46. Chan C, Paul R, Samoray D, Amiot NC, Giese B, Jenal U, Schirmer T. Structural basis of activity and allosteric control of diguanylate cyclase. Proc Natl Acad Sci U S A. 2004 Dec 7;101(49):17084–17089. PMCID: PMC535365
47. Christen M, Christen B, Folcher M, Schauerte A, Jenal U. Identification and characterization of a cyclic di-GMP-specific phosphodiesterase and its allosteric control by GTP. J Biol Chem. 2005 Sept 2;280(35):30829–30837. PMID: 15994307
48. Chang AL, Tuckerman JR, Gonzalez G, Mayer R, Weinhouse H, Volman G, Amikam D, Benziman M, Gilles-Gonzalez MA. Phosphodiesterase A1, a regulator of cellulose synthesis in Acetobacter xylinum, is a heme-based sensor. Biochemistry. 2001 Mar 27;40(12):3420–3426. PMID: 11297407
49. Gjermansen M, Ragas P, Sternberg C, Molin S, Tolker-Nielsen T. Characterization of starvation-induced dispersion in Pseudomonas putida biofilms. Environ Microbiol. 2005 June;7(6):894–906. PMID: 15892708
50. Drenkard E, Ausubel FM. Pseudomonas biofilm formation and antibiotic resistance are linked to phenotypic variation. Nature. 2002 Apr 18;416(6882):740–743. PMID: 11961556
51. Hengge R. Principles of c-di-GMP signalling in bacteria. Nat Rev Microbiol. 2009 Apr;7(4):263–273. PMID: 19287449
52. Shyp V, Dubey BN, Böhm R, Hartl J, Nesper J, Vorholt JA, Hiller S, Schirmer T, Jenal U. Reciprocal growth control by competitive binding of nucleotide second messengers to a metabolic switch in Caulobacter crescentus. Nat Microbiol. 2021 Jan;6(1):59–72. PMID: 33168988
53. Gundlach J, Mehne FMP, Herzberg C, Kampf J, Valerius O, Kaever V, Stülke J. An Essential Poison: Synthesis and Degradation of Cyclic Di-AMP in Bacillus subtilis. J Bacteriol. 2015 Oct;197(20):3265–3274. PMCID: PMC4573722
54. Commichau FM, Heidemann JL, Ficner R, Stülke J. Making and Breaking of an Essential Poison: the Cyclases and Phosphodiesterases That Produce and Degrade the Essential Second Messenger Cyclic di-AMP in Bacteria. J Bacteriol. 2019 Jan 1;201(1):e00462-18. PMCID: PMC6287462
55. Pham TH, Liang ZX, Marcellin E, Turner MS. Replenishing the cyclic-di-AMP pool: regulation of diadenylate cyclase activity in bacteria. Curr Genet. 2016 Nov;62(4):731–738. PMID: 27074767
56. Huynh TN, Woodward JJ. Too much of a good thing: regulated depletion of c-di-AMP in the bacterial cytoplasm. Curr Opin Microbiol. 2016 Apr;30:22–29. PMCID: PMC4821758
57. Zarrella TM, Bai G. The Many Roles of the Bacterial Second Messenger Cyclic di-AMP in Adapting to Stress Cues. J Bacteriol. 2020 Dec 7;203(1):e00348-20. PMCID: PMC7723955
58. Pham HT, Nhiep NTH, Vu TNM, Huynh TN, Zhu Y, Huynh ALD, Chakrabortti A, Marcellin E, Lo R, Howard CB, Bansal N, Woodward JJ, Liang ZX, Turner MS. Enhanced uptake of potassium or glycine betaine or export of cyclic-di-AMP restores osmoresistance

in a high cyclic-di-AMP Lactococcus lactis mutant. PLoS Genet. 2018 Aug;14(8):e1007574. PMCID: PMC6108528
59. Rao F, See RY, Zhang D, Toh DC, Ji Q, Liang ZX. YybT is a signaling protein that contains a cyclic dinucleotide phosphodiesterase domain and a GGDEF domain with ATPase activity. J Biol Chem. 2010 Jan 1;285(1):473–482. PMCID: PMC2804195
60. Corrigan RM, Bowman L, Willis AR, Kaever V, Gründling A. Cross-talk between two nucleotide-signaling pathways in Staphylococcus aureus. J Biol Chem. 2015 Feb 27;290(9):5826–5839. PMCID: PMC4342491
61. Peterson BN, Young MKM, Luo S, Wang J, Whiteley AT, Woodward JJ, Tong L, Wang JD, Portnoy DA. (p)ppGpp and c-di-AMP Homeostasis Is Controlled by CbpB in Listeria monocytogenes. mBio. 2020 Aug 25;11(4):e01625-20. PMCID: PMC8549634
62. Krüger L, Herzberg C, Wicke D, Bähre H, Heidemann JL, Dickmanns A, Schmitt K, Ficner R, Stülke J. A meet-up of two second messengers: the c-di-AMP receptor DarB controls (p)ppGpp synthesis in Bacillus subtilis. Nat Commun. 2021 Feb 22;12(1):1210. PMCID: PMC7900238
63. Poudel A, Pokhrel A, Oludiran A, Coronado EJ, Alleyne K, Gilfus MM, Gurung RK, Adhikari SB, Purcell EB. Unique Features of Alarmone Metabolism in Clostridioides difficile. J Bacteriol. 2022 Apr 19;204(4):e0057521. PMCID: PMC9017329
64. Gaca AO, Kudrin P, Colomer-Winter C, Beljantseva J, Liu K, Anderson B, Wang JD, Rejman D, Potrykus K, Cashel M, Hauryliuk V, Lemos JA. From (p)ppGpp to (pp)pGpp: Characterization of Regulatory Effects of pGpp Synthesized by the Small Alarmone Synthetase of Enterococcus faecalis. J Bacteriol. 2015 Sept;197(18):2908–2919. PMCID: PMC4542164
65. Anderson BW, Fung DK, Wang JD. Regulatory Themes and Variations by the Stress-Signaling Nucleotide Alarmones (p)ppGpp in Bacteria. Annu Rev Genet. 2021 Nov 23;55:115–133. PMID: 34416118
66. Rodnina MV. Translation in Prokaryotes. Cold Spring Harb Perspect Biol. 2018 Sept 4;10(9):a032664. PMCID: PMC6120702
67. Bange G, Brodersen DE, Liuzzi A, Steinchen W. Two P or Not Two P: Understanding Regulation by the Bacterial Second Messengers (p)ppGpp. Annu Rev Microbiol. 2021 Oct 8;75:383–406. PMID: 34343020
68. Hamel E, Cashel M. Guanine nucleotides in protein synthesis. Utilization of pppGpp and dGTP by initiation factor 2 and elongation factor Tu. Arch Biochem Biophys. 1974 May;162(1):293–300. PMID: 4598531
69. Milon P, Tischenko E, Tomsic J, Caserta E, Folkers G, La Teana A, Rodnina MV, Pon CL, Boelens R, Gualerzi CO. The nucleotide-binding site of bacterial translation initiation factor 2 (IF2) as a metabolic sensor. Proc Natl Acad Sci U S A. 2006 Sept 19;103(38):13962–13967. PMCID: PMC1599896
70. Mitkevich VA, Ermakov A, Kulikova AA, Tankov S, Shyp V, Soosaar A, Tenson T, Makarov AA, Ehrenberg M, Hauryliuk V. Thermodynamic characterization of ppGpp binding to EF-G or IF2 and of initiator tRNA binding to free IF2 in the presence of GDP, GTP, or ppGpp. J Mol Biol. 2010 Oct 8;402(5):838–846. PMID: 20713063
71. Diez S, Ryu J, Caban K, Gonzalez RL, Dworkin J. The alarmones (p)ppGpp directly regulate translation initiation during entry into quiescence. Proc Natl Acad Sci U S A. 2020 July 7;117(27):15565–15572. PMCID: PMC7354938

72. Persky NS, Ferullo DJ, Cooper DL, Moore HR, Lovett ST. The ObgE/CgtA GTPase influences the stringent response to amino acid starvation in Escherichia coli. Mol Microbiol. 2009 July;73(2):253–266. PMCID: PMC2771346
73. Rodnina MV, Wintermeyer W. GTP consumption of elongation factor Tu during translation of heteropolymeric mRNAs. Proc Natl Acad Sci U S A. 1995 Mar 14;92(6):1945–1949. PMCID: PMC42399
74. Rodnina MV, Beringer M, Wintermeyer W. How ribosomes make peptide bonds. Trends Biochem Sci. 2007 Jan;32(1):20–26. PMID: 17157507
75. Holtkamp W, Cunha CE, Peske F, Konevega AL, Wintermeyer W, Rodnina MV. GTP hydrolysis by EF-G synchronizes tRNA movement on small and large ribosomal subunits. EMBO J. 2014 May 2;33(9):1073–1085. PMCID: PMC4193938
76. Hamel E, Cashel M. Role of guanine nucleotides in protein synthesis. Elongation factor G and guanosine 5'-triphosphate,3'-diphosphate. Proc Natl Acad Sci U S A. 1973 Nov;70(11):3250–3254. PMCID: PMC427210
77. Legault L, Jeantet C, Gros F. Inhibition of in vitro protein synthesis by ppGpp. FEBS Lett. 1972 Oct 15;27(1):71–75. PMID: 11946810
78. Miller DL, Cashel M, Weissbach H. The interaction of guanosine 5'-diphosphate, 2' (3')-diphosphate with the bacterial elongation factor Tu. Arch Biochem Biophys. 1973 Feb;154(2):675–682. PMID: 4570843
79. Rojas AM, Ehrenberg M, Andersson SG, Kurland CG. ppGpp inhibition of elongation factors Tu, G and Ts during polypeptide synthesis. Mol Gen Genet MGG. 1984;197(1):36–45. PMID: 6392824
80. Mc K, H K, A K. Ribosome recycling: An essential process of protein synthesis. Biochem Mol Biol Educ Bimon Publ Int Union Biochem Mol Biol [Internet]. Biochem Mol Biol Educ; 2007 Jan [cited 2025 July 14];35(1). Available from: https://pubmed.ncbi.nlm.nih.gov/21591054/ PMID: 21591054
81. Coatham ML, Brandon HE, Fischer JJ, Schümmer T, Wieden HJ. The conserved GTPase HflX is a ribosome splitting factor that binds to the E-site of the bacterial ribosome. Nucleic Acids Res. 2016 Feb 29;44(4):1952–1961. PMCID: PMC4770234
82. Zhang Y, Mandava CS, Cao W, Li X, Zhang D, Li N, Zhang Y, Zhang X, Qin Y, Mi K, Lei J, Sanyal S, Gao N. HflX is a ribosome-splitting factor rescuing stalled ribosomes under stress conditions. Nat Struct Mol Biol. 2015 Nov;22(11):906–913. PMID: 26458047
83. Zhang Y, Zborníková E, Rejman D, Gerdes K. Novel (p)ppGpp Binding and Metabolizing Proteins of Escherichia coli. mBio. 2018 Mar 6;9(2):e02188-17. PMCID: PMC5845004
84. Corrigan RM, Bellows LE, Wood A, Gründling A. ppGpp negatively impacts ribosome assembly affecting growth and antimicrobial tolerance in Gram-positive bacteria. Proc Natl Acad Sci U S A. 2016 Mar 22;113(12):E1710-1719. PMCID: PMC4812758
85. Ross W, Vrentas CE, Sanchez-Vazquez P, Gaal T, Gourse RL. The magic spot: a ppGpp binding site on E. coli RNA polymerase responsible for regulation of transcription initiation. Mol Cell. 2013 May 9;50(3):420–429. PMCID: PMC3654024
86. Muchmore CR, Krahn JM, Kim JH, Zalkin H, Smith JL. Crystal structure of glutamine phosphoribosylpyrophosphate amidotransferase from Escherichia coli. Protein Sci Publ Protein Soc. 1998 Jan;7(1):39–51. PMCID: PMC2143822
87. Ross W, Sanchez-Vazquez P, Chen AY, Lee JH, Burgos HL, Gourse RL. ppGpp Binding to a Site at the RNAP-DksA Interface Accounts for Its Dramatic Effects on Transcription

Initiation during the Stringent Response. Mol Cell. 2016 June 16;62(6):811–823. PMCID: PMC4912440
88. Paul BJ, Barker MM, Ross W, Schneider DA, Webb C, Foster JW, Gourse RL. DksA: a critical component of the transcription initiation machinery that potentiates the regulation of rRNA promoters by ppGpp and the initiating NTP. Cell. 2004 Aug 6;118(3):311–322. PMID: 15294157
89. Paul BJ, Berkmen MB, Gourse RL. DksA potentiates direct activation of amino acid promoters by ppGpp. Proc Natl Acad Sci U S A. 2005 May 31;102(22):7823–7828. PMCID: PMC1142371
90. Lemke JJ, Durfee T, Gourse RL. DksA and ppGpp directly regulate transcription of the Escherichia coli flagellar cascade. Mol Microbiol. 2009 Dec;74(6):1368–1379. PMCID: PMC2806482
91. My L, Rekoske B, Lemke JJ, Viala JP, Gourse RL, Bouveret E. Transcription of the Escherichia coli fatty acid synthesis operon fabHDG is directly activated by FadR and inhibited by ppGpp. J Bacteriol. 2013 Aug;195(16):3784–3795. PMCID: PMC3754556
92. Lemke JJ, Sanchez-Vazquez P, Burgos HL, Hedberg G, Ross W, Gourse RL. Direct regulation of Escherichia coli ribosomal protein promoters by the transcription factors ppGpp and DksA. Proc Natl Acad Sci U S A. 2011 Apr 5;108(14):5712–5717. PMCID: PMC3078377
93. Barker MM, Gaal T, Josaitis CA, Gourse RL. Mechanism of regulation of transcription initiation by ppGpp. I. Effects of ppGpp on transcription initiation in vivo and in vitro. J Mol Biol. 2001 Jan 26;305(4):673–688. PMID: 11162084
94. Barker MM, Gaal T, Gourse RL. Mechanism of regulation of transcription initiation by ppGpp. II. Models for positive control based on properties of RNAP mutants and competition for RNAP. J Mol Biol. 2001 Jan 26;305(4):689–702. PMID: 11162085
95. Haugen SP, Berkmen MB, Ross W, Gaal T, Ward C, Gourse RL. rRNA promoter regulation by nonoptimal binding of sigma region 1.2: an additional recognition element for RNA polymerase. Cell. 2006 June 16;125(6):1069–1082. PMID: 16777598
96. Krásný L, Gourse RL. An alternative strategy for bacterial ribosome synthesis: Bacillus subtilis rRNA transcription regulation. EMBO J. 2004 Nov 10;23(22):4473–4483. PMCID: PMC526457
97. Sonenshein AL. CodY, a global regulator of stationary phase and virulence in Gram-positive bacteria. Curr Opin Microbiol. 2005 Apr;8(2):203–207. PMID: 15802253
98. Bergara F, Ibarra C, Iwamasa J, Patarroyo JC, Aguilera R, Márquez-Magaña LM. CodY is a nutritional repressor of flagellar gene expression in Bacillus subtilis. J Bacteriol. 2003 May;185(10):3118–3126. PMCID: PMC154071
99. Molle V, Nakaura Y, Shivers RP, Yamaguchi H, Losick R, Fujita Y, Sonenshein AL. Additional targets of the Bacillus subtilis global regulator CodY identified by chromatin immunoprecipitation and genome-wide transcript analysis. J Bacteriol. 2003 Mar;185(6):1911–1922. PMCID: PMC150151
100. Serror P, Sonenshein AL. CodY is required for nutritional repression of Bacillus subtilis genetic competence. J Bacteriol. 1996 Oct;178(20):5910–5915. PMCID: PMC178446
101. Kriel A, Brinsmade SR, Tse JL, Tehranchi AK, Bittner AN, Sonenshein AL, Wang JD. GTP dysregulation in Bacillus subtilis cells lacking (p)ppGpp results in phenotypic amino acid auxotrophy and failure to adapt to nutrient downshift and regulate biosynthesis genes. J Bacteriol. 2014 Jan;196(1):189–201. PMCID: PMC3911124

102. Nagarajan SN, Rosenthal A, Dworkin J. (p)ppGpp-dependent activation of gene expression during nutrient limitation [Internet]. bioRxiv; 2025 [cited 2025 July 22]. p. 2025.04.25.650602. Available from: https://www.biorxiv.org/content/10.1101/2025.04.25.650602v1
103. Schreiber G, Ron EZ, Glaser G. ppGpp-mediated regulation of DNA replication and cell division in Escherichia coli. Curr Microbiol. 1995 Jan;30(1):27–32. PMID: 7765879
104. Levine A, Vannier F, Dehbi M, Henckes G, Séror SJ. The stringent response blocks DNA replication outside the ori region in Bacillus subtilis and at the origin in Escherichia coli. J Mol Biol. 1991 June 20;219(4):605–613. PMID: 1905358
105. Wang JD, Sanders GM, Grossman AD. Nutritional control of elongation of DNA replication by (p)ppGpp. Cell. 2007 Mar 9;128(5):865–875. PMCID: PMC1850998
106. Denapoli J, Tehranchi AK, Wang JD. Dose-dependent reduction of replication elongation rate by (p)ppGpp in Escherichia coli and Bacillus subtilis. Mol Microbiol. 2013 Apr;88(1):93–104. PMCID: PMC3640871
107. Kamarthapu V, Epshtein V, Benjamin B, Proshkin S, Mironov A, Cashel M, Nudler E. ppGpp couples transcription to DNA repair in E. coli. Science. 2016 May 20;352(6288):993–996. PMCID: PMC4917784
108. McGlynn P, Lloyd RG. Modulation of RNA polymerase by (p)ppGpp reveals a RecG-dependent mechanism for replication fork progression. Cell. 2000 Mar 31;101(1):35–45. PMID: 10778854
109. Rudner R, Murray A, Huda N. Is there a link between mutation rates and the stringent response in Bacillus subtilis? Ann N Y Acad Sci. 1999 May 18;870:418–422. PMID: 10415512
110. Wright BE. The effect of the stringent response on mutation rates in Escherichia coli K-12. Mol Microbiol. 1996 Jan;19(2):213–219. PMID: 8825767
111. Trautinger BW, Jaktaji RP, Rusakova E, Lloyd RG. RNA polymerase modulators and DNA repair activities resolve conflicts between DNA replication and transcription. Mol Cell. 2005 July 22;19(2):247–258. PMID: 16039593
112. Bharati BK, Gowder M, Zheng F, Alzoubi K, Svetlov V, Kamarthapu V, Weaver JW, Epshtein V, Vasilyev N, Shen L, Zhang Y, Nudler E. Crucial role and mechanism of transcription-coupled DNA repair in bacteria. Nature. 2022 Apr;604(7904):152–159. PMCID: PMC9370829
113. Weaver JW, Proshkin S, Duan W, Epshtein V, Gowder M, Bharati BK, Afanaseva E, Mironov A, Serganov A, Nudler E. Control of transcription elongation and DNA repair by alarmone ppGpp. Nat Struct Mol Biol. 2023 May;30(5):600–607. PMCID: PMC10191844
114. Kingston RE, Nierman WC, Chamberlin MJ. A direct effect of guanosine tetraphosphate on pausing of Escherichia coli RNA polymerase during RNA chain elongation. J Biol Chem. 1981 Mar 25;256(6):2787–2797. PMID: 7009598
115. Krohn M, Wagner R. Transcriptional pausing of RNA polymerase in the presence of guanosine tetraphosphate depends on the promoter and gene sequence. J Biol Chem. 1996 Sept 27;271(39):23884–23894. PMID: 8798619
116. Tedin K, Norel F. Comparison of DeltarelA strains of Escherichia coli and Salmonella enterica serovar Typhimurium suggests a role for ppGpp in attenuation regulation of branched-chain amino acid biosynthesis. J Bacteriol. 2001 Nov;183(21):6184–6196. PMCID: PMC100096

117. Lemos JA, Lin VK, Nascimento MM, Abranches J, Burne RA. Three gene products govern (p)ppGpp production by Streptococcus mutans. Mol Microbiol. 2007 Sept;65(6):1568–1581. PMID: 17714452
118. Wang B, Grant RA, Laub MT. ppGpp Coordinates Nucleotide and Amino-Acid Synthesis in E. coli During Starvation. Mol Cell. 2020 Oct 1;80(1):29-42.e10. PMCID: PMC8362273
119. Anderson BW, Schumacher MA, Yang J, Turdiev A, Turdiev H, Schroeder JW, He Q, Lee VT, Brennan RG, Wang JD. The nucleotide messenger (p)ppGpp is an anti-inducer of the purine synthesis transcription regulator PurR in Bacillus. Nucleic Acids Res. 2022 Jan 25;50(2):847–866. PMCID: PMC8789054
120. Ontai-Brenning A, Hamchand R, Crawford JM, Goodman AL. Gut microbes modulate (p)ppGpp during a time-restricted feeding regimen. mBio. 2023 Nov 16;e0190723. PMID: 37971266
121. Kundra S, Colomer-Winter C, Lemos JA. Survival of the Fittest: The Relationship of (p)ppGpp With Bacterial Virulence. Front Microbiol. 2020;11:601417. PMCID: PMC7744563
122. Chen E, Shaffer MG, Bilodeau RE, West RE, Oberly PJ, Nolin TD, Culyba MJ. Clinical rel mutations in Staphylococcus aureus prime pathogen expansion under nutrient stress. mSphere. 2023 Sept 26;e0024923. PMID: 37750686
123. Geiger T, Goerke C, Fritz M, Schäfer T, Ohlsen K, Liebeke M, Lalk M, Wolz C. Role of the (p)ppGpp synthase RSH, a RelA/SpoT homolog, in stringent response and virulence of Staphylococcus aureus. Infect Immun. 2010 May;78(5):1873–1883. PMCID: PMC2863498
124. Kazmierczak KM, Wayne KJ, Rechtsteiner A, Winkler ME. Roles of rel(Spn) in stringent response, global regulation and virulence of serotype 2 Streptococcus pneumoniae D39. Mol Microbiol. 2009 May;72(3):590–611. PMCID: PMC2739083
125. Klinkenberg LG, Lee JH, Bishai WR, Karakousis PC. The stringent response is required for full virulence of Mycobacterium tuberculosis in guinea pigs. J Infect Dis. 2010 Nov 1;202(9):1397–1404. PMCID: PMC2949470
126. Xu X, Yu H, Zhang D, Xiong J, Qiu J, Xin R, He X, Sheng H, Cai W, Jiang L, Zhang K, Hu X. Role of ppGpp in Pseudomonas aeruginosa acute pulmonary infection and virulence regulation. Microbiol Res. 2016 Nov;192:84–95. PMID: 27664726
127. Balaban NQ, Helaine S, Lewis K, Ackermann M, Aldridge B, Andersson DI, Brynildsen MP, Bumann D, Camilli A, Collins JJ, Dehio C, Fortune S, Ghigo JM, Hardt WD, Harms A, Heinemann M, Hung DT, Jenal U, Levin BR, Michiels J, Storz G, Tan MW, Tenson T, Van Melderen L, Zinkernagel A. Definitions and guidelines for research on antibiotic persistence. Nat Rev Microbiol. 2019 July;17(7):441–448. PMCID: PMC7136161
128. Hartman BJ, Tomasz A. Low-affinity penicillin-binding protein associated with beta-lactam resistance in Staphylococcus aureus. J Bacteriol. 1984 May;158(2):513–516. PMCID: PMC215458
129. Aedo S, Tomasz A. Role of the Stringent Stress Response in the Antibiotic Resistance Phenotype of Methicillin-Resistant Staphylococcus aureus. Antimicrob Agents Chemother. 2016 Apr;60(4):2311–2317. PMCID: PMC4808156
130. Takada H, Mandell ZF, Yakhnin H, Glazyrina A, Chiba S, Kurata T, Wu KJY, Tresco BIC, Myers AG, Aktinson GC, Babitzke P, Hauryliuk V. Expression of Bacillus subtilis ABCF antibiotic resistance factor VmlR is regulated by RNA polymerase pausing,

transcription attenuation, translation attenuation and (p)ppGpp. Nucleic Acids Res. 2022 June 24;50(11):6174–6189. PMCID: PMC9226507
131. Singh M, Matsuo M, Sasaki T, Morimoto Y, Hishinuma T, Hiramatsu K. In Vitro Tolerance of Drug-Naive Staphylococcus aureus Strain FDA209P to Vancomycin. Antimicrob Agents Chemother. 2017 Feb;61(2):e01154-16. PMCID: PMC5278750
132. Honsa ES, Cooper VS, Mhaissen MN, Frank M, Shaker J, Iverson A, Rubnitz J, Hayden RT, Lee RE, Rock CO, Tuomanen EI, Wolf J, Rosch JW. RelA Mutant Enterococcus faecium with Multiantibiotic Tolerance Arising in an Immunocompromised Host. mBio. 2017 Jan 3;8(1):e02124-16. PMCID: PMC5210501
133. Bryson D, Hettle AG, Boraston AB, Hobbs JK. Clinical Mutations That Partially Activate the Stringent Response Confer Multidrug Tolerance in Staphylococcus aureus. Antimicrob Agents Chemother. 2020 Feb 21;64(3):e02103-19. PMCID: PMC7038295
134. Gaca AO, Kajfasz JK, Miller JH, Liu K, Wang JD, Abranches J, Lemos JA. Basal levels of (p)ppGpp in Enterococcus faecalis: the magic beyond the stringent response. mBio. 2013 Sept 24;4(5):e00646-00613. PMCID: PMC3781836
135. Salzer A, Keinhörster D, Kästle C, Kästle B, Wolz C. Small Alarmone Synthetases RelP and RelQ of Staphylococcus aureus Are Involved in Biofilm Formation and Maintenance Under Cell Wall Stress Conditions. Front Microbiol. 2020;11:575882. PMCID: PMC7533549
136. Pokhrel A, Poudel A, Castro KB, Celestine MJ, Oludiran A, Rinehold AJ, Resek AM, Mhanna MA, Purcell EB. The (p)ppGpp Synthetase RSH Mediates Stationary-Phase Onset and Antibiotic Stress Survival in Clostridioides difficile. J Bacteriol. 2020 Sept 8;202(19):e00377-20. PMCID: PMC7484180
137. Yang J, Barra JT, Fung DK, Wang JD. Bacillus subtilis produces (p)ppGpp in response to the bacteriostatic antibiotic chloramphenicol to prevent its potential bactericidal effect. mLife. 2022;1(2):101–113.
138. Spira B, Ospino K. Diversity in E. coli (p)ppGpp Levels and Its Consequences. Front Microbiol. 2020;11:1759. PMCID: PMC7434938
139. Mirouze N, Prepiak P, Dubnau D. Fluctuations in spo0A transcription control rare developmental transitions in Bacillus subtilis. PLoS Genet. 2011 Apr;7(4):e1002048. PMCID: PMC3084206
140. Balaban NQ. Persistence: mechanisms for triggering and enhancing phenotypic variability. Curr Opin Genet Dev. 2011 Dec;21(6):768–775. PMID: 22051606
141. Dworkin J, Harwood CS. Metabolic Reprogramming and Longevity in Quiescence. Annu Rev Microbiol. 2022 Sept 8;76:91–111. PMID: 35417196
142. Pacios O, Blasco L, Bleriot I, Fernandez-Garcia L, Ambroa A, López M, Bou G, Cantón R, Garcia-Contreras R, Wood TK, Tomás M. (p)ppGpp and Its Role in Bacterial Persistence: New Challenges. Antimicrob Agents Chemother. 2020 Sept 21;64(10):e01283-20. PMCID: PMC7508602
143. Salzer A, Wolz C. Role of (p)ppGpp in antibiotic resistance, tolerance, persistence and survival in Firmicutes. microLife. 2023;4:uqad009. PMCID: PMC10117726
144. Balaban NQ, Gerdes K, Lewis K, McKinney JD. A problem of persistence: still more questions than answers? Nat Rev Microbiol. 2013 Aug;11(8):587–591. PMID: 24020075
145. Kaldalu N, Hauryliuk V, Tenson T. Persisters-as elusive as ever. Appl Microbiol Biotechnol. 2016 Aug;100(15):6545–6553. PMCID: PMC4939303

146. Randerath K, Randerath E. ION-EXCHANGE CHROMATOGRAPHY OF NUCLEOTIDES ON POLY-(ETHYLENEIMINE)-CELLULOSE THIN LAYERS. J Chromatogr. 1964 Oct;16:111–125. PMID: 14226338
147. Kuroda A, Murphy H, Cashel M, Kornberg A. Guanosine tetra- and pentaphosphate promote accumulation of inorganic polyphosphate in Escherichia coli. J Biol Chem. 1997 Aug 22;272(34):21240–21243. PMID: 9261133
148. Payne SH, Ames BN. A procedure for rapid extraction and high-pressure liquid chromatographic separation of the nucleotides and other small molecules from bacterial cells. Anal Biochem. 1982 June;123(1):151–161. PMID: 7051895
149. Varik V, Oliveira SRA, Hauryliuk V, Tenson T. HPLC-based quantification of bacterial housekeeping nucleotides and alarmone messengers ppGpp and pppGpp. Sci Rep. 2017 Sept 8;7(1):11022. PMCID: PMC5591245
150. Zborníková E, Knejzlík Z, Hauryliuk V, Krásný L, Rejman D. Analysis of nucleotide pools in bacteria using HPLC-MS in HILIC mode. Talanta. 2019 Dec 1;205:120161. PMID: 31450400
151. Cassels R, Oliva B, Knowles D. Occurrence of the regulatory nucleotides ppGpp and pppGpp following induction of the stringent response in staphylococci. J Bacteriol. 1995 Sept;177(17):5161–5165. PMCID: PMC177300
152. Kavita K, Breaker RR. Discovering riboswitches: the past and the future. Trends Biochem Sci. 2023 Feb;48(2):119–141. PMCID: PMC10043782
153. Nahvi A, Sudarsan N, Ebert MS, Zou X, Brown KL, Breaker RR. Genetic control by a metabolite binding mRNA. Chem Biol. 2002 Sept;9(9):1043. PMID: 12323379
154. Mandal M, Breaker RR. Gene regulation by riboswitches. Nat Rev Mol Cell Biol. 2004 June;5(6):451–463. PMID: 15173824
155. McCown PJ, Corbino KA, Stav S, Sherlock ME, Breaker RR. Riboswitch diversity and distribution. RNA N Y N. 2017 July;23(7):995–1011. PMCID: PMC5473149
156. Vitreschak AG, Rodionov DA, Mironov AA, Gelfand MS. Riboswitches: the oldest mechanism for the regulation of gene expression? Trends Genet TIG. 2004 Jan;20(1):44–50. PMID: 14698618
157. Breaker RR. Riboswitches: from ancient gene-control systems to modern drug targets. Future Microbiol. 2009 Sept;4(7):771–773. PMCID: PMC5340290
158. Breaker RR. Riboswitches and the RNA world. Cold Spring Harb Perspect Biol. 2012 Feb 1;4(2):a003566. PMCID: PMC3281570
159. Breaker RR. The Biochemical Landscape of Riboswitch Ligands. Biochemistry. 2022 Feb 1;61(3):137–149. PMCID: PMC9971707
160. Breaker RR. Prospects for riboswitch discovery and analysis. Mol Cell. 2011 Sept 16;43(6):867–879. PMCID: PMC4140403
161. Weiss CA, Hoberg JA, Liu K, Tu BP, Winkler WC. Single-Cell Microscopy Reveals That Levels of Cyclic di-GMP Vary among Bacillus subtilis Subpopulations. J Bacteriol. 2019 Aug 15;201(16):e00247-19. PMCID: PMC6657594
162. Nelson JW, Plummer MS, Blount KF, Ames TD, Breaker RR. Small molecule fluoride toxicity agonists. Chem Biol. 2015 Apr 23;22(4):527–534. PMCID: PMC4617673
163. Perkins KR, Atilho RM, Moon MH, Breaker RR. Employing a ZTP Riboswitch to Detect Bacterial Folate Biosynthesis Inhibitors in a Small Molecule High-Throughput Screen. ACS Chem Biol. 2019 Dec 20;14(12):2841–2850. PMCID: PMC8023010

164. Barth KM, Hiller DA, Belem de Andrade G, Kavita K, Fernando CM, Breaker RR, Strobel SA. Decoding the Complex Functional Landscape of the ykkC Riboswitches. Biochemistry. 2025 Apr 20; PMID: 40254862
165. Sherlock ME, Sudarsan N, Stav S, Breaker RR. Tandem riboswitches form a natural Boolean logic gate to control purine metabolism in bacteria. eLife. 2018 Mar 5;7:e33908. PMCID: PMC5912903
166. Nelson JW, Atilho RM, Sherlock ME, Stockbridge RB, Breaker RR. Metabolism of Free Guanidine in Bacteria Is Regulated by a Widespread Riboswitch Class. Mol Cell. 2017 Jan 19;65(2):220–230. PMCID: PMC5360189
167. Sherlock ME, Sadeeshkumar H, Breaker RR. Variant Bacterial Riboswitches Associated with Nucleotide Hydrolase Genes Sense Nucleoside Diphosphates. Biochemistry. 2019 Feb 5;58(5):401–410. PMCID: PMC6713212
168. Sherlock ME, Sudarsan N, Breaker RR. Riboswitches for the alarmone ppGpp expand the collection of RNA-based signaling systems. Proc Natl Acad Sci U S A. 2018 June 5;115(23):6052–6057. PMCID: PMC6003355
169. Reiss CW, Xiong Y, Strobel SA. Structural Basis for Ligand Binding to the Guanidine-I Riboswitch. Struct Lond Engl 1993. 2017 Jan 3;25(1):195–202. PMCID: PMC5317007
170. Jagodnik J, Tjaden B, Ross W, Gourse RL. Identification and characterization of RNA binding sites for (p)ppGpp using RNA-DRaCALA. Nucleic Acids Res. 2023 Jan 25;51(2):852–869. PMCID: PMC9881157
171. Sun Z, Wu R, Zhao B, Zeinert R, Chien P, You M. Live-Cell Imaging of Guanosine Tetra- and Pentaphosphate (p)ppGpp with RNA-based Fluorescent Sensors*. Angew Chem Int Ed Engl. 2021 Nov 2;60(45):24070–24074. PMCID: PMC8545912
172. Hydorn M, Nagarajan SN, Fones E, Harwood CS, Dworkin J. Analysis of (p)ppGpp metabolism and signaling using a dynamic luminescent reporter. PLoS Genet. 2025 Aug;21(8):e1011691. PMCID: PMC12373219
173. Wendrich TM, Marahiel MA. Cloning and characterization of a relA/spoT homologue from Bacillus subtilis. Mol Microbiol. 1997 Oct;26(1):65–79. PMID: 9383190
174. Sørensen MA. Charging levels of four tRNA species in Escherichia coli Rel(+) and Rel(-) strains during amino acid starvation: a simple model for the effect of ppGpp on translational accuracy. J Mol Biol. 2001 Mar 30;307(3):785–798. PMID: 11273701
175. Zhu M, Dai X. Stringent response ensures the timely adaptation of bacterial growth to nutrient downshift. Nat Commun. 2023 Jan 28;14(1):467. PMCID: PMC9884231
176. Dittmar KA, Sørensen MA, Elf J, Ehrenberg M, Pan T. Selective charging of tRNA isoacceptors induced by amino-acid starvation. EMBO Rep. 2005 Feb;6(2):151–157. PMCID: PMC1299251
177. Hughes J, Mellows G. Inhibition of isoleucyl-transfer ribonucleic acid synthetase in Escherichia coli by pseudomonic acid. Biochem J. 1978 Oct 15;176(1):305–318. PMCID: PMC1186229
178. Fernández-Coll L, Cashel M. Contributions of SpoT Hydrolase, SpoT Synthetase, and RelA Synthetase to Carbon Source Diauxic Growth Transitions in Escherichia coli. Front Microbiol. 2018;9:1802. PMCID: PMC6085430
179. Traxler MF, Chang DE, Conway T. Guanosine 3’,5’-bispyrophosphate coordinates global gene expression during glucose-lactose diauxie in Escherichia coli. Proc Natl Acad Sci U S A. 2006 Feb 14;103(7):2374–2379. PMCID: PMC1413745
180. Monod J. Recherches sur la croissance des cultures bactériennes. Hermann; 1942.

181. Srivatsan A, Wang JD. Control of bacterial transcription, translation and replication by (p)ppGpp. Curr Opin Microbiol. 2008 Apr;11(2):100–105. PMID: 18359660
182. Srivatsan A, Han Y, Peng J, Tehranchi AK, Gibbs R, Wang JD, Chen R. High-precision, whole-genome sequencing of laboratory strains facilitates genetic studies. PLoS Genet. 2008 Aug 1;4(8):e1000139. PMCID: PMC2474695
183. Schäfer H, Beckert B, Frese CK, Steinchen W, Nuss AM, Beckstette M, Hantke I, Driller K, Sudzinová P, Krásný L, Kaever V, Dersch P, Bange G, Wilson DN, Turgay K. The alarmones (p)ppGpp are part of the heat shock response of Bacillus subtilis. PLoS Genet. 2020 Mar;16(3):e1008275. PMCID: PMC7098656
184. Radeck J, Kraft K, Bartels J, Cikovic T, Dürr F, Emenegger J, Kelterborn S, Sauer C, Fritz G, Gebhard S, Mascher T. The Bacillus BioBrick Box: generation and evaluation of essential genetic building blocks for standardized work with Bacillus subtilis. J Biol Eng. 2013 Dec 2;7(1):29. PMCID: PMC4177231
185. Scott M, Gunderson CW, Mateescu EM, Zhang Z, Hwa T. Interdependence of cell growth and gene expression: origins and consequences. Science. 2010 Nov 19;330(6007):1099–1102. PMID: 21097934
186. Ackermann M. A functional perspective on phenotypic heterogeneity in microorganisms. Nat Rev Microbiol. 2015 Aug;13(8):497–508. PMID: 26145732
187. Elowitz MB, Levine AJ, Siggia ED, Swain PS. Stochastic gene expression in a single cell. Science. 2002 Aug 16;297(5584):1183–1186. PMID: 12183631
188. Rosenthal AZ, Qi Y, Hormoz S, Park J, Li SHJ, Elowitz MB. Metabolic interactions between dynamic bacterial subpopulations. eLife. 2018 May 29;7:e33099. PMCID: PMC6025961
189. Pavlou A, Cinquemani E, Pinel C, Giordano N, Mathilde VMG, Mihalcescu I, Geiselmann J, de Jong H. Single-cell data reveal heterogeneity of investment in ribosomes across a bacterial population. Nat Commun. 2025 Jan 2;16(1):285. PMCID: PMC11695989
190. McNulty R, Sritharan D, Pahng SH, Meisch JP, Liu S, Brennan MA, Saxer G, Hormoz S, Rosenthal AZ. Probe-based bacterial single-cell RNA sequencing predicts toxin regulation. Nat Microbiol. 2023 May;8(5):934–945. PMCID: PMC10159851
191. Kuchina A, Brettner LM, Paleologu L, Roco CM, Rosenberg AB, Carignano A, Kibler R, Hirano M, DePaolo RW, Seelig G. Microbial single-cell RNA sequencing by split-pool barcoding. Science. 2021 Feb 19;371(6531):eaba5257. PMCID: PMC8269303
192. Ma P, Amemiya HM, He LL, Gandhi SJ, Nicol R, Bhattacharyya RP, Smillie CS, Hung DT. Bacterial droplet-based single-cell RNA-seq reveals antibiotic-associated heterogeneous cellular states. Cell. 2023 Feb 16;186(4):877-891.e14. PMCID: PMC10014032
193. Imdahl F, Vafadarnejad E, Homberger C, Saliba AE, Vogel J. Single-cell RNA-sequencing reports growth-condition-specific global transcriptomes of individual bacteria. Nat Microbiol. 2020 Oct;5(10):1202–1206. PMID: 32807892
194. Blattman SB, Jiang W, Oikonomou P, Tavazoie S. Prokaryotic single-cell RNA sequencing by in situ combinatorial indexing. Nat Microbiol. 2020 Oct;5(10):1192–1201. PMCID: PMC8330242
195. Wang B, Lin AE, Yuan J, Novak KE, Koch MD, Wingreen NS, Adamson B, Gitai Z. Single-cell massively-parallel multiplexed microbial sequencing (M3-seq) identifies rare bacterial populations and profiles phage infection. Nat Microbiol. 2023 Aug 31; PMID: 37653008

196. Samanta P, Cooke SF, McNulty R, Hormoz S, Rosenthal A. ProBac-seq, a bacterial single-cell RNA sequencing methodology using droplet microfluidics and large oligonucleotide probe sets. Nat Protoc. 2024 Oct;19(10):2939–2966. PMID: 38769144
197. Scott M, Hwa T. Bacterial growth laws and their applications. Curr Opin Biotechnol. 2011 Aug;22(4):559–565. PMCID: PMC3152618
198. Bosdriesz E, Molenaar D, Teusink B, Bruggeman FJ. How fast-growing bacteria robustly tune their ribosome concentration to approximate growth-rate maximization. FEBS J. 2015 May;282(10):2029–2044. PMCID: PMC4672707
199. Brettner L, Geiler-Samerotte K. Single-cell heterogeneity in ribosome content and the consequences for the growth laws. BioRxiv Prepr Serv Biol. 2024 Oct 8;2024.04.19.590370. PMCID: PMC11185559
200. Kaspy I, Rotem E, Weiss N, Ronin I, Balaban NQ, Glaser G. HipA-mediated antibiotic persistence via phosphorylation of the glutamyl-tRNA-synthetase. Nat Commun. 2013;4:3001. PMID: 24343429
201. Blattman SB, Jiang W, McGarrigle ER, Liu M, Oikonomou P, Tavazoie S. Identification and genetic dissection of convergent persister cell states. Nature. 2024 Dec;636(8042):438–446. PMCID: PMC11634777
202. Fung DK, Barra JT, Yang J, Schroeder JW, She F, Young M, Ying D, Stevenson DM, Amador-Noguez D, Wang JD. A shared alarmone-GTP switch controls persister formation in bacteria. Nat Microbiol. 2025 July;10(7):1617–1629. PMCID: PMC12221987
203. Baumann C, Hydorn M, Cooke SF, Dworkin J, Rosenthal AZ. Simultaneous measurements of translation rate and transcriptome in single bacterial cells by scTR-seq uncovers linked regulation within a specialized active cell population [Internet]. bioRxiv; 2025 [cited 2025 Aug 21]. p. 2025.04.22.649982. Available from: https://www.biorxiv.org/content/10.1101/2025.04.22.649982v1
204. Walls AW, Rosenthal AZ. Bacterial phenotypic heterogeneity through the lens of single-cell RNA sequencing. Transcription. 2024;15(1–2):48–62. PMCID: PMC11093040
205. Weinreb C, Wolock S, Tusi BK, Socolovsky M, Klein AM. Fundamental limits on dynamic inference from single-cell snapshots. Proc Natl Acad Sci U S A. 2018 Mar 6;115(10):E2467–E2476. PMCID: PMC5878004
206. Pisithkul T, Schroeder JW, Trujillo EA, Yeesin P, Stevenson DM, Chaiamarit T, Coon JJ, Wang JD, Amador-Noguez D. Metabolic Remodeling during Biofilm Development of Bacillus subtilis. mBio. 2019 May 21;10(3):e00623-19. PMCID: PMC6529636
207. Tran P, Lander SM, Prindle A. Active pH regulation facilitates Bacillus subtilis biofilm development in a minimally buffered environment. mBio. 2024 Mar 13;15(3):e0338723. PMCID: PMC10936434
208. Härtig E, Frädrich C, Behringer M, Hartmann A, Neumann-Schaal M, Jahn D. Functional definition of the two effector binding sites, the oligomerization and DNA binding domains of the Bacillus subtilis LysR-type transcriptional regulator AlsR. Mol Microbiol. 2018 Sept;109(6):845–864. PMID: 30039521
209. Dworkin J. Understanding the Stringent Response: Experimental Context Matters. mBio. 2023 Feb 28;14(1):e0340422. PMCID: PMC9973329
210. Scott M, Klumpp S, Mateescu EM, Hwa T. Emergence of robust growth laws from optimal regulation of ribosome synthesis. Mol Syst Biol. 2014 Aug 22;10(8):747. PMCID: PMC4299513

211. Hambraeus G, von Wachenfeldt C, Hederstedt L. Genome-wide survey of mRNA half-lives in Bacillus subtilis identifies extremely stable mRNAs. Mol Genet Genomics MGG. 2003 Aug;269(5):706–714. PMID: 12884008
212. Syvertsson S, Wang B, Staal J, Gao Y, Kort R, Hamoen LW. Different Resource Allocation in a Bacillus subtilis Population Displaying Bimodal Motility. J Bacteriol. 203(12):e00037-21. PMCID: PMC8316123
213. Rosenberg A, Sinai L, Smith Y, Ben-Yehuda S. Dynamic Expression of the Translational Machinery during Bacillus subtilis Life Cycle at a Single Cell Level. PLoS ONE. 2012 July 25;7(7):e41921. PMCID: PMC3405057
214. Cormack BP, Valdivia RH, Falkow S. FACS-optimized mutants of the green fluorescent protein (GFP). Gene. 1996;173(1 Spec No):33–38. PMID: 8707053
215. Mathy N, Bénard L, Pellegrini O, Daou R, Wen T, Condon C. 5'-to-3' exoribonuclease activity in bacteria: role of RNase J1 in rRNA maturation and 5' stability of mRNA. Cell. 2007 May 18;129(4):681–692. PMID: 17512403
216. Richards J, Liu Q, Pellegrini O, Celesnik H, Yao S, Bechhofer DH, Condon C, Belasco JG. An RNA pyrophosphohydrolase triggers 5'-exonucleolytic degradation of mRNA in Bacillus subtilis. Mol Cell. 2011 Sept 16;43(6):940–949. PMCID: PMC3176438
217. Piton J, Larue V, Thillier Y, Dorléans A, Pellegrini O, Li de la Sierra-Gallay I, Vasseur JJ, Debart F, Tisné C, Condon C. Bacillus subtilis RNA deprotection enzyme RppH recognizes guanosine in the second position of its substrates. Proc Natl Acad Sci U S A. 2013 May 28;110(22):8858–8863. PMCID: PMC3670357
218. Jones PG, Cashel M, Glaser G, Neidhardt FC. Function of a relaxed-like state following temperature downshifts in Escherichia coli. J Bacteriol. 1992 June;174(12):3903–3914. PMCID: PMC206098
219. Kanjee U, Gutsche I, Alexopoulos E, Zhao B, El Bakkouri M, Thibault G, Liu K, Ramachandran S, Snider J, Pai EF, Houry WA. Linkage between the bacterial acid stress and stringent responses: the structure of the inducible lysine decarboxylase. EMBO J. 2011 Mar 2;30(5):931–944. PMCID: PMC3049219
220. Mahat DB, Tippens ND, Martin-Rufino JD, Waterton SK, Fu J, Blatt SE, Sharp PA. Single-cell nascent RNA sequencing unveils coordinated global transcription. Nature. 2024 July;631(8019):216–223. PMCID: PMC11222150
221. Middleton R, Hofmeister A. New shuttle vectors for ectopic insertion of genes into Bacillus subtilis. Plasmid. 2004 May;51(3):238–245. PMID: 15109830
222. Patrick JE, Kearns DB. Laboratory strains of Bacillus subtilis do not exhibit swarming motility. J Bacteriol. 2009 Nov;191(22):7129–7133. PMCID: PMC2772471
223. Ducret A, Quardokus EM, Brun YV. MicrobeJ, a tool for high throughput bacterial cell detection and quantitative analysis. Nat Microbiol. 2016 June 20;1(7):16077. PMCID: PMC5010025

Appendix A: Materials and methods

Strain construction

Strains were derived from *B. subtilis* 168 *trpC2* except as noted and are listed in Table 1. Strains were constructed by transformation using conventional methodology and where necessary, media was supplemented with either 100 µg/mL spectinomycin, 10 µg/mL kanamycin, 5 µg/mL chloramphenicol, or 1X MLS. Reporters at *sacA* were constructed using pSac-cm (221) derived plasmids (Table 2), confirmed via whole plasmid sequencing via Plasmidsaurus or Genewiz, and *sacA* integration was confirmed by assaying growth on TSS/glc and nongrowth on TSS sucrose plates. Constructs at *amyE* were constructed using pDG1730 derived plasmids, confirmed via whole plasmid sequencing, and *amyE* integration was confirmed by assaying on LB starch plates. Bacitracin-inducible constructs were designed as described previously (184), using P_{liaI} promoter upstream of induced gene (Table 2). Marker free site-directed mutagenesis of the *B. subtilis* chromosome was done using pMINIMad2 methodology as described (222), confirming via whole plasmid sequencing and mutated locus sequence by amplification and Sanger sequencing (Genewiz).

(p)ppGpp reporter construction

The various (p)ppGpp reporter strains were constructed by fusing their respective gBlocks (Table 3) downstream of IPTG-inducible promoter, $P_{hyperspank}$, and upstream of firefly luciferase or GFPmut2 gene, using a pSac-cm cloning vector via conventional restriction enzyme and Gibson assembly cloning techniques. Plasmids were sequenced verified and are listed in Table 2. The vectors were transformed into *B. subtilis*, selecting on LB Agar supplemented with 5 µg/mL chloramphenicol, and *sacA* integration was verified using TSS/glc and TSS sucrose plating.

Media composition

S7 media is composed of 1X MOPS (Teknova), 1.32 mM K_2HPO_4, 1% glucose, 0.1% glutamic acid, 40 µg/mL L-Trp. S7+CAA media is composed of 1X MOPS (Teknova), 1.32 mM K_2HPO_4, 1% glucose, 0.1% glutamic acid, 0.01% casamino acids, 40 µg/mL L-Trp.

Luminescence measurements

Luminescence was measured in a Tecan Infinite M200 Pro instrument with continuous shaking at 37°C, taking OD_{600} and luminescence reads every 10 minutes. Cultures were grown from single colonies grown overnight on LB plates at 37°C. Single colonies were picked into 2 mL S7+CAA (1X MOPS (Teknova), 1.32 mM K_2HPO_4, 1% glucose, 0.1% glutamic acid, 0.01% casamino acids, 40 µg/mL L-Trp), unless otherwise stated, and grown at 37°C in a roller drum for ~3.5 hours. OD_{600} measurements were taken to ensure colonies remained in early exponential phase (between OD_{600} 0.3-0.6). The cultures were then diluted to OD_{600}=0.05 in 0.5 mL fresh S7+CAA supplemented with 4.7 mM D-luciferin (Goldbio) and 10 µM IPTG (Goldbio). Note that a spectrophotometer OD_{600} reading of 0.05 is equivalent to a plate reader reading of ~0.01. Cultures were aliquoted in triplicate in wells amounting 150 µL each in a 96-well white-walled, flat and clear bottom plate (Greiner Bio-One). Media only cells were used for background subtraction.

HPLC-MS nucleotide quantification

Cultures were grown from single colonies grown overnight on LB plates at 37°C. Single colonies were picked into 2 mL S7+CAA and grown at 37°C in a roller drum for ~3.5 hours. OD_{600}

measurements were taken to ensure colonies remained in early exponential phase (between OD_{600} 0.3-0.6). The cultures were back diluted to OD_{600} 0.05 in 20 mL S7+CAA supplemented with 4.7mM D-luciferin and 10μM IPTG in baffled flasks. The cultures were incubated at 37°C with shaking in a water bath. At 120, 180, and 300 min, 450 μL were sampled for measuring luminescence and OD_{600} via Tecan Infinite M200 Pro plate reader, aliquoting 150 μL in triplicate wells. Media only wells were used for background subtraction. Simultaneously, 5 mL of culture were concentrated on 0.2 μm pore (d = 0.47 mm) cellulose acetate membrane filter (Sartorius) via vacuum filtration. The filter was immediately washed with 1 mL ice cold 1M acetic acid solution containing 1 μg/mL ^{15}N-ATP (Sigma) and 1 μg/mL ^{15}N-GTP (Sigma) in a 50 mL conical tube, repeatedly washing the solution over the filter surface using the force of a pipette. Conical tubes were vortexed for 3-5 seconds, and the solution was transferred to 2 mL cryo-vials. Solutions were stored at -80°C. Cold acid nucleotide extractions were performed by thawing samples on ice for 60 minutes, vortexing occasionally. Samples were then re-frozen using liquid nitrogen and lyophilized for 6 hours using a VirTis Benchtop Freeze Dryer. Lyophilized samples were dissolved in 200 μl ice-cold HPLC-grade water, centrifuged at maximum speed for 30 minutes, and clear supernatant was collected for quantification via UHPLC-MS/MS.

UHPLC-MS/MS was performed using an ACQUITY Premier UPLC System coupled with a Waters XEVO TQ-S triple quadrupole mass spectrometer. UPLC was performed on a Hypercarb 2.1x50 mm porous graphitic carbon column (3 μm particle size) using a 10-90% linear gradient of solvent B (0.1% ammonium hydroxide in acetonitrile) in solvent A (0.1 ammonium acetate in water, adjusted to pH 9.5 with ammonium hydroxide) within 10 minutes and a flow rate of 0.3

ml/min. MS/MS analysis was operated in negative ionization mode and a multiple reaction monitoring (MRM) mode was adopted. MassLynx was used to quantify peak intensities.

Amino acid downshift

After 60 min growth in the plate reader, cultures were collected in sterile microcentrifuge tubes, pelleted by centrifugation, and resuspended in equal volume of S7 lacking CAA. Cultures were returned to the plate reader, taking OD_{600} and luminescence reads every 10 minutes for remainder of assay.

Mupirocin treatment

After 90 min growth in plate reader, mupirocin was added to the cultures at noted concentrations, and OD_{600} and luminescence measurements were resumed for remainder of assay.

Diauxic shift

Cultures were grown in either 2.5 mg/ml glucose or a mixture of 0.5 mg/mL glucose and 2.0 mg/mL arabinose.

OPP Labeling

Click-iT Plus OPP Protein Synthesis Assay Kit (Invitrogen) was used to label cells with OPP following manufacturer's instructions. 1000 µL of cells at given time points were transferred to disposable glass tubes. OPP was added to a final concentration of 10 µM. OPP incorporation was performed at 37 ºC on a roller drum for 20 min and all subsequent steps were done at RT. Cells were fixed by adding formaldehyde to a final concentration of 1%. Cells were fixed for 30 min,

harvested by centrifugation at 15k x *g* for 3 mins, and permeabilized using 100 µL of 0.5% Triton X-100 in PBS for 15 min. Cells were labelled using 100 µL of 1X Click-iT cocktail for 20 min in the dark. Cells were harvested and washed one time using Click-iT rinse buffer and then re-suspended in 20-100 µL of PBS for imaging.

Fluorescence *in situ* hybridization (FISH)

yfp FISH probes (Table 3) were designed and synthesized with CAL Fluor® Red 590 Dye (LGC Biosearch Technologies). FISH imaging was performed as described (190) with minor modifications. Briefly, 2 ml cells from mid or late-log cultures grown in S7+CAA media were collected and fixed with 1% formaldehyde (final concentration) at room temperature for 30 min. The cells were then harvested by centrifugation at 6000 RPM for 3 min at room temperature and washed with 0.02% saline sodium citrate (SSC, Invitrogen). The cell pellets were resuspended in 300 µl MAAM mix (4:1 V:V dilution of methanol to glacial acetic acid) and incubated at -20 ℃ for 15 minutes, followed by 1X PBS (from 10X PBS, Invitrogen) wash to remove traces of MAAM. Cells were permeabilized in 200µl PBS containing 350 U µl-1 of lysozyme (Epicenter ready-lyse) for 30 min at 37°C. After permeabilization, cells were washed once with 500 µl PBS. The cells were resuspended in 100 µl Stellaris® RNA FISH Hybridization Buffer containing 10% formamide and 12.5 µM reconstituted *yfp* oligo probes for hybridization. The cell-probe mix was incubated in a 30°C water bath overnight. Cells were harvested and washed with 500 µl of reconstituted Stellaris® RNA FISH Wash Buffer A containing 10% formamide and incubated at 30°C water bath for 1 hour. The washing step was repeated one more time to remove the excess probe. The cells were harvested and resuspended in 0.5 ml Stellaris® RNA FISH Wash Buffer B and incubated for 5 minutes at room temperature. Finally, the cells were harvested and

resuspended in 20-40 µl of PBS with 1µl SlowFade™ Gold Antifade Mountant (Invitrogen). A non-fluorescent control strain, treated with *yfp* probes, was used as a control to subtract background and autofluorescence in each channel. Phase contrast and fluorescence images (mCherry (ET Sputter Ex560/40 Dm585 Em630/75)) of bacterial cells immobilized on agarose pads were acquired.

Microscopy

Microscopy was performed on cells immobilized on 1% agarose pads prepared with PBS. Imaging was performed using a Nikon 90i microscope with a Phase contrast objective (CFI Plan Apo Lambda DM ×100 Oil, NA 1.45), an X-Cite light source, a Hamamatsu Orca ER-AG, and the following filter cubes: mCherry (ET Sputter Ex560/40 Dm585 Em630/75), FITC (ET Sputter Ex480/40 Dm505 Em510/0). Phase contrast and fluorescence images of bacterial cells immobilized on agarose pads were acquired. The image stacks were analyzed in the software Fiji with the help of the MicrobeJ plugin (223). The straighten and intensity options in the MicrobeJ plugin were used to measure the average fluorescence per pixel within each cell. A non-fluorescent control strain was used to subtract background and autofluorescence in each channel.

Fluorescence-activated cell sorting (FACS)

Adapted from (29). Cultures were grown to early log phase and diluted 100-fold with additional S7 media to obtain the optimal density of 1×10^{-6} cells/mL for flow cytometry. The resulting samples were vortexed vigorously prior to measurement to disrupt aggregates. Flow cytometry and sorting were performed on a BD Biosciences FACS Aria II-SORP. GFP was detected using a blue laser (488 nm) with a 525/50 dichroic, and a 505 long pass filter. Fluorescence values

were quantitatively compared between experiments by rescaling each experiment by the mean fluorescence of a control sample. Sorting was performed with a 70 μm nozzle at 70 PSI. Detection voltages were set such that the non-fluorescent control had a median value of ~100. The sorting thresholds were chosen such that the "high" expression gate corresponds to approximately 5% of the starting population and can be sorted in ~10 min. The simple random sample (SRS) was a selection of cells in the population at random and can be sorted in ~30 sec.

Survival assays

Adapted from (29). 2.0×10^4 cells were sorted by fluorescence and dispensed into 2 mL of defined growth media (S7). Cultures were incubated in a roller drum at 37 °C for 15 min, then 1 mL was treated with 1 μg/ml ciprofloxacin for 1.5 h. Serial dilutions of each population were plated for colony forming units (CFUs) on LB every 15 mins and grown overnight at 30 °C and survival ratios were calculated by comparing the CFU/mL values between the initial CFU/mL count and subsequent counts.

Appendix B: Strains, plasmids, and oligos

Table 1. Strain list

Strain	Genotype	Source
JDB3	*Prototroph (PY79)*	Lab collection
JDB1772	*trpC2*	Lab collection
JDE3129	*MG1655 rpoZ-kanR rpoC-tetAR (1+, 2+)*	Gourse Lab
JDE3168	*MG1655 relA::kanR spoT::catR*	Gourse Lab
JDB4294	*trpC2 relA::erm sasA(ywaC)::kan yjbM::tet*	(71)
JDB4300	*trpC2 relA-Y308A*	(71)
JDB4440	*trpC2 yjbM-F42A*	(31)
JDB4525	*trpC2 relA-Y200A*	This thesis
JDB4729	*trpC2 relA D264G*	This thesis
JDB4496	*trpC2 sacA::$P_{hyperspank}$-ilvE riboswitch-luciferase cmR*	This thesis
JDB4512	*relA::erm ywaC::kan yjbM::tet sacA::$P_{hyperspank}$-D. hafniense ilvE riboswitch-luciferase-cmR*	This thesis
JDB4631	*trpC2 sacA::$P_{hyperspank}$-M9+M11 riboswitch-luciferase-cmR*	This thesis
JDB4524	*trpC2 sacA::Phyperspank-luciferase-cmR*	This thesis
JDB4599	*trpC2 sacA::Phyperspank-M9 riboswitch-luciferase-cm*	This thesis
JDB4522	*trpC2 sacA::Phyperspank-M11 riboswitch-firefly luciferase-cm*	This thesis
JDB4730	*trpC2 sacA::Phyperspank-Clostridiales natA riboswitch-luciferase-cmR*	This thesis
JDB4731	*trpC2 sacA::Phyperspank-Oxobacter pfennigii livK riboswitch-luciferase-cmR*	This thesis
JDB4508	*trpC2 ywaC::kan yjbM::tet sacA::Phyperspank-D. hafniense ilvE riboswitch-luciferase-cmR*	This thesis

JDB4515	*trpC2 ywaC::kan sacA::Phyperspank-D. hafniense ilvE riboswitch-firefly luciferase-cmR*	This thesis
JDB4516	*trpC2 yjbM::tet sacA::Phyperspank-D. hafniense ilvE riboswitch-firefly luciferase-cmR*	This thesis
JDB4741	*trpC2 relA D264G sacA::Phyperspank-D. hafniense ilvE riboswitch-luciferase-cmR*	This thesis
JDB4568	*trpC2 ykuL::kan sacA::Phyperspank-D. hafniense ilvE riboswitch-luciferase-cmR*	This thesis
JDB4675	*trpC2 relA::erm ywaC::kan yjbM::tet sacA::Phyperspank-D. hafniense ilvE riboswitch-luciferase-cmR amyE::PliaI-relA-specR*	This thesis
JDB4676	*trpC2 relA::erm ywaC::kan yjbM::tet sacA::Phyperspank-D. hafniense ilvE riboswitch-luciferase-cmR amyE::PliaI-relA D78A-specR*	This thesis
JDB4567	*trpC2 yvcI::erm sacA::Phyperspank-D. hafniense ilvE riboswitch-luciferase-cmR*	This thesis
JDB4568	*trpC2 ykuL::kan sacA::Phyperspank-D. hafniense ilvE riboswitch-luciferase-cmR*	This thesis
JDB4711	*trpC2 yjbM F42A sacA::Phyperspank-D. hafniense ilvE riboswitch-luciferase-cmR*	This thesis
JDB4528	*trpC2 relA Y200A sacA::Phyperspank-D. hafniense ilvE riboswitch-luciferase-cmR*	This thesis
JDB4656	*PY79 sacA::Phyperspank-D. hafniense ilvE riboswitch-luciferase-cmR*	This thesis
JDB4657	*PY79 sacA::Phyperspank-M9+M11 riboswitch-luciferase-cmR*	This thesis
JDB4759	*trpC2 sacA::PserA-luciferase-cmR*	This thesis
JDB4765	*trpC2 sacA::PhomA-luciferase-cmR*	This thesis
JDB4792	*trpC2 sacA::PilvB-luciferase-cmR*	This thesis

JDB4798	*trpC2 sacA::PmetE-luciferase-cmR*	This thesis
JDB4793	*trpC2 relA D264G sacA::PserA-luciferase-cmR*	This thesis
JDB4794	*trpC2 relA D264G sacA::PhomA-luciferase-cmR*	This thesis
JDB4795	*trpC2 relA D264G sacA::PilvB-luciferase-cmR*	This thesis
JDB4799	*trpC2 relA D264G sacA::PmetE-luciferase-cmR*	This thesis
JDB4803	*trpC2 sacA::PpurE-luciferase-cmR*	This thesis
JDB4804	*trpC2 relA Y308A ywaC::kan yjbM::tet sacA::PpurE-firefly -cmR*	This thesis
JDB4303	*trpC2 sacA::Phyperspank-D. hafniense ilvE. riboswitch-yfp-cmR*	This thesis
JDB4623	*trpC2 sacA::Phyperspank-D. hafniense ilvE. riboswitch-yfp-cmR amyE::P Phyperspank-D. hafniense ilvE. riboswitch-luciferase-specR*	This thesis
JDB4784	*trpC2 sacA::PalsS-luciferase-cmR*	This thesis
JDB4786	*trpC2 alsR::alsR-GFP*	This thesis
JDB4787	*trpC2 sacA::PalsS-luciferase-cmR alsR::alsR-GFP*	This thesis
JDB4632	*trpC2 sacA::Phyperspank-D. hafniense ilvE riboswitch-gfpmut2-cmR*	This thesis
JDB4661	*trpC2 sacA::Phyperspank-M9+M11 riboswitch-gfpmut2-cmR*	This thesis
DS3290	*PY79 amyE::Phyperspank-lytF-specR*	Kearns Lab
JDB4839	*trpC2 amyE::Phyperspank-lytF-specR*	This thesis
JDB4841	*trpC2 sacA::Phyperspank-D. hafniense ilvE riboswitch-gfpmut2-cmR amyE::Phyperspank-lytF-specR*	This thesis
JDE3185	*MG1655 pMH11-ampR rpoZ-kanR rpoC-tetAR (1+, 2+)*	This thesis
JDE3187	*MG1655 pMH11-ampR relA::kanR spoT::catR*	This thesis

Table 2. Plasmid list

Plasmid	**Description**	**Source**
pSac-cm	*B. subtilis sacA* integration vector	Lab collection

pDR111	Vector for Phyperspank integration at *B. subtilis amyE*	Lab collection
pMINIMad2	Chromosomal integration of a mutation in *B. subtilis*	Lab collection
pGL3	Vector containing firefly luciferase gene	Lab collection
pEL47	pSac-cm-Phyperspank	Lab collection
pMH9	pSac-cm-Phyperspank-(p)ppGpp riboswitch-yfp	This thesis
pMH11	pSac-cm-Phyperspank-(p)ppGpp riboswitch-firefly luciferase	This thesis
pMH13	pSac-cm-Phyperspank-M9 riboswitch-firefly luciferase	This thesis
pMH15	pSac-cm-Phyperspank-M11 riboswitch-firefly luciferase	This thesis
pMH16	pSac-cm-Phyperspank-firefly luciferase	This thesis
pMH17	pMINIMad2 relA Y200A	This thesis
pMH25	pDG1730-Phyperspank-(p)ppGpp riboswitch-firefly luciferase	This thesis
pMH31	pSac-cm-Phyperspank-M9+M11 riboswitch-firefly luciferase	This thesis
pMH39	pDG1730-PliaI-relA	This thesis
pMH40	pDG1730-PliaI-relA D78A	This thesis
pMH42	pMINIMad2 relA D264G	This thesis
pMH45	pSac-cm-Phyperspank-pppGpp riboswitch-firefly luciferase	This thesis
pMH46	pSac-cm-Phyperspank-ppGpp riboswitch-firefly luciferase	This thesis

pMH50	pSac-cm-PserA-firefly luciferase	This thesis
pMH67	pSac-cm-PilvB-firefly luciferase	This thesis
pMH68	pSac-cm-PmetE-firefly luciferase	This thesis
pSN27	pSac-cm-PpurE-firefly luciferase	This thesis
pMH62	pKL147-alsR 3' frag-GFP	This thesis
pMH63	pSac-cm-PalsS-firefly luciferase	This thesis
pMH35	pSac-cm-Phyperspank-(p)ppGpp riboswitch-GFPmut2	This thesis
pMH38	pSac-cm-Phyperspank-M9+M11 riboswitch-GFPmut2	This thesis

Table 3. Oligo list

Source	Number	Name	Sequence
(27)	MES153	IDT G-block containing the WT D. hafniense ilvE riboswitch and controlled by the B. subtilis lysC promoter, for serving as a dsDNA template for in vitro transcription termination assays	GCGCACATGAGAATTCCAGCGACGCTGTT GATCCTTTTAAATAAGTCTGATAAAATGT GAACTAAAGTTATAAATGAAAGAATGTAT TATAACAGCAGGAAGTGTACCTAGGGTTC CGGGAGCTGCTCCGTCTGGTCCGAGCGGT ACAAAATCCAGAGCATGGATTTACACCGT GGGCAGAAAATACCCGAGCGGAAAGTTCC TCGAGAGGGTAGGAACACCGCTCGGTTTT CTATAATATTCAGAGGATCCCCAGCTGCG C
This thesis		ilvE riboswitch gBlock	AGTTATAAATGAAAGAATGTATTATAACA GCAGGAAGTGTACCTAGGGTTCCGGGAGC TGCTCCGTCTGGTCCGAGCGGTACAAAAT CCAGAGCATGGATTTACACCGTGGGCAGA AAATACCCGAGCGGAAAGTTCCTCGAGAG GGTAGGAACACCGCTCGGTTTTCTATAAT ATTCAGAGGATCCCCAGCTGCGC
This thesis		natA riboswitch gBlock	ACTGTCAAGCTTCAATCATATTATAATATT AACAATAAGAGAGTGTATCTAGGGTTCCG GTCAATAGATGTCTGGTCCGAGCGATACA

			GGATTTCAATCTACACTTTTAGGAAAAAA GCCTAAAGGACGAGTCTCTGCAAAGAGAT TTGTTCTTGGGCTTTATTTTTTTATCTTTAT TTAAGGGGGCGGCCGCTGAGTC
This thesis		livK riboswitch gBlock	AGTCTGAAGCTTTAATTTATAATGACAAA TTAATTATGTTGATAAGAGGCTAACTAGG GTTCCGATGGTTTCATGCTGGTCCAAGCGT TAGCAAACATACTGAGGAAGGTATGTTAC ACCGTTAGTACAAAAGGCTCGGCGGGAGG TCTTATCCTTAGATGGACAAGGCCCCCCTA CGAGTTTTTTTATTAAACTTGTTGACATAA TGTGTCATTATATGGCGGCCGCTGACTG
This thesis		ilvE riboswitch F1 F	CCCGGGAAGCTTAGTTATAAATGAAAGAA TGTATTATAACAGCAG
This thesis		rbs-YFP F2 R	CCCGGGGCTAGCTTTATTTATACAGTTCGT CCATACCGTG
This thesis		ilvE riboswitch F1 R	GCTCATAATGTGACTTTCCTCCTTTGCGCA GCTGGGGATCCTC
This thesis		rbs-YFP F2 F	ATATTCAGAGGATCCCCAGCTGCGCAAAG GAGGAAAGTCACATTATGAGCA
This thesis	MH53	pSacA with luciferase F	GCGGAAAGATCGCCGTGTAAAGCTAGCCG CATGC
This thesis	MH54	pSacA with luciferase R	ATGTTTTTGGCGTCTTCCATAATGTGACTT TCCTC
This thesis	MH55	luciferase in pSacA F	CAAAGGAGGAAAGTCACATTATGGAAGA CGCCAAAA
This thesis	MH56	luciferase in pSacA R	TAGCTTGCATGCGGCTAGCTTTACACGGC GATCTTTC
This thesis	MH145	M9 Q5 SDM F	GGTCCGAGAGGTACAAAATCCAGAGC
This thesis	MH146	M9 Q5 SDM R	AGACGGAGCAGCTCCCG
This thesis	MH50	M11 Q5 SDM F	CCGCTCGGTTTTTTATAATATTCAG
This thesis	MH51	M11 Q5 SDM R	CTGAATATTATAAAAAACCGAGCGG
This thesis	MH65	luciferase in pSac-cm-Physpank F	ATTAAGCTTaggaggAGCCACCATG
This thesis	MH66	luciferase in pSac-cm-Physpank R	CGGCTAGCTTACACGGCGATCTTT
This thesis	MH22	relA EcoRI F pMINIMAD2	gggcccgaattcCATCTTTCGTTTTTTTCTTG
This thesis	MH23	relA BamHI R pMINIMAD2	gggcccggatccTGGGCTTCATTCGTTTTG
This thesis	MH67	relA Y200A F	ACCCTCAGCAAgcgTACAGAATTGT
This thesis	MH68	relA Y200A R	ACAATTCTGTAcgcTTGCTGAGGGT

This thesis	MH167	EcoRI PliaI F	CAGTCAGAATTCATTGGCCAAAGCAGAAAGGTCC
This thesis	MH168	SalI PliaI R	CTGACTGTCGACTCGTTTTCCTTGTCTTCATCTTATAC
This thesis	MH57	relA D78A F	ATTTTTGCACgcgGTCGTGGAAG
This thesis	MH58	relA D78A R	CTTCCACGACcgcGTGCAAAAAT
This thesis	MH121	Pspac RS luc EcoRI F	GTCAAACATGAGAATTCGACTCTCTAGCTTG
This thesis	MH122	Pspac RS luc EcoRI R	gggaaagaattcCTCACATTAATTGCGTTGCGCTCAC
This thesis	MH205	natA riboswitch gBlock F	ACTGTCAAGCTTCAATCATATTATAATATTAACAATAAG
This thesis	MH206	natA riboswitch gBlock R	GACTCAGCGGCCGCC
This thesis	MH207	livK riboswitch gBlock F	AGTCTGAAGCTTTAATTTATAATGACAAATTAATTATGTTG
This thesis	MH208	livK riboswitch gBlock R	CAGTCAGCGGCCGCCA
This thesis	MH209	NotI luciferase F	CTGACAGCGGCCGCAAAGGAGGAAAGTCACATTATG
This thesis	MH210	NheI luciferase R	GCATGCGGCTAGCTTTACAC
This thesis	MH231	BamHI PserA F	CTGACAGGATCCCGAATCCTGCTGTAAAGACAGC
This thesis	MH232	HindIII PserA R	TGACTGAAGCTTGACAAACTAAATATCTGATAATTTAACATATTCTC
This thesis	MH265	BamHI PilvB F	CTGACAGGATCCGAAATTGAAATGGATTG
This thesis	MH266	NheI PilvB R	CTGACAGCTAGCGGATTTTCATCCTTTAAAGATCATC
This thesis	MH271	BamHI PmetE F	CAGTCAGGATCCCACATCATGTAAATAAAAATTTCAAATTC
This thesis	MH272	HindIII PmetE R	AGTCTGAAGCTTTTATATGTAAAACACTCTCTTTCACC
This thesis	NSN139	PpurE luc F	ccggcgctcaggatccGGAAATTGATCTAAAACACGAAC
This thesis	NSN140	PpurE luc R	ACCGGAATGCCAAGCTTAATGCTTTTGTTTTCAGAAAAT
This thesis		*yfp* FISH probe 1	aaagttcttctcctttacgc
This thesis		*yfp* FISH Probe 2	agaattgggacaactccagt
This thesis		*yfp* FISH Probe 3	cccattaacatcaccatcta
This thesis		*yfp* FISH Probe 4	cctctccactgacagaaaat
This thesis		*yfp* FISH Probe 5	gtaagttttccgtatgttgc
This thesis		*yfp* FISH Probe 6	gtagttttccagtagtgcaa
This thesis		*yfp* FISH Probe 7	acaagtgttggccatggaac

This thesis		*yfp* FISH Probe 8	tgaacaccccaagtcaaagt
This thesis		*yfp* FISH Probe 9	tcatgccgtttcatatgatc
This thesis		*yfp* FISH Probe 10	gggcatggcactcttgaaaa
This thesis		*yfp* FISH Probe 11	ttctttcctgtacataacct
This thesis		*yfp* FISH Probe 12	gttcccgtcatctttgaaaa
This thesis		*yfp* FISH Probe 13	tgacttcagcacgtgtcttg
This thesis		*yfp* FISH Probe 14	taacaagggtatcaccttca
This thesis		*yfp* FISH Probe 15	atacctttaactcgattct
This thesis		*yfp* FISH Probe 16	gaatgtttccatcttcttta
This thesis		*yfp* FISH Probe 17	ttgtattccaatttgtgtcc
This thesis		*yfp* FISH Probe 18	gtttatctgcagtgatgtat
This thesis		*yfp* FISH Probe 19	tgagctttgattccattctt
This thesis		*yfp* FISH Probe 20	ccatcttcaatgttgtgtct
This thesis		*yfp* FISH Probe 21	atggtctgctagttgaacgc
This thesis		*yfp* FISH Probe 22	cgccaattggagtattttgt
This thesis		*yfp* FISH Probe 23	ttgtctggtaaaagggcagg
This thesis		*yfp* FISH Probe 24	cagattgtgtggacaggtaa
This thesis		*yfp* FISH Probe 25	ttttcgttgggatctttcga
This thesis		*yfp* FISH Probe 26	aagaaggaccatgtggtctc
This thesis		*yfp* FISH Probe 27	tcccagcagctgttacaaac
This thesis		*yfp* FISH Probe 28	Ttatacagttcgtccatacc
This thesis	MH259	EcoRI 3' alsR F	CTGACAGAATTCCAAAGCAGCCCTTGTGTTTTAG
This thesis	MH260	XhoI 3' alsR R	CTGACAGAATTCCAAAGCAGCCCTTGTGTTTTAG

This thesis	MH261	BamHI PalsS F	CAGTCAGGATCCCGTTTTGTCCTTTTCAGAAG
This thesis	MH262	HindIII PalsS R	AGTCTGAAGCTTGCATTTTAAACGTAAAATTTTAAATATC

Appendix C: Assessing (p)ppGpp in *E. coli*

A large number of studies on (p)ppGpp have investigated the molecule in the Gram-negative model organism, *E. coli*, including the seminal study that identified the signaling nucleotide (6). Researchers have long been utilizing *E. coli* in laboratories to investigate how (p)ppGpp may play a role in pathogenicity and antibiotic tolerance (138). While other researchers have established a riboswitch-based, fluorescent RNA reporter in *E. coli* (171), I sought to ensure our RsFluc reporter, validated and characterized in *B. subtilis*, functioned to report on (p)ppGpp in *E. coli*.

To investigate RsFluc activity in *E. coli*, I transformed the plasmid carrying the shuttle vector with the RsFluc construct (pMH11, Table 2) into wild-type MG1655. I also transformed this into a (p)ppGpp^0 (Δ*relA*Δ*spoT*) MG1655 strain. When the luminescent signal from the wildtype strain was normalized to the (p)ppGpp^0 strain, there was a sharp spike of activity that occurred as the cells were exiting exponential growth (Figure Appendix C.1). Notably, this spike in RsFluc activity occurs in approximately the same point along the growth curve in similar growth conditions as an observed spike in ppGpp as quantified by HPLC-MS by Varik *et al.* ((149), Fig. 4). Thus, the RsFluc reporter can report on ppGpp production in both Gram-positive and -negative model organisms, *B. subtilis* and *E. coli*.

The demonstration of RsFluc in *E. coli* is compelling, as *E. coli* is a commonly used laboratory strain for investigating other Gram-negative pathogens. When investigating possible new therapeutics against Gram-negative infections, the use of RsFluc in *E. coli* could be instrumental in evaluating how (p)ppGpp is affected by new treatments. It also demonstrates the robustness of this reporter across different species, which can be helpful for researchers investigating (p)ppGpp in other organisms.

This work demonstrated that the propagation of the plasmid that carries the RsFluc construct was a sufficient (p)ppGpp reporter in *E. coli*. However, this system was not optimized. To better investigate (p)ppGpp metabolism in *E. coli*, it would be pertinent to integrate this construct into the genome as a single copy, as was done in *B. subtilis*. It is challenging to control for plasmid copy number; however, integration into the genome ensures that there is only one singular copy in a growing cell until the DNA replicates.

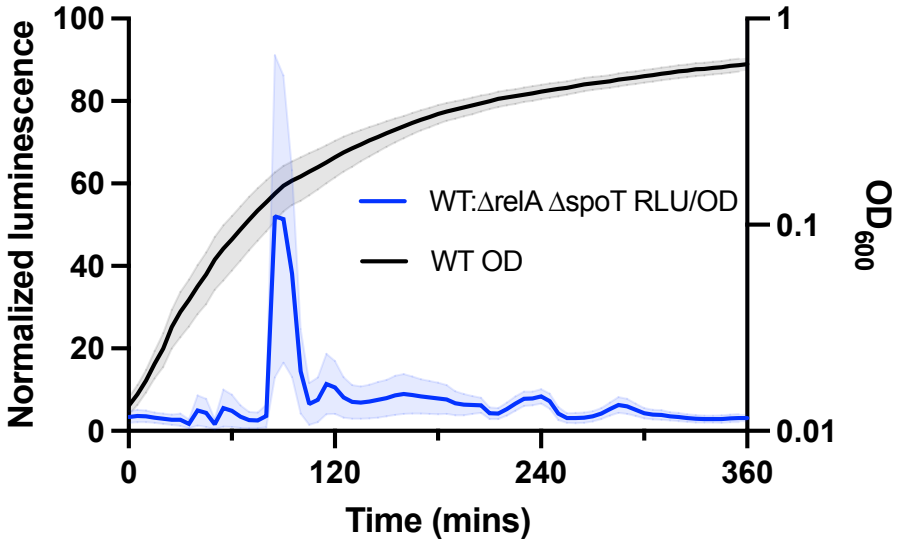

Figure Appendix C.1. RsFluc luminescence throughout growth in *E. coli*. Luminescence (RLU/OD_{600}) of RsFluc in wildtype (JDE3185) normalized to luminescence of RsFluc in Δ*relA*Δ*spoT* (JDE3187) background (blue). Growth (OD_{600}) of RsFluc in wildtype (black).